Stray Magnetic Field Based Health Monitoring of Electrical Machines

Zheng Liu, BSc MSc

School of Engineering

Newcastle University

A thesis submitted for the degree of

Doctor of Philosophy

February 2018

Abstract

Electrical machines are widely used in industrial and transportation applications which are essential to industrial processes. However, the lack of reliability and unpredictable life cycles of these machines still present opportunities and challenges for condition monitoring research. The breakdown of an electrical machine leads to expensive repairs and high losses due to downtime. The motivation of this research is to improve the reliability of electrical machines and to classify different kinds of failures via non-intrusive methods for condition-based maintenance and early warning of failure. Major potential failure types in electrical machines are winding and mechanical failures, which are caused by dynamic load state, component ageing and harsh working environments. To monitor and characterise these abnormal situations in the early stages, this thesis proposes stray magnetic field-based condition monitoring allowing fault diagnosis with the help of finite element models and advanced signal processing technology. By investigating the interaction between stray flux variations and machine failure, different kinds of faults can be classified and distinguished via numerical and experimental studies.

A non-intrusive stray flux monitoring system has been developed and can provide both static and transient stray flux information and imaging. The designed monitoring system is based on a giant magnetoresistance (GMR) sensor used to capture low stray flux fields outside the electrical machine's frame. Compared with other monitoring systems, its small size, low cost, non-inventive and ease of setting up make the designed system more attractive for in many long-term monitoring applications. Additionally, integration with the wireless sensor network (WSN) means that the latter's unique characteristics makes the proposed system suitable for electrical machine monitoring in industrial applications replacing existing expensive wired systems. The proposed system can achieve real-time data collection and on-line monitoring with the help of spectrogram and independent component analysis.

Three cases studies are conducted to validate the proposed system with different failures and loading states, using load fatigue, winding short-circuit failure and mechanical testing. In these case studies, electrical and mechanical failures and dynamic loads are investigated, collecting stray flux information with different kinds and sizes of electrical machines using both simulation and experimental approaches. Stray flux information is collected for different situations of winding failure, unbalanced load and bearing failures. Comprehensive transient feature extraction using spectrogram is implemented with respect to multiple failures and load variations. Spectrograms of stray flux can provide time-frequency information allowing the

discrimination of different failures and load states. Different faults can be distinguished through independent component analysis of stray flux data. Compared with traditional and current detection strategies, stray flux-based monitoring can not only provide failure indicator and better resolution but also gives location information. Additionally, by applying different feature extraction methods, different failure types can be separated based on stray flux information, which is likely to be difficult to achieve using traditional monitoring approaches. However, stray flux monitoring systems suffer from issue of noise and instability, and more case studies and investigations are needed for further refinement.

Acknowledgment

I would like to take this opportunity to express my sincere gratitude to those who have supported this project and helped me during my PhD study.

Firstly, special thanks go to Prof. Wenping Cao and Prof. Guiyun Tian, who supervised me throughout this research with their time, patience and knowledge. It has been such a pleasant and unforgettable experience to work with Prof. Tian and Prof. Cao, whose expertise in the field of condition monitoring and electrical machines has helped me through all the tough days.

I would like to thank my colleagues Dr. Mohammed Alamin, Dr. Hong Zhang, Dr. Jun Zhang, Dr. Min Zhang, Dr. Bin Ji, Dr. Chukwuma Junior Ifedi, Dr. Haimeng Wu, Dr. Zheng Tan, Dr. Aijun Yin, Dr Danping Huang, Dr Jianping Peng, Mr Yunlai Gao, Mr Kongjing Li, Mr Chen Wang, Mr Kaiwen Yu and all researchers in the Sensor Technology Research Team and Electrical Power Research Group at Newcastle University, who have provided their help and fruitful suggestions.

My deepest thanks go to my parents Hongxia and Dianxuan as well as my wife Jia. I could not have done my PhD without their support, love and perseverance throughout all my endeavours.

List of Publications:

[J1] Z. Liu, G. Tian, W. Cao, X. Dai, B. Shaw, “Non-invasive load monitoring of induction motor drives using magnetic flux sensors,” IET Power Electronics, Accepted.

[J2] S. Gao, X. Dai, Z. Liu, G. Tian, “High-performance wireless piezoelectric sensor network for distributed structural health monitoring,” International Journal of Distributed Sensor Networks, vol. 12, no 3, Mar. 2016.

[J3] Z. Tan, X. Song, W. Cao, Z. Liu, Y. Tong, “DFIG machine design for maximizing power output based on surrogate optimization algorithm,” IEEE Transactions on Energy Conversion, vol. 30, issue 3, pp. 1154-1162, Sep. 2015.

[J4] Z. Tan, X. Song, B. Ji, Z. Liu, J. Ma, W. Cao, “3D thermal analysis of a permanent magnet motor with cooling fans.” In Journal of Zhejiang University Science A, vol. 16, no 8, pp. 616-621, Aug 2015.

[C1] Z. Liu, W. Cao, P. Huang, G. Tian, J.L. Kirtley, “Non-invasive winding fault detection for induction machines based on stray flux magnetic sensors,” 2016 IEEE PES General Meeting Conference, Boston, MA, 2016.

[C2] S. Gao, X. Dai, Z. Liu, G. Tian, S. Yuan, "A wireless piezoelectric sensor network for distributed structural health monitoring," Wireless for Space and Extreme Environments (WiSEE), 2015 IEEE International Conference on, Orlando, FL, pp. 1-6, 2015.

[C3] Z. Liu, W. Cao, Z. Tan, X. Song, B. Ji and G. Tian, "Electromagnetic and temperature field analyses of winding short-circuits in DFIGs," Diagnostics for Electric Machines, Power Electronics and Drives (SDEMPED), 2013 9th IEEE International Symposium on, Valencia, pp. 269-273, 2013.

[C4] N. Yang, W. Cao, Z. Liu, Z. Tan, Y. Zhang, S. Yu, J. Morrow, "Novel asymmetrical rotor design for easy assembly and repair of rotor windings in synchronous generators," IEEE in Magnetics Conference (INTERMAG), Beijing, pp. 11-15, May 2015.

[C5] Z. Liu, W. Cao, Z. Tan, B. Ji, X. Song, G. Tian, “Condition monitoring of doubly-fed induction generators in wind farms,” the Ninth International Symposium on Linear Drives for Industry Applications (LDIA’13), Hangzhou, 2013.

[C6] Z. Tan, W. Cao, Z. Liu, X. Song, B. Zahawi, “Optimization of doubly fed induction generators (DFIGs) for wind power system,” the Ninth International Symposium on Linear Drives for Industry Applications (LDIA’13), Hangzhou, 2013.

Contents

List of Figures

List of Tables

List of Symbols

$\vec{A}$	Magnetic vector potential
B	Magnetic flux density
c	Capacity
D	Diameter
f	Frequency
i	Current
j	The complex number
K	Constant
k	Constant
L	Inductance
M	Mature Inductance
m	Constant
P	Power
p	Number of motor poles
r	Resistance
R	Radius
s	Slip
t	Time
T	Torque
V	Voltage
ω	Rotation an
Ψ	Flux
ϕ	Angular position
σ	Electrical conductivity
μ	Magnetic permeability
ζ	Damping factor
α	Contact angle
λ	Constant
β	Constant
v	Velocity
ρ	Density

List of Acronyms

GMR	Giant magneto resistance
DSP	Digital signal processing
MMFs	Magnetic motive force
UMP	Unbalanced magnetic pull
MSCA	Motor current signature analysis
FFT	Fast Fourier transform
AC	Alternating current
DC	Direct current
EMF	Electrical magnetic force
STFT	Short time fourier transform
AMR	Anisotropic magnetoresistive
DMA	Direct memory access
PWM	Pulse-width modulators
ADC	Analog-to-digital conversion
DAC	Digital-to-analog conversion
SPI	Serial peripheral interface
SRAM	Static random access memory
VSD	Variable speed drive
FOC	Field-oriented controller
VSI	And voltage-source inverter
FE	Finite element
FEA	Finite element analysis

Chapter 1 Introduction

This chapter provides the motivation for the research and illustrates the challenges and opportunities of current condition monitoring technologies for electrical machines. The stray flux detection method is then proposed for the characterisation and evaluation of the health state and potential failures in electrical machines. The major achievements of the research are then listed. Finally, the structure of this thesis is explained.

1.1 Research background

Electrical machines play an essential role in industrial drives and power generation plants worldwide. They are found in use in motor drive systems from a few watts to several megawatts. In recent years, electrical machine diagnosis and predictive maintenance research has experienced spectacular dynamism. Condition monitoring technologies have been also incorporated into many industrial systems and applications. However, failures in electrical machines, may lead to severe repercussions in economic terms as well as other less tangible costs, and this is a crucial issue for current industrial applications. In these circumstances, it is essential to develop new monitoring techniques able to detect the early stage of failure sufficiently in advance so that proper maintenance action can be planned and adopted.

Electrical machines typically operate in harsh environments, which leading to annual failure rate of approximately 6%. Faulty motors and generators may cause whole electrical systems to shut down or even catastrophic damage. Failures in Bearings and stator winding and eccentricity-related faults are the most prevalent types and, thus, demand special attention. These types of failure share several of the same symptoms, including unbalanced voltage/current, decreased average torque, reductions in efficiency and excessive heating or vibration. Therefore, it is important to develop reliable and accurate condition monitoring systems to safeguard machine operation.

For the purpose of detecting and distinguishing failures inside machines, many diagnostic methods and indicators have been developed so far. Electrical methods are based on the measurement of electrical terminal quantities such as current. Motor current signature analysis (MCSA) utilizes the results of spectral analysis of the current of an induction machine

(IM) to pinpoint existing or the predict failures in the motor [1]. As a result of abnormalities occurring in the machine, additional frequency components will appear in the current spectrum [2]. Meanwhile, diagnostic analysis has been reported in which current is sensed during the normal operation and transient state, measuring variables such as the sequence components of current, park vector, wavelet transform and zero crossing instants [3-5]. Vibration signals can also be analysed to detect the possible development of a faulty condition in IMs. This technique is generally used for detecting mechanical faults, such as bearing problems, gear mesh defects, rotor misalignment and unbalanced mass [6, 7]. However, these methods shares a common drawback, which is that due to their 'global' character they cannot provide sufficient ability to discriminate between different kinds of faults and give location information, because of the influence of changes in the power supply and dynamic load [8]. Additionally, detailed information on the characteristics of motor design and geometry is required, such as knowledge of frequency response functions [9]. This is because mechanical and electrical responses vary at different accelerometer positions, which makes the quantification of faults difficult. Current monitoring technologies may require sensors to be placed inside of machines and cables, which may lead to possible damage, and in any case these locations are not always accessible.

To address the aforementioned problems, this research concentrates on how magnetic flux detection can be applied to estimate and monitor the health of electrical machines. Magnetic flux is one of the most important parameters of a machine and is related to the magnetic state of the machine. Once a tiny abnormality occurs in a machine, its magnetic flux will change depending on different situations and types of faults.

Stray flux is magnetic flux that radiates from the outside of the machine frame and is inherently and strictly connected to the magnetic state of the machine. Stray flux is induced by stator and rotor currents, both of which produce magnetic flux with different spectral components. Depending on the physical location around the motor body where measurement is performed, the magnetic field can contain information on stator and rotor states together, which reflects on different spectrum and harmonics.

Three specific challenges have arisen for the condition monitoring of electrical machines. Firstly, methods should be non-invasive approach and easy to implement. Secondly, the detection and classification of different types of failures outside the machines is necessary. Thirdly, quantitative non-destructive evaluation is required to distinguish between different types of faults. To address these issues, a novel condition monitoring system is developed in this study based on GMR sensors which can capture stray flux escaping outside the machine's

frame. In term of distinguishing different failures, spectrogram and ICA are used to obtain time-frequency information and provide failure separation.

1.2 Aim and objectives

The overall aim of this research is the design and development of a new generation of non-invasive evaluation health monitoring system to detect different faults in the electrical machines.

The objectives of this research can be summarized as follows:

1) To undertake a literature survey and investigation of the application of different parameters based condition monitoring system for electrical machine monitoring including the challenges for failure detection and diagnostics.

2) To design and develop a stray flux-based sensing system for machine monitoring diagnosis and to validate the proposed system in different case studies, which includes the elements listed below:

a) To develop a magnetic sensor system for stray magnetic field capture with wired and wireless network which is suitable for the applications of electrical machine condition monitoring.
b) To develop and have a deep understanding of finite element models concentrating on stray flux distribution in electrical machines with different types of faults;
c) To monitor the load variation of electrical machines during both the steady-state and transient states by using the designed stray flux-based sensing system.
d) To investigate the relationship between stray magnetic/**thermal** field and stator winding short-circuits in electrical machines; to identify and evaluate the health state of the machine in different situations of stator winding failures.
e) To understand and classify different mechanical failures based on the proposed stray flux sensing system for machine health monitoring in order demonstrate the system's capability and merits, to compare traditional detection technology with stray flux monitoring and identify the suitable approach for monitoring and diagnosis of electrical machines.

1.3 Main achievements

The main achievements of this research are shown below:

1. A comprehensive review of condition monitoring technologies of electrical machines is undertaken. To provide a non-invasive approach, the design of a GMR sensor-based system for monitoring failures and the healthy state of electrical machines is proposed. The designed stray magnetic sensor system is able to capture stray flux and is integrated with wired and wireless monitoring systems via several experimental case studies.

2. Finite element models concentrating on the distribution of stray flux in electrical machines with different stator winding and mechanical failures are built. Additionally, depending on the simulation results, the optimal location of the GMR sensor is determined, which is at the centre of the machine's external frame. The z-direction of the stray flux provides the strongest signal among the three directions.

3. Real-time load monitoring is achieved through the application of the designed stray flux system. By analysing the static and dynamic feature extraction using spectrograms, the time-frequency information of stray flux and load variation can be illustrated. The transient time of stray flux can be an indicator of load variation, which provides better performance than amplitude measurements during the steady state.

4. Different stator winding failures are investigated through numerical and experimental studies using stray flux information. The link between the stray flux signal and winding failures is demonstrated. Phase-to-phase and phase-to-ground stator short-circuit failures are tested in the experiments. By referencing different harmonic components, especially those at half of the fundamental frequency, different winding failures can be separated using the designed stray flux monitoring system and feature extraction approach.

5. The inspection of electrical machines for mechanical failures including unbalanced load and bearing misalignment, is investigated using simulation and experimental studies. By using independent component analysis, different mechanical failures can be separated due to the different failure harmonic indicator. Compared with the measurement current, stray flux-based monitoring provides better performance in defect detection and classification through spectrogram.

1.4 Thesis layout

Chapter 1 gives a brief introduction of the study, including the research background, aim and objectives, main achievements and an outline of the thesis.

Chapter 2 presents a comprehensive survey of possible failures inside electrical machines. Meanwhile, state-of-the-art condition monitoring technologies for machines are analysed and compared. The advantage and disadvantages of current methods are discussed. Additionally, previous stray flux monitoring methods are also reviewed.

Chapter 3 shows the methodologies and the overall process of this research to elaborate different case studies and milestones. This chapter provides the theoretical background of stray flux condition monitoring in electrical machines, followed by a brief description of the stray flux monitoring system. The signal processing methods for collecting stray flux information and feature extraction in the frequency domain using spectrograms are also mentioned in this chapter.

Chapter 4 presents the design and set-up of a novel stray flux condition monitoring system. Depending on FEA simulation results, the choice of sensors, optimized sensor location and direction can be determined. In this research, the giant magnetoresistance (GMR) sensor is chosen as the magnetic flux sensor to capture low magnetic flux field. This chapter also explained the data acquisition system and wired/wireless communication system design which based on an NI data acquisition card and DSP board. The proposed system provides a non-invasive method to inspect the health state inside of electrical machines.

Chapter 5 focuses on one of the case studies investigating load monitoring using the proposed stray flux monitoring system. Experimental validation including two case studies is also carried out via static and transient magnetic field measurements. In steady-state operation, the static features from a GMR sensor are applied for load monitoring and characterization. Loading can also be measured by using the feature extraction of different transients. Firstly, when induction motors start up with different loads, the first peak value of the output voltage of the magnetic sensor is an indicator of variable loads. Secondly, a spectrogram is used to provide patterns over time with varying harmonics. By referencing the transient time information of the spectrogram patterns of the external magnetic flux, load variations can be illustrated during experiments. Compared with static analysis and results, the transient response time can provide more effective and better results for dynamic load states. Load monitoring experiments are carried out in two different test benches. The results show that the proposed load monitoring system can be suitable for different machines with differing ranges of power.

Chapter 6 shows the second case study based on the detection and separation of different kinds of stator winding failures. The proposed stray flux method offers wide range spectrum response, and high resolution of low-level magnetic field detection. Simulation results from

different stator winding short-circuits can provide information about changes in the stray flux. Based on this information, GMR sensors and arrays can be chosen and developed to meet the test requirements. Experimental results have confirmed that the proposed condition monitoring system is capable of capturing stray magnetic flux even though the leaking flux signal is quite weak. By studying the measured stray flux in the time domain and especially in the frequency domain, several significant harmonic components can be used as the indicators of stator winding faults. The time-frequency spectrogram can provide better harmonic patterns and information compared with the frequency spectrum.

Chapter 7 considers presents two different mechanical failures of unbalanced load and bearing misalignment in an experimental case study. A theoretical analysis illustrates the relevant harmonics once these mechanical failures happen inside of the electrical machines. By implemented the proposed GMR sensor system outside the tested machine, stray flux information can be collected. Combining the measured stray flux data and spectrograms, unbalanced loads and bearing misalignments can be detected by the proposed system. In this chapter, stray flux detection is also compared with a current-based monitoring system, and is shown to offer richer information and higher efficiency.

Chapter 8 summarizes all of the studies. Additionally, it presents the conclusions of the research so far and gives recommendations for future work. The research has proposed and validated a novel non-invasive condition monitoring system for electrical machines. With the help of spectrograms, stray flux information can be an effective indicator of load monitoring, stator winding failures and mechanical failures.

1.5 Chapter summary

This chapter introduces the PhD research work which focuses on the condition monitoring of electrical machines using stray flux information. The research background is shown, and the aim and objective of this research are presented. The major contributions of the research are listed as well. Following this, an outline of the thesis is given and the contents of each chapter are described.

Chapter 2 Literature Review

A comprehensive literature review is given in this chapter. To determine the aims and objectives of the condition monitoring system, types of failure are explained, which include winding, bearing and rotor failure. By analysing failures in electrical machines, it is possible to assess the importance and priority of different types of failure which need to be monitored. Different kinds of condition monitoring technologies are then illustrated and their advantages and disadvantages are discussed. Compared with other approaches, the stray flux monitoring approach provides rich information and is non-destructive. Additionally, by reviewing current monitoring technologies, the challenges and problems arising are also summarized.

2.1 Failure models

Induction machines typically operate in harsh environments leading to failure rates of approximately 6% each year [10-12]. Faulty induction machines may cause whole drive systems to shut down or even catastrophic damage. Several surveys have investigated and illustrated in detail types and rates of failure in these machines [13]. Common failures in induction machines include those due to stator winding faults, bearing faults, rotor bar/ring faults and shaft faults. Stator winding faults are one of the most frequent types of failures in drive systems [14]. Fig 2.1 shows the failures rates of typical motor drive applications. From this, it is very important to develop reliable and accurate condition monitoring systems to safeguard machine operation.

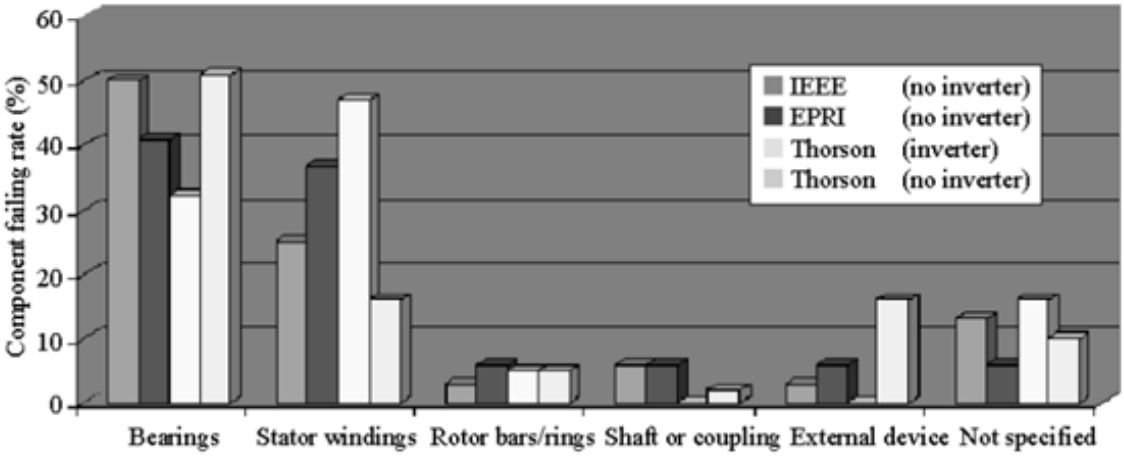

Figure 2.1 Failure rate of induction machines [3, 13, 15, 16]

From the data above, winding faults in the rotors and stators are a major type of failures, and are extremely common in electrical machine systems. Once winding failure occurs, generators cannot supply stable and high quality electric power. Moreover, if a short-circuit in the windings is not detected until a very late stage, it can lead to the catastrophic failure of generators or even the breakdown of whole systems. An example of a rotor winding fault is shown in Fig. 2.2.

Figure 2.2 Catastrophic failure of a wind turbine generator due to faulty rotor winding [17].

2.1.1 Stator failures

Industrial surveys and other research have shown that a large percentage of failures in electrical machines result from a fault related to the stator winding and core. Many studies have indicated that the majority of motor stator winding failures result from the destruction of the turn insulation [6, 18-20]. Typically, winding faults are divided into open circuits and short-circuits in machines. Winding short-circuits are the major and most common types of winding faults. Possible winding faults in generators may be turn-to-turn, coil-to-coil, phase-to-phase, phase-to-ground and winding-to-iron faults. Fig. 2.3 shows the positions and patterns of the different winding short-circuit faults in electrical machines.

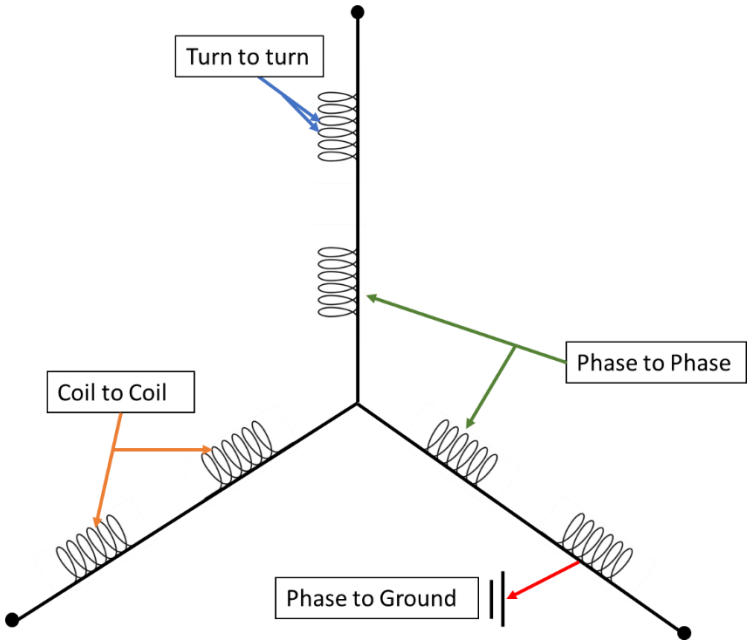

Figure 2.3 Possible winding failures in the rotors and stators of the machines

Shorted turns in the stator winding belong to a class of faults that may often have a negligible effect on the performance of the machine, but the presence of which may eventually lead to catastrophic failure. Therefore, stringent demands are made for means to minimise the occurrence and mitigate the effects of turn insulation breakdown [8, 21, 22].

In electrical machines, the stator and rotor winding insulation is exposed to a combination of thermal, electrical, vibrational, thermo-mechanical, and environmental stresses during operation. In the long term, these multiple stresses cause ageing, which finally leads to insulation breakdown [18, 23-25]. For this reason, it is important to estimate the integrity of the remaining insulation in winding after a period of operating time. Deterioration of the winding insulation usually begins as an inter-turn fault involving a few turns of the winding. A turn fault in the stator winding of an electrical machine causes a large circulating current to flow in the shorted turns. Such a circulating current is of the magnitude of twice the locked rotor current,

and it causes severe localised heating and sustains favourable conditions for the fault to rapidly spread to a larger section of the winding. If left undetected, turn faults can propagate, leading to catastrophic phase-ground or phase-phase faults. Excessive heating caused by turn-to-turn shorts is the reason why motors in this condition will almost always fail in a matter of minutes, if not seconds. A basic rule of thumb to consider is that every additional 10°C causes the winding to deteriorate twice as fast as when operation takes place in the allowable temperature range [26, 27]. Failure of the insulation between the winding and ground can cause a large ground current, which would result in irreversible damage to the core of the machine. This fault may be so severe that the machine might even have to be removed from service. If the fault is detected at an early stage, however, the machine can be put back into service by just re-winding the stator; while, on the other hand, replacing the whole motor means increased downtime [28].

Regular monitoring provides the opportunity for the early detection of problems and possible remedial action, thereby prolonging the life of the machine. For smaller machines, the development of a time delay between a direct turn-to-turn short-circuit and ground insulation failure can be from some minutes up to as much as hours, depending on the severity of the fault and the loading of the motor. Another types of fault associated with the stator winding is called "single-phasing" [22, 29]. In this case, one supply line or phase winding becomes open-circuited. The resulting motor connection has a line voltage directly across two phases (assuming a "star" connected machine) which is equivalent to a single-phase circuit. The effect of an insulation fault between turns is to eliminate a turn or group of turns from the stator winding [30]. This will be of little direct consequence, but will be quantifiable in the flux distribution in the air-gap. Fig. 2.4 shows an inter-turn short-circuit between two points, a and b, of a complete stator winding. The path to the circulating current between these points is closed and the path A–A' can be expanded into two independent circuits [19, 23]. Fig. 2.4 shows that the two currents, the phase current and the current which flows in the short-circuited part, produce opposite MMFs. Therefore, inter-turn short-circuits have a cumulative effect in decreasing the MMF in the vicinity of the short-circuited turn(s). Firstly, when a short-circuit occurs, the phase winding has fewer turns and, therefore, lower MMF. Secondly, the short-circuit current MMF is opposite to the MMF of the phase winding. The circulating current Ic is a result of the galvanic contact between points a and b, but also due to the contribution brought about by the transformer effect or mutual induction.

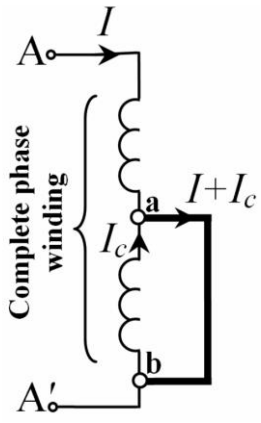

Figure 2.4 Inter-turn short-circuit

2.1.2 Rotor failures

Unlike with stator design, rotor design and manufacturing has undergone little change over the years. As a result, rotor failures now account for around 20% of total induction motor failures [13, 31, 32]. However, in the field of fault diagnosis and the condition monitoring of electrical machines, most of the research presented in the literature deals with induction motor rotor failures, while bearing-related failures, which account for 50-60% of failures, are not so widely discussed [12, 17]. Rotor cage-related faults have perhaps received so much attention in the literature as a result of their well-defined associated fault frequency components.

Under normal operating conditions, large mechanical and thermal stresses are present, especially if the machine is being continually stopped and restarted or if it is heavily loaded [33]. It is well known that the rotor current during starting can be as much as ten times the normal full load current and that the effects of these large currents are represented by very large thermal stresses in the rotor circuit. The starting period is also characterised by minimal cooling and maximum mechanical forces, which over-stress the rotor bars.

The sequence of events following the cracking of a rotor bar can be described as follows [13]. The cracked bar will increase in resistance and will overheat at the crack. The bar will break completely and arcing will occur across the break. This arcing will then damage the rotor laminations around the faulty bar [34, 35]. The neighbouring bars will carry an increased current and will be subject to increased stresses, eventually causing these bars to fail. Finally, the broken bars may lift outwards because of centrifugal forces and could catastrophically damage the stator windings.

Machine eccentricity is defined as a condition of the asymmetric air-gap that exists between the stator and rotor [1, 36, 37]. The presence of a certain level of eccentricity is

common in rotating electrical machines. Some manufacturers and users specify a maximum permissible level of 5 per cent, whereas in other cases, a maximum level of 10 per cent of the air-gap length may be allowed by the user. However, manufacturers normally try to keep total eccentricity at even lower levels in order to reduce vibration and noise and minimise unbalanced magnetic pull (UMP) [38]. Since the air-gap in an induction machine is considerably smaller than in other types of machines with a similar size and performance, this type of machine is more sensitive to changes in the length of the air-gap. There are two types of air-gap eccentricity: static air-gap eccentricity and dynamic air-gap eccentricity. In the case of static air-gap eccentricity, the position of the minimal radial air-gap length is fixed in space, while in the case of dynamic eccentricity, the centre of the rotor is not at the centre of rotation and the position of the minimum air-gap rotates with the rotor [34, 39]. However, static and dynamic eccentricities are only a basic classification, since further varieties and modifications, such as unilateral eccentricities as well as angular and radial misalignments, are also possible.

In reality, both static and dynamic eccentricities tend to co-exist. An inherent level of static eccentricity exists even in newly manufactured machines as a result of the manufacturing and assembly method used. This causes a steady UMP in one direction, and with usage this may lead to a bent rotor shaft and bearing wear and tear, resulting in some degree of dynamic eccentricity [35]. Unless detected early, this eccentricity becomes large enough so that high unbalanced radial forces develop that may cause stator-to-rotor rub, leading to a major breakdown of the machine.

2.1.3 Bearing failures

Because of the close relationship between motor system development and bearing assembly performance, it is difficult to imagine the progress of modern rotating machinery without considering the wide application of bearings. Bearing faults may account for 42%-50% of all motor failures [31, 40-42]. Motor bearings may cost between 3 and 10% of the actual cost of the motor, but the hidden costs involved in downtime and lost production combine to make bearing failure a rather expensive abnormality [43]. Bearing faults might manifest themselves as rotor asymmetry faults, which are usually included in the category of eccentricity-related faults. Otherwise, ball bearing-related defects can be categorised as outer bearing race defects, inner bearing race defects, ball defects, and train defects [42, 44, 45].

Different stresses acting upon a bearing may lead to excessive audible noise, uneven running, reduced working accuracy, and the development of mechanical vibrations and, as a result, increased wear [9, 46]. As long as these stresses are kept within the design capabilities

of the bearing, premature failure should not occur. However, if any combination of them exceeds the capacity of the bearing, then its lifetime may be drastically diminished and a catastrophic failure could occur.

2.2 Main reasons for faults

There are many reasons leading to faults in electrical machines. This section presents the major causes of these faults showing three main reasons for faults in electrical machines. By understanding and investigating the causes of faults, the development of failure can be traced and this helps in the design of condition monitoring system and in predicting the progress of the fault process. The major reasons for faults in electrical machines can be important parameters to monitor during machine operation.

2.2.1 Environment

The environment of electrical machines may be extremely harsh and complicated. Due to the special environments, moisture, dust and salt can corrode machines parts. Adverse environment all conditions easily lead to insulation faults in windings. The working environments of electrical machines often include aggressive chemicals, and high humidity, contamination and radiation, which lead to not only corrosion but also contamination. Corrosion and contamination can accelerate the thermal deterioration of electrical machines, increasing thermal stress in every component. Additionally, unexpected corrosion can generate surface currents and electrical tracking during machine service, which increase the degradation of the winding insulations and bearings.

2.2.2 Voltage spikes of PWM control

In a drive system, a PWM power converter is linked to the windings directly to control the whole machine. Generally speaking, the operating voltage of the stator windings is 690 volts; however, there will be almost 2500 volts peak voltage spikes with very high switching frequency, which are generated by the power converter and sent to the winding [27, 47]. This high voltage can damage and break down the insulation of the rotor windings, and result in a turn-to-turn short-circuit. Fig. 2.5 shows an example of a turn-to-turn winding fault in an induction machine.

Figure 2.5 Turn to turn winding fault in an induction machine [47].

2.2.3 Dynamic load

Wind speed in an offshore wind farm is not a constant parameter. The generator is directly affected by wind speed, and its speed is also changing all the time. By controlling the excitation current in the rotor windings, the generators can create satisfactory electric input. The rotor windings are twisted all the time by electromagnetic force, which is the same situation as in broken rotor bars in the squirrel cage induction motors [22, 48]. Moreover, given the dynamic wind speed, the rotor windings are unstable all the time. Meanwhile, there will be an excessive minor movements between windings [18], which may lead to rubbing against the insulation and then to short-circuit situations. Subsequently, due to the dynamic load, the rotor windings create lots of heat, and most of the heat will be conducted to the air through the main machine body which depends on a cooling system [47]. But the end windings are directly connected to the air, and moreover the thermal conductivity coefficient of the air is much higher than that inside the generator body [49]. In this case, the insulation of the end windings and the generators will be damaged and break down due to the high temperature.

2.3 The state-of-the-art of condition monitoring technologies

From the review above of the modes of failure and their causes in electrical machines, it is clearly necessary to develop condition monitoring technologies for these drive systems. To reduce maintenance and operating costs, much condition monitoring research has been conducted in recent 10 years. The following review of monitoring methods includes motor current detection, stray flux monitoring, surge testing and temperature monitoring. The merits

and drawbacks of different condition monitoring technologies are then compared. An overall perspective on recent advanced condition monitoring technologies is then provided.

2.3.1 Motor current

The current is the most important characteristics in machines and is easy to measure. Due to its low cost and simplicity, motor current signature analysis (MSCA) is the most widely used condition monitoring technology in commercial applications. The main idea of this technology is the use of spectral analysis to detect winding faults in both rotors and stators [10-12, 17].

In the recent years, researchers have proposed several ways to conduct spectral analysis. Firstly, the application of Fast Fourier transform (FFT) analysis is able to determine the amplitude of each different harmonic component [50]. During winding faults in rotors and stators, the harmonics at even numbers or specific frequencies are quite different compared with those in healthy machines. The advantage of using the FFT is that accurate results can be obtained to detect winding fault in machines. Furthermore, it is also able to detect bearing faults, eccentricity and other faults in an entire wind turbine system [31, 51]. However, due to the characteristics of this diagnostic approach, it is only suitable for cases of fixed frequency [52]. Given a variable wind speed load, the slip and the frequency are changing all the time, and this is the main drawback for the use of the Fast Fourier transform in MSCA.

Alternatively, the wavelet transform is also able to be used in this condition monitoring technology. The wavelet transform is an approach which provides the necessary information in the time-frequency domain for non-stationary signals [53]. In recent years, this approach has been applied by various researchers to failure detection in the doubly-fed induction generators [54-58]. The advantage of the wavelet transform is that there is no influence on the results if a machine is running with variable speed, which is the most significant difference comparing with other kinds of power generations [55, 56]. Although the wavelet transform seems to be appropriate for monitoring wind generators, it does not yield very satisfactory results when the generator suffers from an unbalanced load or a poor excitation current [50, 54].

Additionally, the Park's vector approach is an alternative way to detect faults, and has been widely used to identify turn-to-turn winding fault in rotors and stators and rotor eccentricity [55, 59]. The Park's vector approach is able to use 2-D representation for three-phase induction generators. The relevant equations are shown below [24]:

$$\begin{cases} i_d = \sqrt{\frac{2}{3}} i_a - \frac{1}{\sqrt{6}} i_b - \frac{1}{\sqrt{6}} i_b \\ i_q = \frac{1}{\sqrt{2}} i_b - \frac{1}{\sqrt{2}} i_c \end{cases} \quad (2.1)$$

In equation 1.1, the (i_a, i_b, i_c) are the currents of the three phases in the induction generator, and the(i_q, i_d) are the current Park's vector components. In this case, the Park's vector can be expressed as the following equations:

$$\begin{cases} i_d = \frac{\sqrt{6}}{2} i_M \sin \omega t \\ i_q = \frac{\sqrt{6}}{2} i_M \sin(\omega t - \frac{\pi}{2}) \end{cases} \quad (2.2)$$

where i_M is the maximum value of the phase current; and ω is the frequency. From equation 2.2, the healthy generators can provide a perfect circle, in which $\sqrt{i_d^2 + i_q^2}$ is constant. On the other hand, if there are some winding faults in the generators, the circle will instead be elliptical, and in this case the fault can be detected. Besides this, the frequency of the Park's vector is twice the fundamental frequency, and its amplitude also shows how serious the fault is [24, 59]. The advantage of the Park's vector approach is that it can give very good results at a certain frequency or steady state, and is sensitive to winding failures. Its drawbacks are that, using this method, the location of winding faults cannot be determined; moreover, it cannot be used when there are rapid changing in wind speed or the transient states [10].

2.3.2 Flux signature analysis

Flux is one of the most important characteristics in a machine. Firstly, in healthy machines, no axial homo-polar flux is created as the current flowing in the rotor and stator circuits is balanced. However, if winding faults occur in the electrical machine, a measurable axial leakage flux will be created which can be detected by search coils [60, 61]. By referencing the harmonic of the axial leakage flux, turn-to-turn winding faults in the machine can be detected.

Additionally, air-gap flux is one of the most important parameters, and any changes in machines are reflected in the air-gap flux and the distribution of the MMF, which can be detected by flux sensors [62]. By using FFT, the harmonics of the air-gap flux density can be obtained which can then be used to detect winding faults.

The flux signature analysis is able to detect failures rapidly. Furthermore, it also shows the locations of winding faults, which reduces the repair time once technicians arrive. In this

case, it can be a very good online methods for condition monitoring. However, its disadvantage is that flux sensors or search coils are required to be installed in the machine, which makes it an invasive method [62]. Moreover, in the special environment of an offshore wind farm, flux sensors might be damaged as well, which would be obviously reduces the reliability and accuracy of flux signature analysis.

2.3.3 Surge test

The surge test is an established and predictive method for detecting winding faults in both the rotors and stators, and it can also provide early warnings if weak insulation between winding turns before short-circuit faults occur. During the test, two high frequency pulses are injected into two phase windings of the generator with the third phase grounded. By comparing the reflected signals, winding faults or weak insulation between turns can be detected directly [63]. With the development of system identification technologies, surge tests can provide not only information about insulation ageing, but can also show other parameters of machines such as the inductance of the stator and rotor windings.

During a real experimental test, the surge test is based on offline measurement data using a locked rotor test with DC voltage step response, AC sinusoidal voltage or a multi-sinusoidal signal as the injected signal. By controlling the average phase voltage and injecting the test signal, the motor can be represented in an analytical model as an RLC circuit. If there is anything wrong with the insulation or windings, changes in the magnitude and frequency of the reflected signal can be observed. In this way, the machine impedance can also be measured for different DC values of the quadrature and direct-current components, which allows an analysis to be carried out of the influence of saturation and magnetic interaction on machine impedance. Thus the health state of an electrical machine can be monitored.

The advantage of the surge test is that it can accurately determine the location of winding failures, and predictions can be made prior to the occurrences of faults, making it attractive for reducing maintenance costs [64]. The drawback is that the surge test cannot set as an online condition monitoring method for machines; moreover, it requires the machines to be stopped which is not suitable for in-service machines. Furthermore, the surge test voltage signal is likely to reduce the lifetime of the testing winding.

2.3.4 Temperature

All winding faults will create hotspots and excessive heat inside the machine, which gives rise to the increasing temperature of the machine. From the knowledge of mechanisms of winding faults, data of the heat flow and distribution of the temperature field can be used to

directly illustrate the progress of the failure from the initial turn-to-turn winding faults to catastrophic damage [65]. In this case, a focus on thermal performance and the temperature in the machine can provide an effective method of condition monitoring.

The general arrangement for monitoring winding temperatures is to use thermal sensors or cameras. Additionally, temperature monitoring can also be accomplished by using a method which analyses the thermal mode or a motor parameter-based method.

Firstly, a lumped thermal circuit model has been reported for the estimation of the thermal performance of machines, which includes variables of parameters such as the thermal resistance, capacitance and the heat source [19]. The thermal resistors provide the performance of the heat conduction and convection inside and outside the machines. The thermal capacitors give temperature rise of the machines, and the heat source is equated to the power losses in the machines. By building a lumped thermal model, the temperatures of stator and rotor, and even the windings are able to be predicted [26]. Hence, temperature condition monitoring systems can be applied in the onshore and offshore wind farms as well as any in- service machines.

Consequently, the temperature of the windings in stators and rotors can be estimated using calculation of motor parameters. In this method, the currents and the voltages in the rotors and stators, the active power and the rotor speed can be measured and used to calculate the resistance of the rotors and stators [66]. Due to the relationship between temperature and the characteristics of materials, the winding temperatures in the rotors and stators can be estimated with reasonable accuracy [20].

The advantage of these two methods is non-intrusive nature, where no temperature sensors are required. Furthermore, they avoid drift errors in thermal sensors after long periods of service [19, 20, 26]. Moreover, this technology is able to be applied in an online system, which can give rapid response and results. Nonetheless, all the parameters to be measured are very sensitive and are collected at certain frequencies. More specifically, the results will be not satisfactory for transient states. Additionally, the cooling system used in different machines and unstable conditions may lead to some deviations in data during evaluation [27].

2.3.5 Comparisons

Generally, online condition monitoring and diagnostics requires the sensing and analysis of such signals that contain specific information which is characteristic of the degradation process, problem or fault to be detected. Various factors need to be considered when selecting the most appropriate monitoring technique for application in an industrial environment. The system should meet the following requirements as blow:

1. The sensor should be non-invasive;

2. The sensor and instrumentation system must be reliable;
3. The diagnosis must be reliable;
4. The severity of the fault should be quantified;
5. Ideally, an estimation of the remaining lifetime should be given;
6. Ideally, a prediction of the fundamental cause of failures should be provided via online information from the sensors.
7. Resolution and sensitivity should be as high as possible to provide more accurate results.

Table 2-1 Comparisons of different methods of condition monitoring

Parameters	**Potential information richness**	**Measurement device**	**Possible of analysis methods**
Current [7-9]	Average	Hall effect transducers	RMS trending, phase relationship, spectrum analysis
Voltage [51,52]	Average	Diagnostic Voltage Meter	RMS trending, phase relationship, spectrum analysis
Flux [64,65,82]	Very high	Search coil	RMS trending, time analysis, spectrum analysis, statistical methods
Vibration [42,43,47]	High	Accelerometer	spectrum analysis,
Acoustics [88,90,91]	High	Microphone	RMS trending, time analysis, spectrum analysis,
Temperature [17,36,57]	Average	Thermocouple	Trending, Visual interpretation
Torque [2,76]	High	Torque meter, encoders	RMS trending, time analysis,

Table 2-I shows the basis of the several technologies for condition monitoring referencing different parameters. Motor current signature analysis (MCSA) is the most commonly used at the moment [7-9]. Researchers have developed many ways to conduct the possible methods in the analysis, including RMS trending, phase relationships, spectrum analysis and statistical methods. But MCSA cannot provide sufficient ability to discriminate

between different faults. Moreover, the current spectrum is also influenced by the power supply, dynamic load and the machine geometry. Additionally, each MCSA diagnostic system will only matches a certain type of motor which is universalizability and complex to integrate on the control board.

However, the table 2-I shows that magnet flux detection can collect the richest information which provide more useful information and more accurate results. It has the capability of detecting different kinds of faults such as windings short-circuits, bearing fault and eccentricities at the same time. The signature of the magnet flux during fault occurrence in the motor is not influenced by machine geometry; meanwhile, data coming from the dynamic load will provide very useful and transient information. According to previous research [29, 67], the characteristics of a failure situation do not change when the method is applied to machines with different size, which means it can be used with any size of machine or generator. The search coil was developed several decades ago, and in recent years many magnet sensors have been invented which are highly sensitive and accurate. In this case, it is necessary to develop the new magnet flux condition monitoring system using new sensors.

2.4 Magnetic field imaging and stray flux detections

Various non-invasive magnet detection devices have been applied in research. The search coil shown in Fig 2.6 can detect motor faults. The advantage is that different types of failure can be detected, such as turn-to-turn faults, bearing faults and broken rotor bars, and it has been found to be more effective than MCSA. One drawbacks is that the diameter of the air coil has to be much lower than the total height of the machine body, in order to measure the flux in an area covering the width of several stator slots [68]. This means that different sizes of motor require different sizes of coil.

Figure 2.6 Search coil (Emerson M-343F-1204) [7]

Figs 2.6 and 2.7 show the different ways in which measuring the radial magnetic field can be measured with a sensor positioned in the vicinity of an induction machine. There is also a compression between line current detection and radial magnetic field detection [39, 69]. The Radial magnetic field detection is much more sensitive than MCSA. The value of the indicator frequency $(1+k_r N^r(1+S))$*f is 750, 850 and 1550 HZ with side band, when k_r= 1,-1,2.

Figure 2.7 Search coil

Figure 2.8 C shape magnet flux coil

The flux probe proposed here is similar to the sensor used elsewhere, consisting of a ferrite core on which 300 turns of enameled copper of 0.1 mm^2 thickness have been wound (Fig. 2.8) [8]. The signal collected is an EMF, which is a the derivative of the flux. For this research, measurements have been carried out with the sensors located in three different positions in order to collect the fluxes on the axial body, radial body and end-winding of the motor in Fig. 2.9. The dimensions of this sensor allow its use it for different sizes of motor, placed in any type of industrial environment, and power can be supplied by the mains or by an inverter [33, 67].

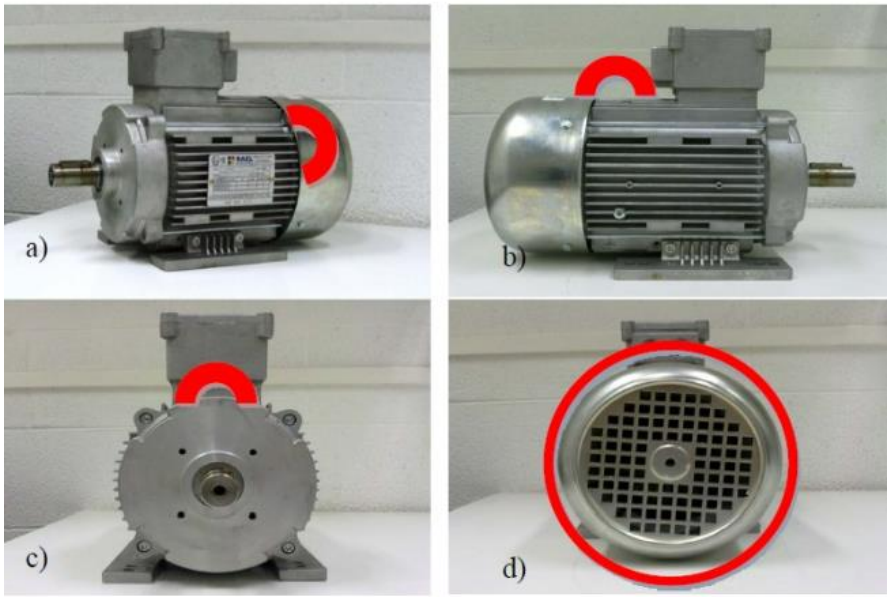

Figure 2.9 Positions of the sensor placed

Furthermore, compared with the MCSA, electrical machine are not in practice equipped with a convenient system able to measure and analyse current online [62]. The disadvantage of using external magnetic field analysis is that some sensitive indicators also exist in healthy machines, especially when with the load during operation. Additionally, the machine user may not have a record of the flux signature in the healthy mode. However, one advantage of this

method is that there is no requirement for the healthy former state of the machines to be presumed. The sensor used in this method has a circular area of 8.04 cm^2, with 200 turns of the coil. The drawbacks of a coil sensor are that do not give localized information, and in order to have more localized information, the sensor has to be small compared to the machine size.

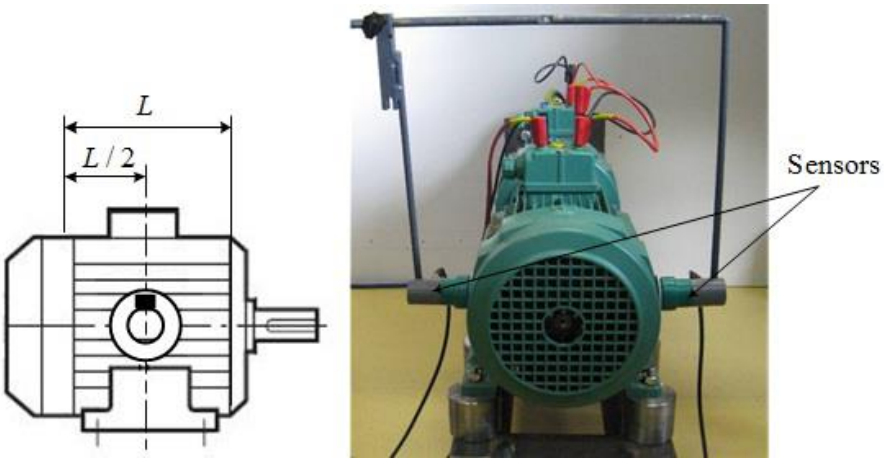

Figure 2.10 Proposed sensor and detect position [12]

Different magnetic sensors such as search coils, and giant magnetoresistance (GMR) sensors have been widely applied for magnetic flux measurement. Recently, search coils have been installed at one end of the motor shaft, allowing detection of the axial magnetic flux linkage of the machine. By analysing the different spectra in the frequency domain from magnetic flux measurements, various kinds of defects can be detected. For example, Kokko [69] applied a search coil with frequency analysis for the identification of different types of failure, such as shorted turns and broken bars and end rings. Furthermore, flux leaking outside the machine in the axial direction was detected and the threshold values of these axial flux harmonics were set as the indicator to distinguish between faulty and healthy machines. Negrea *et al.* [70] showed that measurements of the radial magnetic field with a coil sensor positioned in the vicinity of an induction machine can detect not only stator and rotor faults, but also load oscillations using the spectrum of static responses. Henao *et al.* [17, 21] also proved that leakage flux analysis is more effective in detecting stator faults when compared to the motor current signature analysis method. However, measurement sensitivity and bandwidth may not be suitable for monitoring systems with different failure types. As the sensitivity of the search coil is at a minimum for low frequencies, a sensitivity problem can arise for variable speed motor drive systems when running at low speeds. In recent years, researchers have developed new magnetic flux detection devices to increase measurement sensitivity, response frequency bandwidth and accurate of monitoring systems [67]. For instance, a ‘C’ shape magnetic core flux probe was developed by Frosini as part of an experimental sensing modality of monitoring system measurement of multiple parameters [29]. The probe has a soft magnetic iron core,

which leads to a dramatic improvement in its characteristics compared with previous search coils. However, this leads to a loss of linearity at high flux magnitudes and frequencies. One of the disadvantages of coil sensor-based measurement instruments is that they cannot measure static magnetic fields.

From the review of stray flux monitoring technologies above, there are several problems and challenges which still need to be solved. Firstly, the common stray flux data is collected by the impedance coil, which suffers from sensitivity problems at low speeds and non-linearity problems at high supply frequency. This issue leads to the stray flux monitoring system providing inaccuracy diagnostic result. Secondly, traditional stray flux technology only applies to single failures and is unable to detect several simultaneous faults as well as the load monitoring. Additionally, traditional stray flux monitoring approaches provide global information by using a winding coil, but location information is lacking.

For magnetic sensors such as GMR sensors, the sensitivity and frequency of their responses to magnetic fields are improved compared to coil impedance measurements. This provides a new opportunity for the non-invasive sensing and dynamic monitoring of a motor's condition. GMR sensors have been applied in the field of non-destructive testing and evaluation, such as in defect detections in ferromagnetic materials and electrical conductors. The key advantages of GMR sensors are their high sensitivity and spatial resolution. For example, GMR sensors have been applied to the non-destructive measurement of cracks within ferromagnetic materials in combination with an eddy-current method in [71, 72]. This technique also allows the detection and localization of sub-surface cracks and failures. The devices have a wide field of application in the inspection of plates, bearings and rails to detect fatigue cracks of different depths and orientations [71]. Nonetheless, no applications have yet been proposed for inspection of defects in the magnetic circuit of induction machines.

2.5 Chapter summary

This chapter has carried out a comprehensive literature review focusing on the condition monitoring of electrical machines. Condition monitoring technologies provide an extensive way to improve the reliability of electrical machines. Moreover, the potential for reductions in maintenance costs and downtime means that a condition monitoring system in an essential part of an industrial drive system. A survey of potential failure modes in electrical machines was carried out to identify the major failure types to be monitored. Based on previous research, bearing and winding failure are the most frequent failure modes found in various types of electrical machines. Additionally, dynamic loads are one of the major reasons which lead to

machine faults. Therefore, this research focuses on detecting and monitoring winding failures, load variations and mechanical bearing failures.

Many condition monitoring technologies are available for electrical machines, each approach has its own merits and drawbacks. Methods may be based on current, stray flux, surge testing and temperature monitoring. A literature review and comparison of common monitoring technologies was also carried out. Among these approaches, flux monitoring provides rich and precise information, as flux is the most important parameter of electrical machines. To collect flux information, several researchers have applied search coils and customized coils. However, these impedance coils have disadvantages which include invasiveness, non-linearity, and low sensitivity at high frequency. The problems and challenges identified in current stray flux monitoring research also includes a lack of location information and multiple fault detection. Therefore, this work focuses on developing a non-invasive stray flux condition monitoring system for winding and bearing failures and load monitoring.

Chapter 3 Methodology

As discussed in the literature review, stray flux monitoring technology can provide rich and precise information, and is more efficient than the traditional current signature monitoring approach. However, current stray flux monitoring still has several and challenges, including sensitivity at low speeds, non-linearity problems at high supply frequency, a lack of local information, an inability to detect multiple faults. To investigate and solve these problems, this chapter presents the methodology applied for the health monitoring of electrical machines based on stray flux detection. The theoretical background of stray flux monitoring is discussed in Section 3.1, including electromagnetic modelling and decoupling of the attenuation of flux inside an electrical machine. Section 3.2 then gives the theoretical background of feature extraction method applied in this thesis, which uses spectrograms and independent component analysis.

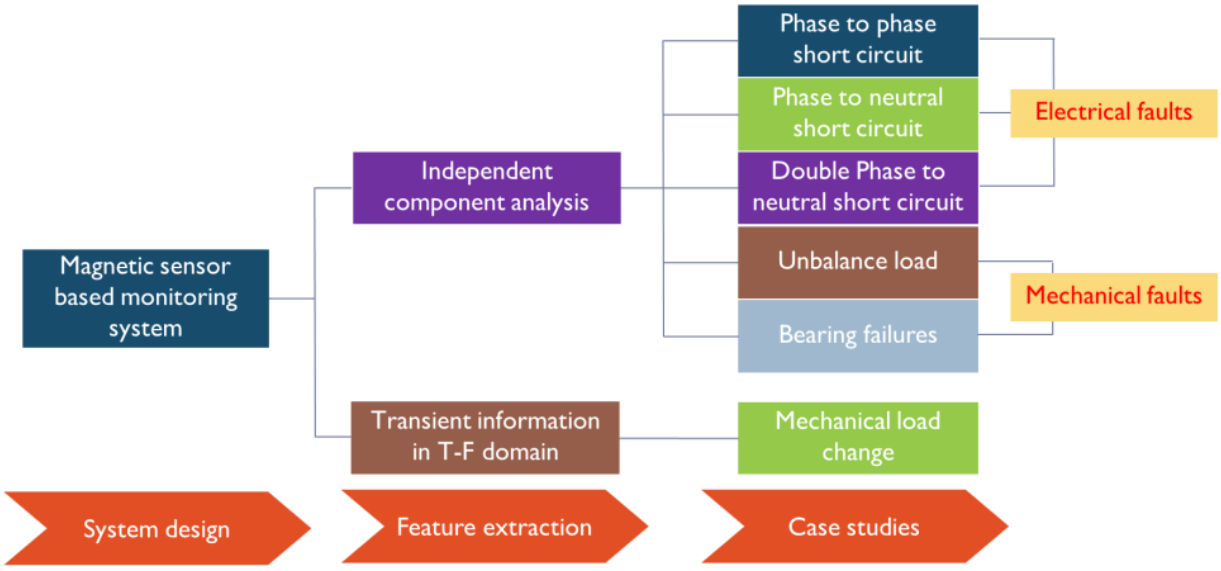

Figure 3.1 Research diagram of magnetic sensor based monitoring system

Fig 3.1 shows the research diagram for a magnetic sensor-based electrical machine condition monitoring system. This research work can be divided into several phases. The first is to design an appropriate magnetic sensor-based monitoring system. With the help of simulation models, the choice of sensor chosen, and the optimization of sensor detection location and direction can be determined as well as the data acquisition transmission systems.

Three case studies consider load monitoring, electrical winding failures, and mechanical bearing failure, and tests are carried out with the proposed sensing system to validates its capability. By applying feature extraction methods, stray flux information from different machine failures is represented through the proposed monitoring system, including spectrograms for time-frequency information and independent component analysis.

3.1 Theoretical background of stray flux in electrical machines

The stray flux of an induction machine is created by both stator and rotor currents. The reference frames can be transformed from the 3 phase (*a-b-c* axis) to the *d-q* axis using Clarke transformation, and then to the $\gamma - \delta$ axis by Park transformation. In this case, the air gap flux is used to link the stray flux with motor load. This air-gap flux can be expressed as follows [73]:

$$\Psi_{rg} = Mi_{\gamma s} + M_{\gamma r} \tag{3.1}$$

$$\Psi_{\delta g} = Mi_{\delta s} + M_{\delta r} \tag{3.2}$$

where the subscripts r and δ indicate the rotor and stator components respectively. Ψ_g is the air-gap flux; M is the mutual inductance; $i_{\gamma s}, i_{\delta s}$ are the stator currents in the $\gamma - \delta$ axis and $i_{\gamma r}, i_{\delta s}$ are the rotor currents in the $\gamma - \delta$ axis respectively.

From equations 3.1 and 3.2, both the stator current and rotor current affect the magnetic field in the air gap. The air gap flux is given by:

$$B_{ag} = \sum_{k,m} B \sin(K\omega t - m\phi - \varphi_{k,m}) \tag{3.3}$$

where B is the component magnitude, B_{ag} is the magnetic flux density in the air gap at a given point, m is the number of pole pairs, ω is the angular speed, k is the harmonic rank, ϕ is the angular position, and $\varphi_{k,m}$ is the initial phase. To show the stray flux model of an electrical machine, several assumptions and simplifications need to be made as below:

1. The slot effect of a machine is not considered in this model, which is replaced by a smooth air gap between stator and rotor as shown in Fig 3.2.
2. The geometry of the whole machine is complex. Thus, it is assumed that there is no air gap between the stator yoke and external frame.
3. To reduce the influence of end windings, the length of the electrical machine is made infinite.
4. The magnetic properties of the materials are constant.

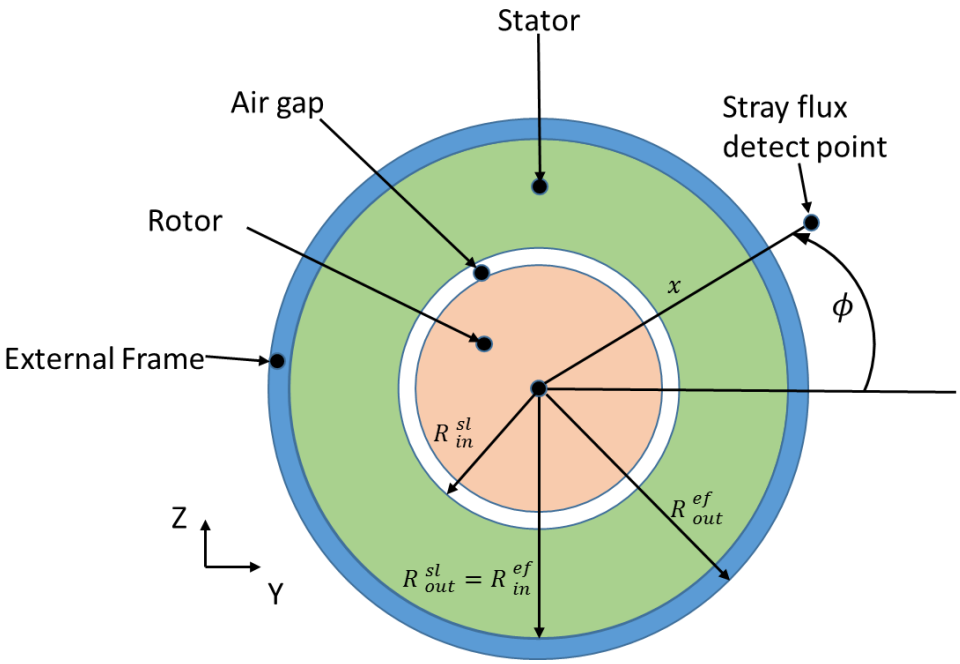

Figure 3.2 Schematic of stray flux in the machine

To build a stray flux model for a machine, the magnetic vector potential can be set as $\vec{A}$, the magnetic permeability μ, and electrical conductivity σ. Thus the relationship among them can be expressed as below:

$$\nabla \times \nabla \times \vec{A} = -\mu\,\sigma\frac{\partial \vec{A}}{\partial t} \tag{3.4}$$

If the eddy current in the laminations is not considered, the conductivity σ is zero, and then $\nabla \times \nabla \times \vec{A} = 0$.

To analyse the radial field of stray flux, the magnetic vector potential $\vec{A}$ is oriented through the Z direction of the machine, which is perpendicular to the machine frame. In this case, $A_{x,\phi}$ is directly related to the distance between the sensor location and machine centre x and the angular position ϕ. If only one magnetic field component is considered at the specific frequency K, then $A_{x,\phi}$ varies sinusoidally.

Thus, $\overline{A_{x,\phi}}$ can be shown as:

$$A_{x,\phi} = \Re\left[A_{x,\phi}e^{j\omega_K t}\right] \tag{3.5}$$

where $\Re$ is the real part of the $\overline{A_{x,\phi}}$ complex quantity, and j is the complex number, where $j^2 = -1$.

In this case, equation 4 can be transferred into a cylindrical referential:

$$\frac{\partial^2 \overline{A_{x,\phi}}}{\partial x^2} + \frac{1}{x}\frac{\partial \overline{A_{x,\phi}}}{\partial x} + \frac{1}{x^2}\frac{\partial^2 \overline{A_{x,\phi}}}{\partial \phi^2} = j\mu\sigma\omega_K \overline{A_{x,\phi}} \tag{3.6}$$

From equation 3.6, it is noticed that if the eddy current is considered in the analytical model, then the results will be related to the angular frequency ω_K. Otherwise, the value of $j\mu\sigma\omega_K \overline{A_{x,\phi}}$ in equation 6 is null.

3.1.1 Attenuation of stray flux in the machine

To investigate the relationship between stray flux and air gap flux, the coefficient of attenuation can be presented as the ratio of the magnitude of flux. In this case, it is likely that the reduction and shifting of stray flux due to the influences of stator lamination, external frame and external air can be decoupled into three different coefficients as shown below.

$$K = K^{sl} K^{ef} K^{air} \tag{3.7}$$

where $K^{sl}, K^{ef}\ and\ K^{air}$ are the coefficients of the stator lamination, external frame and external air stray flux respectively. Each different part of the electrical machine provides a different coefficient because of its different material and electromagnetic properties. These three coefficients are presented as the ratio of magnitude of flux density from the one at the inlet of the machine's part to the one at the outlet as shown in Fig. 3.3. By calculating the individual coefficient of each part, the link between stray flux outside the machine frame and air-gap flux can be illustrated.

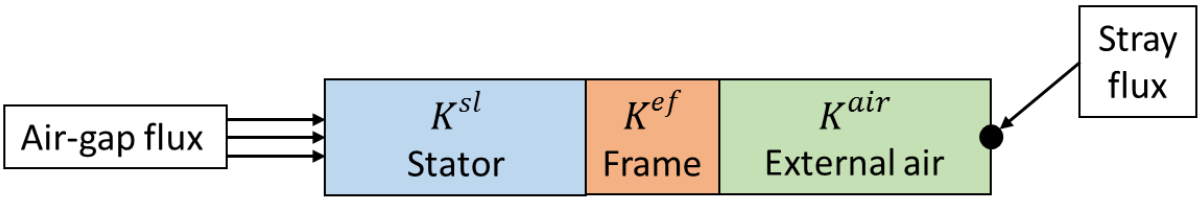

Figure 3.3 Decoupling of attenuation

In this case, by solving the equation 3.6, these three coefficients can be determined separately. The variable separation method is applied to determine the solutions, as below:

$$\overline{A_{x,\phi}} = \overline{A_x}\,\overline{A_\phi} \tag{3.8}$$

From equation 3.8, the subsequent equations are shown below:

$$\begin{cases} \overline{A_\phi}'' + i^2 \overline{A_\phi} = 0 \\ \overline{A_x}''(x) + \frac{1}{x}\overline{A_x}'(x) - \left(\frac{i^2}{x^2} + j\mu\sigma\omega_K\right)\overline{A_x}\ \ (x) = 0 \end{cases} \tag{3.9}$$

The first formula in equation 3.9 can be represented with real variables, where the solutions of the sine functions are: $A_\phi = \gamma_1 \cos i\,\phi + \gamma_2 \sin i\phi$. Additionally, due to the period of sine wave, $A_\phi(2\pi) = A_\phi(0)$, the term i is an integer in the variable separation method. Thus, the solution can be illustrated as follows:

$$\overline{A_{x,\phi}} = \sum_i \overline{A_\iota} \tag{3.10}$$

where $\overline{A_\iota} = \overline{A_{x,\iota}}\,\overline{A_{\phi,\iota}}$

The relationship between flux density and the vector potential can be shown as:

$$\vec{B} = \nabla \times \vec{A} \tag{3.11}$$

Because this project mainly focuses on the radial stray flux of electrical machines, the flux density $\vec{B}$ can be assumed to be the sum of the directional Z, Y components, which are b_Z and b_Y respectively. Both components can be written in a cylindrical referential:

$$\begin{cases} \overline{b_z} = \frac{1}{x}\frac{\partial \overline{A_\iota}}{\partial \phi} \\ \overline{b_Y} = -\frac{\partial \overline{A_\iota}}{\partial x} \end{cases} \tag{3.12}$$

Consequently, to solve the equations above, the boundary conditions need to set as the conservation of b_Z and b_Y. Additionally, the flux density at the inner surface of the stator laminations is the same as that in the air-gap. In this case, one certain air gap flux density component can be presented as below:

$$\overline{b_z} = Be^{-jm\phi} \tag{3.13}$$

This means that $b = \Re\left[\overline{b_z} e^{j\omega_K t}\right]$

So the attenuation coefficient K can be expressed as the ratio between two flux densities in the different positions:

$$K = \frac{\left|\overline{b_z}_{(x=R_{out})}\right|}{\left|\overline{b_z}_{(x=R_{in})}\right|} \tag{3.14}$$

3.1.2 Analytical model of stray flux

If the eddy current of the machine is not considered, and the $\sigma = 0$,thus equation 3.8 gives :

$$\begin{cases} \overline{A_\phi}'' + i^2\overline{A_\phi} = 0 \\ \overline{A_x}''(x) + \frac{1}{x}\overline{A_x}'(x) - \left(\frac{i^2}{x^2}\right)\overline{A_x}\ \ (x) = 0 \end{cases} \tag{3.15}$$

By referring to equation 3.9, the solution of the stray flux model without eddy current is then:

$$\overline{A_\iota} = \overline{A_{x,\iota}}\,\overline{A_{\phi,\iota}} = (\lambda_1 x^i + \lambda_2 x^{-i})(\beta_1 e^{ji\phi} + \beta_2 e^{-ji\phi}) \tag{3.16}$$

In this case, $\overline{b_Z}$ and $\overline{b_Y}$ are represented in the cylindrical reference:

$$\begin{cases} \overline{b_z} = \frac{1}{x}\frac{\partial \overline{A_\iota}}{\partial \phi} = ij(\lambda_1 x^{i-1} + \lambda_2 x^{-i-1})(\beta_1 e^{ji\phi} - \beta_2 e^{-ji\phi}) \\ \overline{b_Y} = -\frac{\partial \overline{A_\iota}}{\partial x} = -i(\lambda_1 x^{i-1} - \lambda_2 x^{-i-1})(\beta_1 e^{ji\phi} + \beta_2 e^{-ji\phi}) \end{cases} \tag{3.17}$$

As mentioned in the previous section, the flux density at the inner surface of stator laminations is equal to that in the air-gap in equation 3.13. In terms of equations 3.13 and 3.17, $i = m$, $\beta_1 = 0$ and $\beta_2 = j$. To derive the $\lambda_1 and\ \lambda_2$, the conservation of $\overline{b_Z}$ and $\overline{b_Y}$ needs to be considered.

3.1.2.1 Stray flux in air

If the distance between the stray flux detection point and the centre of the machine is infinite, the values of $\overline{b_Z}$ and $\overline{b_Y}$ should be null, which leads to $\lambda_1 = 0$, Additionally, the magnitudes of $\overline{b_Z}$ and $\overline{b_Y}$ are the same and shifted by $\frac{\pi}{2}$. To determine the coefficient of external air, the ratio can be shown as :

$$K^{air} = \left(\frac{x}{R_{out}^{ef}}\right)^{-m-1} \tag{3.18}$$

3.1.2.2 Stray flux in stator lamination

As several assumptions have been made at the beginning of this Chapter, and the coefficient K^{sl} is related to the material properties of the stator lamination. By setting μ^{sl} as the relative magnetic permeability of the stator lamination, the coefficient K^{sl} is:

$$K^{sl} = \frac{2}{(\mu^{sl}+1)\left(\frac{R_{in}^{sl}}{R_{out}^{sl}}\right)^{-m-1} - (\mu^{sl}-1)\left(\frac{R_{in}^{sl}}{R_{out}^{sl}}\right)^{m-1}} \tag{3.19}$$

So the coefficient of attenuation in stator lamination, K^{sl}, is related to the internal/external radius of the stator, pole pair number and magnetic permeability.

3.1.2.3 Stray flux in external frame

The coefficient of the external frame, K^{ef}, provides the attenuation ratio of magnetic flux density through the machine frame. To simplify the analytical model, eddy current is also neglected in this section. By setting μ^{ef} as the relative magnetic permeability of the external machine frame, the K^{ef} is shown as below:

$$K^{ef} = \frac{2}{(\mu^{ef}+1)(\frac{R_{in}^{ef}}{R_{out}^{ef}})^{-m-1} - (\mu^{ef}-1)(\frac{R_{in}^{ef}}{R_{out}^{ef}})^{m-1}} \tag{3.20}$$

By identifying these three coefficients, the attenuation of magnetic flux can be found. The relationship between air-gap magnetic flux and stray flux outside the machine frame can be derived by calculating the change in ratio due to the lamination, frame and external air. The simplified analytical model implies that the stray flux is likely to be the same as the air-gap magnetic flux. In this case, the stray flux can reflect any abnormality of the air gap flux, as the air-gap flux is the most important parameter showing the state of the electrical machine. The analytical model of attenuation coefficients thus gives the theoretical background to support the stray flux health monitoring of electrical machines. The magnitude of stray flux depends on the parameters of radius of the rotor and frame, the number of pole pair and the magnetic permeability of the lamination and external frame.

To validate the analytical model, this stray flux model is applied to one of the induction machines in the experiment research, which is a three-phase wound rotor induction machine with ratings of 59kW rated power and 1500rpm rated speed with no load. The parameters are the R_{in}^{sl} is 130mm, R_{out}^{sl} is 150mm, μ^{sl} is 1000, R_{in}^{ef} is 150mm, R_{out}^{ef} is 153mm, μ^{ef} is 1.5. If the amplitude of magnetic flux in the airgap is around 1.8T, considering the pervious analytical model and attenuation coefficients, the amplitude of magnetic flux on the machine's frame with 2mm lift-off is around 3.4mT. The numerical simulation result of the stray flux in this machine is shown in chapter 4. In this case, the analytical model can provide a general idea with the stray flux situation of the electrical machine.

3.2 Feature extraction and analysis of stray flux information

Further signal processing is required to extract the features and characteristics from stray flux data, in order to assess an electrical machine's health state. In this section, the spectrogram is presented which shows the time-frequency features of the machine.

The aim of time-frequency analysis is to transfer a signal into the frequency domain as a function of time. The Short Time Fourier Transform (STFT) is the Fast Fourier Transform with a fixed moving window which is shorter than the total length of the signal. The short window leads to a good localization of the frequency components in time.

The spectrogram is a square modulus of the fixed windowed Fourier transform of a signal:

$$S_x(t,v) = \left|\int_{-\infty}^{+\infty} x(s) * h(s-t) * e^{-i*2\pi vs} ds\right| \tag{3.21}$$

where $x(s)$ is the temporal signal, $h(s-t)$ is the window conjugate form and v is the frequency. By applying the short-time Fourier transform (STFT) to the test data, transient information from the stray flux data is expressed out in the time-frequency domain

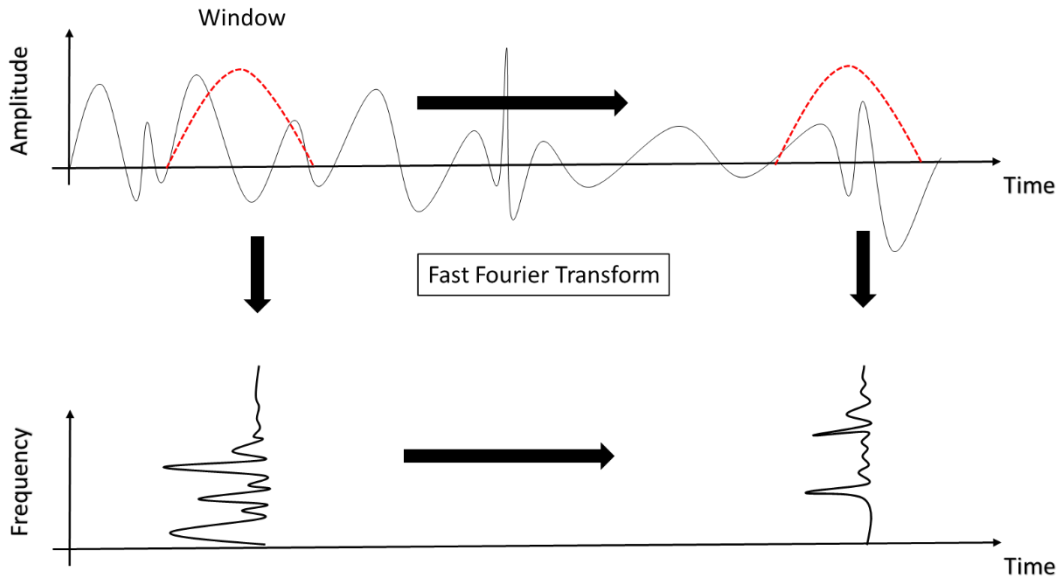

Figure 3.4 STFT of a signal with a fixed window

As shown in Fig 3.4, the STFT provides a pattern of time and frequency, which localizes the spectrum in the time domain. In this case, the different harmonics of electrical machines can be illustrated with time variation. Especially during transient states such as start up and with speed variations, the spectrogram presents an overall idea about the changing harmonics, which is useful in stray flux feature extraction.

3.3 Chapter summary

This chapter explains the overall research methodology in this PhD project, including a description of the research diagram, stray flux monitoring technology and the feature extraction

method. Based on the challenges summarized in chapter 2, the proposed magnetic sensor monitoring system is to be designed with the help of simulation results. The proposed stray flux system is implemented in different experimental studies to monitor the load state, and winding failures and bearing failures in the following chapters.

The theoretical background of stray flux in electrical machines is shown in Section 3.1. By making several assumptions, a simple analytical model is built to represent the relationship between air-gap flux density and stray flux, which is influenced by the geometry of the machine and the electromagnetic properties of the stator lamination and external frame only. As the air-gap flux is an important parameter for the monitoring of an electrical machine and the analytical model, the proposed stray flux monitoring system is also able to show the abnormality of the electrical machine. Additionally, the feature extraction method in this research is explained in Section 3.2, which was the Short Time Fourier Transform. The STFT can provide a spectrogram of the harmonics in electrical machines depending on the time variation. In a transient state, the spectrogram shows the pattern of distribution of and changes in harmonics. The measurement data and signal processing results with different failures in machines are considered in the following chapters.

Chapter 4 Monitoring System Design

In the previous chapter, the theoretical background of stray flux monitoring technology is introduced. In this chapter 4, the design of the stray flux condition monitoring system is presented. More specifically, this chapter explains the choice magnetic sensor, sensor location for the measurement of stray flux, the magnetic sensor array, wireless sensor network and data acquisition system design. Due to the condition monitoring design, the proposed monitoring system shows the capability to collect weak magnetic flux information with very high sampling frequency.

4.1 Choice of sensor

Stray flux condition monitoring technology depends strongly on a sensitive magnetic sensor to collect weak magnetic flux signals. Thus, to choose suitable magnetic sensor in the proposed monitoring system is of considerable importance. There are several commercial candidates for the magnetic sensor in the system design these include the giant magnetoresistive (GMR), anisotropic magnetoresistive (AMR) and Hall sensors. However, AMR sensors have a very low magnetic measurement range and are thus not suitable for this research.

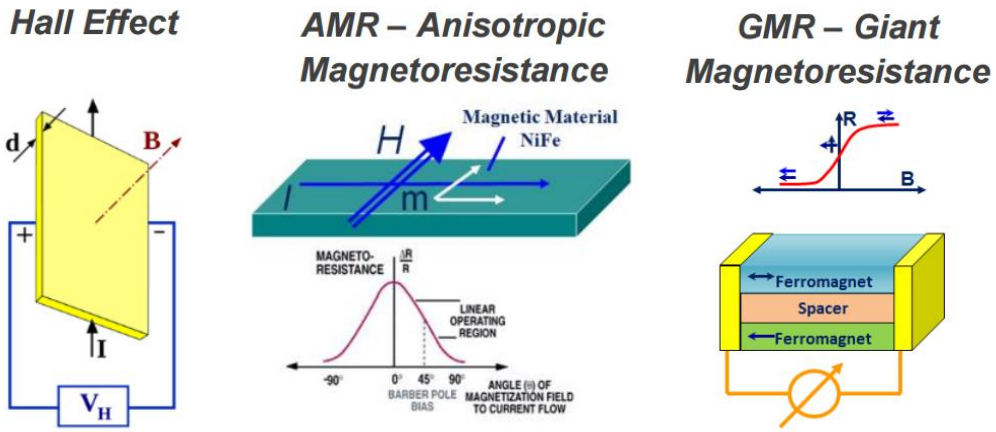

Figure 4.1 Schematics of three different magnetic sensors

There are several ferromagnetic metallic films separated by thin nonmagnetic layers in a GMR sensor, as shown in Fig 4.1. When a GMR sensor is affected by a magnetic field, the resistant of the sensor will change dramatically. NVE AA002 GMR sensors are used in this research work, and they can provide an output signal of a maximum of 200mV with a 5V power supply. One of this advantages is that the GMR sensor has a large detection range of magnetic strength with different levels of output voltage. Additionally, the sensitivity of the device is improved due to the embedded magnetic flux concentrators.

The Hall device is an alternative choice for magnetic flux signal detection. Once an electron is influenced by a magnetic field, it will be affected by the Lorentz force which leads to a perpendicular move in the direction of both the magnetic field and of the movement of the electron. In this case, if there is a current flowing through a magnetic field, a difference in the electrons will appear between two sides, which is the output of the Hall devices. In practice, the output of a Hall device is quite small, and therefore a built-in amplifier is need to magnify the signal and reduce noise. In these circumstances, the outputs of most Hall devices are absolute values.

Table 4-1 General comparisons of three different sensors

Sensor	Hall effect	AMR	GMR
Power Consumption(mA)	5-20	1-10	1-10
Die Size (mm^2)	1*1	1*1	1*2
Field Sensitivity (mV/V/Oe)	~0.05	~1	~3
Dynamic Range (Oe)	1000	10	100
Resolution(mOe)	~500	~0.1	~2
Temperature Performance (^oC)	<150	<150	<150

Table 4-I shows a general comparisons of three different sensors in the commercial market. Although the Hall sensor has a larger magnetic dynamic range than GMR sensors, the latter are more sensitive than the AMR and Hall sensors, and have higher resolution. Additionally, the bandwidth of GMR sensors is much higher than that of Hall sensors. In this case, NVE AA002 GMR sensors are used in this research project.

4.2 Sensor location for measuring stray flux

Stray flux is a magnetic flux that radiates from inside the machine frame and is inherently and strictly connected to the magnetic state of the machine. Stray flux is induced by stator and rotor current; both of which produce magnetic flux with different spectral components. Depending on the physical location around the motor body where the

measurement is performed, the magnetic field can contain information about the state of both the stator and rotor states, which are reflected in different spectra.

Traditionally, the stray flux method uses detection-coil transducers mounted on the device to be tested. However, recent work has focused on the detection of radial magnetic fields, and these magnetic fields can be studied by means of sensing in the axial and radial directions.

To design and select appropriate sensor specifications and locations for installation, simulation on the targeted motors has been carried out in order to understand the strength and distribution of stray magnetic flux. In this case, monitoring the health of a motor can be achieved. The simulation model of the induction machine used for bearing fatigue tests in chapter 5 (Fig 4.2(d)) has been built to find the magnetic sensor specifications and installation location. An FEA simulation model is shown in Fig 4.2(a). Fig 4.2(b) shows the 3D distribution of the magnetic flux under a typical operating current of 15 A, and Fig 4.2(d) indicates the distributions of magnetic flux outside the cage. From the simulation results, the location of the strongest leakage field and magnetic field change is in the middle of the cage, as highlighted in Fig 4.2(b). In addition to the location, Fig 4.2(d) illustrates three different directions and their variations at the detection point, where the z-direction provides the strongest magnetic flux in the simulation (5mT). Compared to the analytical result in Chapter 3, there is a slight difference between the numerical result (5mT) and analytical one (3.4mT), which may due to the eddy current effect and material property. From the numerical results, the sensor location identified is in the middle of the cage, in the z-direction, in order to monitor the magnetic flux field of the induction machine.

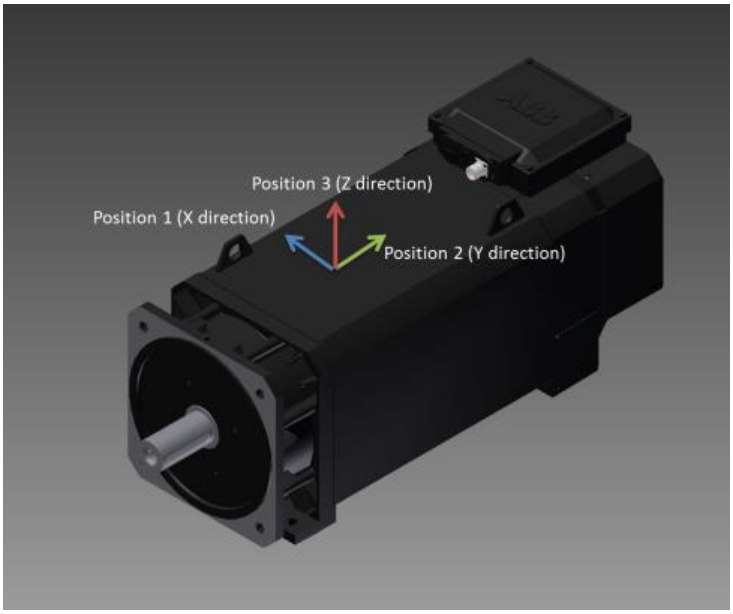

(a) FEA model of tested induction machine

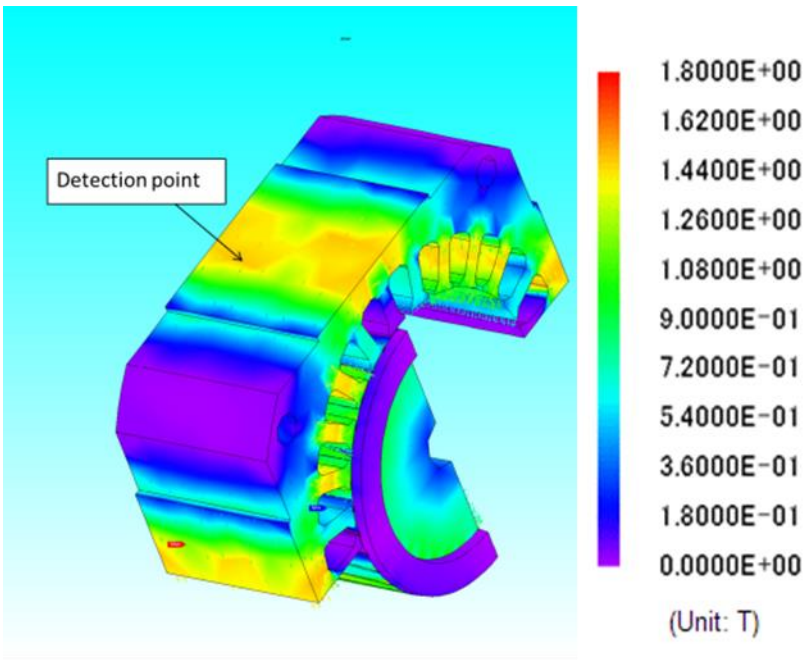

(b) Magnetic field distribution of the machine

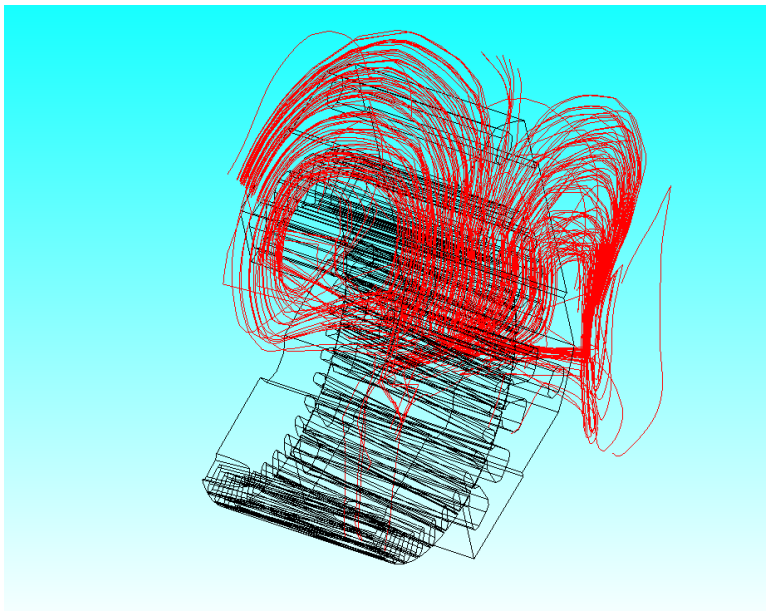

c) Magnetic field flux distribution outside the cage

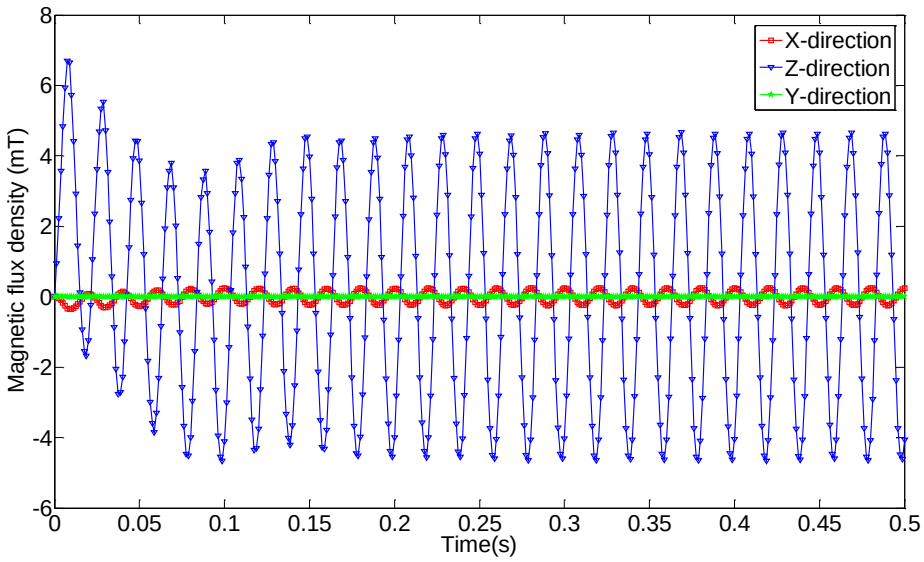

(d) Magnetic flux density in three directions

Figure 4.2 Simulation results of the target induction machine

4.3 Wireless sensor network

Traditional wire-based monitoring systems require long periods of deployment and entail significant costs for cable installation. With the recent maturity of wireless communication techniques, one of the recent challenges for the structural engineering community is the emerging wireless condition monitoring system, which provides a promising solution for rapid, accurate and low-cost structural monitoring.

However, the existing wireless communication protocol, IEEE 802.15.4, and wireless hardware motes (e.g. Mica2, MicaZ and TelosB) in wireless sensor networks are designed for low data rates and low computation applications, which make it is impossible for all of the data to be transmitted to a central server that carries out centralized data processing and feature extraction. To achieve a practical wireless sensor and actuator network for condition monitoring, the wireless senor nodes must be armed with some kind of distributed data processing and compressive sensing capabilities, so that the amount of data to be transmitted over the wireless link can be reduced.

The designed wireless node features with a TMS320F28335 digital signal processor (DSP) and an improved IEEE 802.15.4 wireless data transducer with data rates up to 2Mbps.

4.3.1 Hardware architecture

In the base board, one distinct feature of the TMS320F28335 microcontroller is the capability for high-speed data acquisition. The direct memory access (DMA) module on the

TMS320F28335 allows the wireless PZT node to collect sensor data at a sampling rate up to 10MHZ with 12-bit ADC of 6.25Msps. The core of the base board is the distributed data processing unit. The radio board contains an ATSAMR21G18 microcontroller, DSP module interface, time synchronization and an RF module.

4.3.1.1 Base board

A typical smart wireless sensor node has limited memory, computational ability and battery power. These conditions should be taken into account when the compressive sensing algorithm is embedded into a wireless sensor board. The base board should be chosen according to following conditions. Firstly, it should have an SPI or I2C interface to communicate with the RF board; secondly, it should support high data transmission rates for large amounts of lamb waves or other complex signals; thirdly it should support high enough crystal frequency; and finally it should support sufficient memory storage for the data cache. For low-cost low-power measurement devices, the programmable DSP could be an efficient digital, programmable and real-time platform.

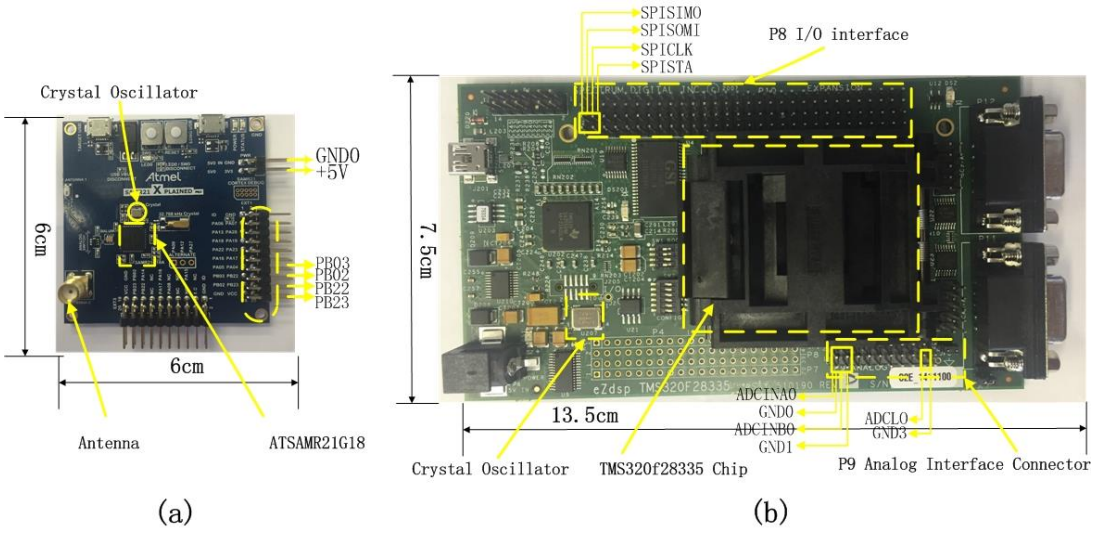

Figure 4.3Circuit prototype of: (a) radio board; (b) base board

The radio board is a four-layer PCB with roughly the size of a Texas Instruments TMS320F28335 microcontroller (real-time digital signal processor with controller features of (the Delfino-family) in the base board, running at up to a clock frequency of 150MHZ, adopted in the wireless sensing node to execute high sampling rates of data acquisition and onboard data processing. Additional important features of this DSP are the on-board DMA-controller, 16-bit enhanced pulse-width modulators PWM (HR-EPWM), 12-bit multi-channel sampling/hold circuit, internal flash memory of the program, and floating point hardware arithmetic. The PWM works at a clock frequency of 100MHZ and can be used for precise digital-to-analog

conversion (DAC) or to trigger analog-to-digital conversion (ADC). The DSP chip also includes a multiplexed ADC of 12-bits resolution with a conversion rate of up to 10MHZ or more and it has 2 simultaneous sample-and-holds. So, this chip has high performance digital-to-analog and analog-to-digital conversion without extra components. In this board, the P8 I/O interface and P9 analog interface connector are used to communicate with the RF board and to acquire sensor data respectively. The ADCL0 pin should be connected to the GND pin to make sure that the ADC module in the DSP adopts the internal reference voltage.

4.3.1.2 Radio board

The radio board detailed in Figure 4.3 is employed in this research. The Atmel SMART SAM R21 board with a low-power microcontroller ATSAMR21G18 is chosen. It adopts a 32-bit ARM Cortex-M0+ Processor and an integrated ultra-low power RF233 as 2.4GHz ISM band transceiver with a maximum data rate of 2Mbps. These devices are available in 48-pin packages with up to 256KB Flash and 32KB of SRAM and operate at a maximum frequency of 48MHz.

Sensor data is sent from the DSP board using the SPI bus (PB03, PB22, PB02 and PB23 from Table 1) to the respective in radio board. The radio board is a two-layer PCB and its size is roughly, as shown in Figure 4.3(a). The two vertical header pins are shown on the right side and bottom side. The 4-pin horizontal headers interface with the base board and map to specific pins on the vertical headers (SPICLK, SPISIMO, SPISOMI, SPISTA in Table 4-1 to enable external data access from the base board. In transmitting state, the radio board consumes 35.5 mW of power (26 mA of power at 1.8 V) but less than 2 μW of power (1.1μW of power at 1.8 V) in power down mode.

Table 4-2 Signals transmitted through bus connections

Symbol	Signal	Symbol	Signal
PB03	SPI clock	ADCINA0	ADCA0 input
PB02	SPI output	GND1	GND for ADCA0
PB22	SPI input	ADCINB0	ADCB0 input
PB23	SPI chip	GND2	GND for ADCB0
+5V	Input supply voltage	ADCL0	Internal/external select
GND0	Input GND	GND3	GND for ADCL0
SPICLK	SPI clock	SPISIMO	SPI input
SPISTA	SPI chip	SPISOMI	SPI output

4.3.1.3 The architecture of high sampling rate operation

The flowchart in Fig 4.4(a) demonstrates the typical data sampling cycle of the conventional design, such as prototypes of wireless nodes, Telosb motes, Imote2, and MICA motes. These conventional motes have an internal 12-bit ADC in the microcontroller. The microcontroller sends a clock signal and control signals to the ADC to trigger sampling cycle conversion. The internal buffer is set up to get data from the ADC. The reading takes 12 periodic operations and an ADC clock signal is generated in each period to fill the buffer bit by bit. After all of the data has been read out entirely, the microcontroller provides a clock signal and control signals to the on-board flash. Before writing the data into the flash bit by bit, the microcontroller takes some instructions to send the address to the flash. The flash saving operation also takes 12 periodic operations, each of which involves several instructions and a few clock cycles. Then, the sampling cycle ends and another sampling cycle may start. This architecture clearly reveals the inefficiency of the wireless sensor node designed with an ordinary microcontroller.

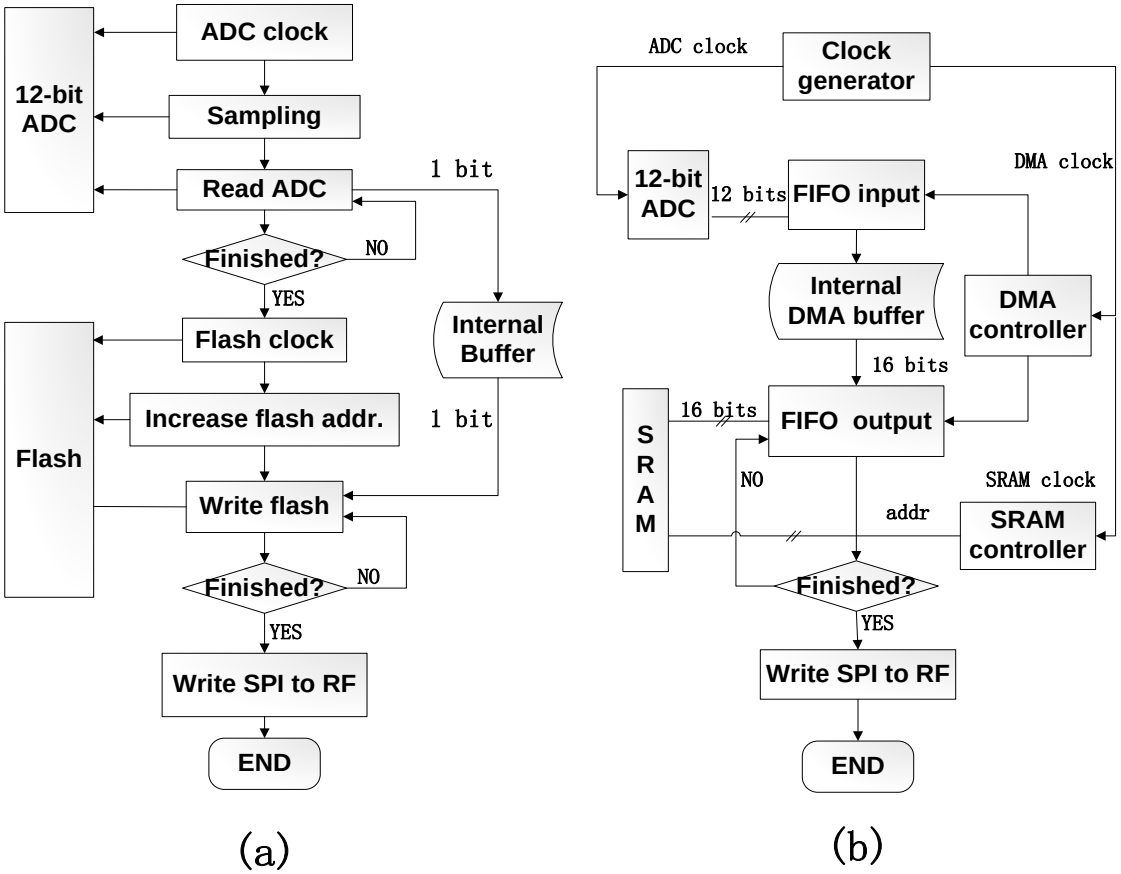

Figure 4.4 (a) Typical data sampling cycle of conventional wireless sensor node; (b) improved sampling operation implemented in the designed wireless sensor node

Figure 4.4 (b) presents an improved sampling design using the TMS320F28335 chip. The chip has some internal controllers, including a first-in-first-out (FIFO) DMA controller for

sampling data input and output, an SRAM controller, and a clock generator. The DMA algorithm has been widely used to allow hardware to access memory independently. To enable a wireless sensor node for high speed applications, various algorithms such as the semi-DMA approach are applied to extend the traditional architecture of the wireless sensor node. In our design with the DMA controller, the main TMS320F28335 microcontroller chip can be released from the task of data transfer. Sampling data transfer and data acquisition can be more efficient when the DMA is adopted. The 12-bit sampling data is acquired by the ADC and saved into the internal DMA buffer in FIFO input mode by the DMA controller. Meanwhile, the DMA controller and address controller controls the data to access the SRAM in FIFO output mode. The sampling data is moved from the internal DMA buffer to SRAM at 16-bit length, which is the I/O width of SRAM. Each clock cycle has 8 continuous sampling operations and one writing operation for writing data for SRAM. As a result, sampling data are encapsulated according to bit alignment in the internal DMA buffer and the DMA, ADC, and the SRAM can be fully utilized without compromise.

4.4 Chapter summary

This chapter provides a detailed description of the design of the proposed condition monitoring system. In comparison with other magnetic sensors, GMR sensors can provide a large detection range, high sensitivity and high bandwidth, and are used in this research work. By using an FEA model, the stray flux density distribution of the electrical machine is illustrated. Depending on the simulation results, the location in which to place the GMR sensor is determined, which is at the middle of the machine's external frame. Additionally, the z-direction of the stray flux provides the strongest signal among the three directions. Subsequently, the NI USB-6125 card is applied for the wire data acquisition system with a fully functional Labview program. Moreover, the wireless sensor network is also built to achieve wireless communication and high sampling rates of data acquisition. In this chapter, the entire stray flux-based condition monitoring system is designed, including the magnetic sensing system, data acquisition system and data transfer system. The monitoring system is ready for evaluation in different case studies involving load variation, winding failures and mechanical bearing failures.

Chapter 5 Load monitoring system

In the literature review, load variation was found to be the one of major reasons for failure in electrical machines. Thus, it is essential to monitor abnormal load and to estimate the machine characteristics. Existing load monitoring methods for electrical machines are generally effective, but suffer from sensitivity problems at low speeds and non-linearity problems at high supply frequencies. Unlike to the conventional methods of measuring stator and/or rotor voltage and current, the proposed stray flux system measures the magnetic field at specific locations and provides time-spectrum features, load response time and stator/rotor characteristics. In this chapter, the proposed GMR condition monitoring system is used to illustrate the load state of the machines. Three induction motors with different initial loading profiles are tested on two separate test benches and the results are analysed in the time-frequency domain. Their steady-state features and dynamic load response times through spectrograms under variable loads are extracted and correlated with load variations based on spectrogram information.

5.1 Vsd induction motor drive

This section describes the variable speed drive (VSD) induction motor and gives a mathematic model of the system. The VSD system consists of an outer speed controller loop, inter field-oriented controller (FOC), pulse-width-modulation (PWM) and voltage-source inverter (VSI), induction motor, the load system and the bearing to be monitored. The induction motor is coupled to a load through a shaft that is supported by the bearing. When the bearing suffers from degradation, it produces additional frictional force or unexpected torque to the shaft. As a result, the additional friction and unexpected torque will have impacts on the motor and VSD. The basic idea of the proposed non-destructive test approach is to monitor the status of the bearing by detecting the changes in VSD performance.

The concept of the FOC implies that the current components supplied to the induction motor are oriented in phases (flux component) and in quadrature (torque component) to the rotor flux vector. This is achieved by controlling not only the magnitude and frequency of the inverter output voltage, but also its phase angle and thus the instantaneous position of the rotor flux. Since the three-phase voltages, currents and fluxes of induction motors can be analysed in

terms of complex space vectors, in the VSD system control is based on projections that transform a three-phase time and speed-dependent system (i.e. the IM) into time invariant system with two coordinates which are the d and q frame. As a result, from the viewpoint of the speed controller, the actual control input of three phase stator currents are represented by a vector, and this enables the implementation of a PI controller in VSD.

The rotor's position θ_r is measured by an encoder and fed to a counter lock that calculates the position of the rotor flux (d-axis) represented by angle θ_e and the electrical rotor angular speed ω_r. Given the rotor speed reference ω_d (measured in electrical rotor angular speed), the speed difference $\omega_d - \omega_r$ between the desired speed ω_d and actual speed ω_r is fed to the speed controller $G_c(s)$. According to the dynamics of the motor and load, the controller $G_c(s)$ computes how much torque current i_{qs} is needed so that enough electrical torque will be generated to adjust the rotor's rotation towards the expected speed. The flux current i_{ds} is specified by the flux function. The outputs $[i_{ds}, i_{qs}]$ of the speed controller are sent to the FOC to drive the motor. With the aid of knowledge of the rotor flux position θ_e, the FOC applies the inverse Park and Clarke transformation to $[i_{ds}, i_{qs}]$ and decides the required three phase currents $[i_a^*, i_b^*, i_c^*]$. At this stage, the magnitude, frequency and phase of the three phase currents are adjusted and oriented to the field of flux. The outputs of the FOC are fed to the pulse width modulation (PWM) and voltage inverter block to generate the actual control voltages/currents. If additional friction or unexpected torque is caused by degradation in the bearing system, the dynamics of the control target (that is, the motor, bearing and load) will change, which results in the VSD's response with a speed adjustments. The performance of the VSD can be measured by the magnetic sensor through changes in the magnetic field.

5.1.1 Modelling of the VSD system

5.1.1.1 Dynamics of IM in dq-coordinate

The dynamics of voltages, currents and flux of a general induction motor can be described as follow [xx]:

$$V = RI + \frac{dI}{dt} \tag{5.1}$$

$$\Psi = LI \tag{5.2}$$

where $V = [v_a\ v_b\ v_c\ v_1\ v_2\ v_3]^T$ are the voltages applied to each stator and rotor phase; $I = [i_a\ i_b\ i_c\ i_1\ i_2\ i_3]^T$ are the phase currents and $\Psi = [\psi_a\ \psi_b\ \psi_c\ \psi_1\ \psi_2\ \psi_3]^T$ are the fluxes linked

to each rotor and stator phases. R and L are the resistance matrix and inductance matrix $|L = \left[\begin{array}{c|c} L_{ss} & L_{sr} \\ \hline L_{rs} & L_{rr} \end{array}\right]$ respectively.

For an ideal induction motor, the d-axis of the synchronously rotating frame is aligned with the rotor flux linkage, so that λ_{rq} and $d(\lambda_{rq})/dt$ are both equal to 0, where λ_{rq} is the q-axis rotor flux linkage. Applying the Clarke and Park transformations to the equations above, the induction motor in dq-coordinate can be expressed in a synchronously rotating reference frame as [62]

$$\frac{d\,x}{dt} = A\,x + B\,u \tag{5.3}$$

For an ideal field-oriented induction motor drive, given the stator current $[i_{ds}\ i_{qs}]$ in the dq-coordinate, the torque generated by the motor is:

$$T_e = \left(\frac{3}{4} p \frac{L_m^2}{L_{rr}} i_{ds}\right)\ i_{qs} = K_t i_{qs} \tag{5.4}$$

where p is the number of motor poles, $L_m$is the stator-rotor mutual inductance matrix, and L_{rr} is the rotor self-inductance matrix.

Given the load torque T_L, torque disturbance ΔT, equivalent friction factor B of the bearing, and the total mechanical inertia constant J of the motor and load, the dynamics of the rotation speed can be described by:

$$T_e = (T_L + \Delta T) + B\omega_r + J\frac{d\omega_r}{dt} \tag{5.5}$$

5.1.1.2 Transient time analysis of the VSD system

Thus the dynamic behaviour of the whole VSD with load and bearing friction can be reasonably represented by the control system block diagram as shown below in Figure 5.1. The FOC is indeed a feed-forwarded controller to actuate the motor at the torque current demanded by the speed controller. In the model of VSD dynamics, both the FOC and IM are regarded as an actuator to generate electromagnetic torque T_e according to the torque current i_{qs}.

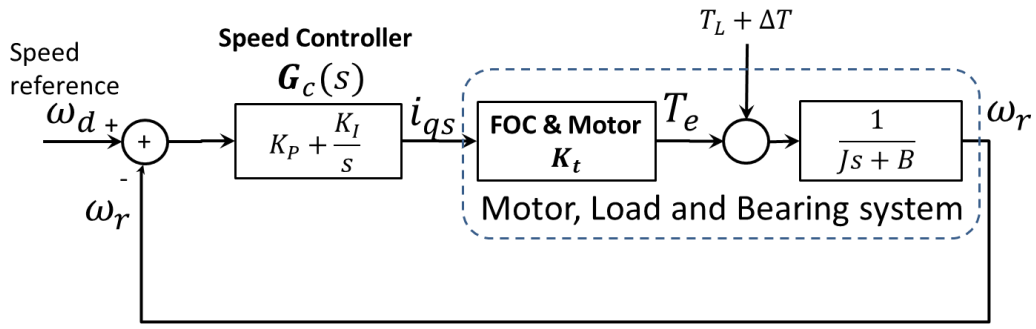

Figure 5.1 System model of VSD behaviour

The transfer function from the torque current i_{ds} to rotational speed ω_r is:

$$G_p(s) = \frac{K_t}{Js+B} \tag{5.6}$$

This can be rewritten as:

$$G_p(s) = \frac{K_t/J}{s+B/J} = \frac{b}{s+a} \tag{5.7}$$

where $a = B/J$ and $b = K_t/J$. It can be noted that the dynamics of the motor, load and bearing system are those of a first-order system.

The transfer function for a PI speed controller is:

$$G_c(s) = K_P + \frac{K_I}{s} \tag{5.8}$$

The closed loop transfer function from the speed reference $\Omega_d(s)$ to the actual speed $\Omega_r(s)$ is

$$G(s) = \frac{\Omega_r(s)}{\Omega_d(s)} = \frac{G_c(s)G_p(s)}{1+G_c(s)G_p(s)} \tag{5.9}$$

where the upper letters denote the Laplace transform of corresponding signals.

By algebraic manipulation, the closed loop transfer function can be rewritten as a second order dynamic system with one zero:

$$G(s) = \frac{\frac{K_tK_I}{J}\left(\frac{K_P}{K_I}s+1\right)}{s^2+\frac{K_tK_P+B}{J}s+\frac{K_tK_I}{J}} \tag{5.10}$$

Substituting $a = B/J$ and $b = K_t/J$ into this equation above gives:

$$G(s) = \frac{b(K_Ps+K_I)}{s^2+(a+bK_p)s+bK_I} \tag{5.11}$$

$$G(s) = \frac{bK_I}{s^2+(a+bK_p)s+bK_I} + \frac{(a+bK_P-a)s}{s^2+(a+bK_p)s+bK_I} \tag{5.12}$$

Let $K_P = \frac{2\zeta\omega_0-a}{b}$ and $K_I = \frac{\omega_0^2}{b}$, we have $a + bK_P = 2\zeta\omega_0$ and $bK_I = \omega_0^2$. It then follows that:

$$G(s) = \frac{\omega_0^2}{s^2+2\zeta\omega_0 s+\omega_0^2} + \frac{(2\zeta\omega_0-a)s}{s^2+2\zeta\omega_0 s+\omega_0^2} \tag{5.13}$$

When $a = B/J$ is tiny, it can be ignored in the nominator, so that:

$$G(s) = \frac{\omega_0^2}{s^2+2\zeta\omega_0 s+\omega_0^2} + \frac{2\zeta\omega_0 s}{s^2+2\zeta\omega_0 s+\omega_0^2} \tag{5.14}$$

$$G(s) = \frac{\omega_0^2}{s^2+2\zeta\omega_0 s+\omega_0^2} + \frac{2\zeta}{\omega_0} \cdot \frac{\omega_0^2 s}{s^2+2\zeta\omega_0 s+\omega_0^2} \tag{5.15}$$

Let $h_0(t)$ be the unit step response of the transfer function

$$G_0(s) = \frac{\omega_0^2}{s^2+2\zeta\omega_0 s+\omega_0^2} \tag{5.16}$$

where $h_0(t) = \left\{1 - e^{-\zeta\omega_0 t}\left(\cos(\omega_0\sqrt{1-\zeta^2}t) + \frac{\zeta}{\sqrt{1-\zeta^2}}\text{sen}(\omega_0\sqrt{1-\zeta^2}t)\right)\right.$

Usually, we have $\zeta = 1$ to achieve critical damping, and the unit step response is

$$h_0(t) = 1 - e^{-\omega_0 t}(1 + \omega_0 t) \tag{5.17}$$

It follows that the step response of $G(s)$ is

$$h(t) = h_0(t) + \frac{2\zeta}{\omega_0} \cdot \frac{dh_0(t)}{dt} \tag{5.18}$$

Since $\frac{d\,h_0(t)}{d\,t} = \omega_0^2 \cdot e^{-\omega_0 t} \cdot t$, the slope of the unit step response is

$$\frac{dh(t)}{dt} = \frac{d\,h_0(t)}{d\,t} + \frac{2\zeta}{\omega_0} \cdot \frac{d^2h_0(t)}{d^2t} \tag{5.19}$$

$$= \omega_0^2 \cdot e^{-\omega_0 t} \cdot t \; + 2\zeta\omega_0 \cdot e^{-\omega_0 t}(1 - \omega_0 t)$$

$$= \; e^{-\omega_0 t}\{2\omega_0 - \omega_0^2 t\} \qquad (for\ \zeta = 1)$$

Recalling the definition,

$$\begin{cases} \frac{K_t K_P + B}{J} = 2\zeta\omega_0 \\ \frac{K_t K_I}{J} = \omega_0^2 \end{cases} \tag{5.20}$$

a conclusion can thus be drawn from the dynamic analysis, that when the bearing suffers degradation and the friction coefficients increases, B increases and the damping factor ζ increases. The increasing value of ζ will slow the VSD's unit step response. In another words, when the degradation of the bearing is present, the VSD's transient time to changes in rotational speed will be longer. How fast the VSD's transient response is can be measured by the slope of the speed change. Since the magnetic sensor's measurement of the stator magnetic field provides information about the electrical rotation speed, analysis of the frequency changes in the magnetic data during the transient period will reveal the status of the bearing.

5.2 Induction machine test benches

Two experimental test benches for machines with different power ranges and with different types of loading strategies have been designed in order to validate the proposed machine load monitoring technique, as shown in Fig. 5.2. The first test induction motor is a three-phase four-pole wound rotor machine with the following parameters: rating 1.5kW, supply voltage 220V/380V, supply frequency 50Hz and rated speed 1500rpm with no load. The stator is star-connected and the rotor is short-circuited. The frame of the test induction machine is made of aluminum. The load has been emulated by a DC motor which is coupled to the induction machine shaft and controlled by a DC load drive. Furthermore, by using a torque meter, an encoder and a current probe, induction machine parameters such as speed, load and output power can be monitored, as shown in Fig. 5.2(c). The GMR sensor (NVE AA002) is placed in the middle of the machine yoke to detect stray magnetic flux. The output voltage from the GMR sensor is measured by an oscilloscope and recorded on a PC. The second induction machine is also a three-phase wound rotor induction machine with ratings of 59kW rated power and 1500rpm rated speed with no load. The machine has a steel frame. The test bench is used to investigate the fatigue progress in a bearing. By using a hydraulic system, variable loads can be applied to the test bearing and to accelerate the ageing of the bearing, as shown in Fig. 5.2(d). With the degradation of the wind turbine main shaft bearing, the load's changing in the whole system can be achieved.

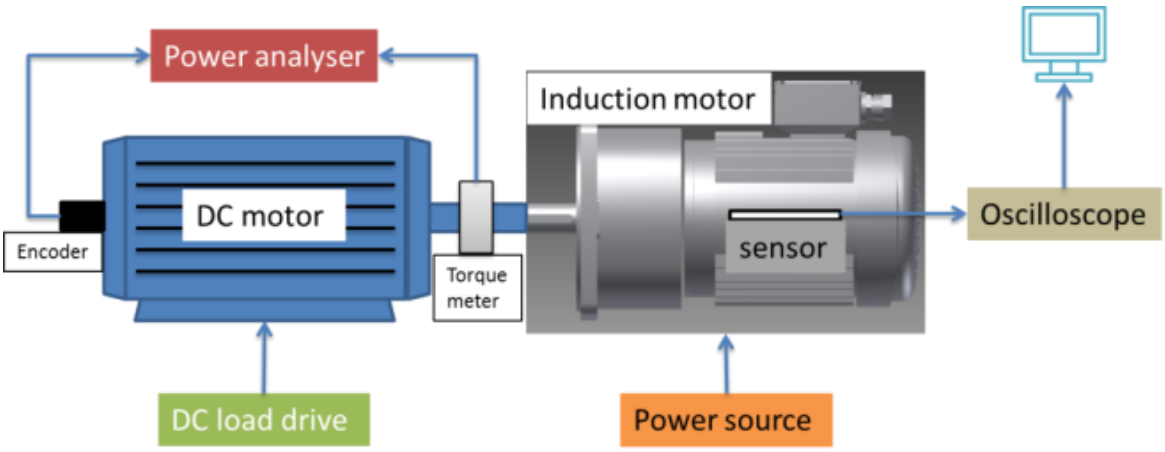

(a) 1.5 kW induction machine test bench

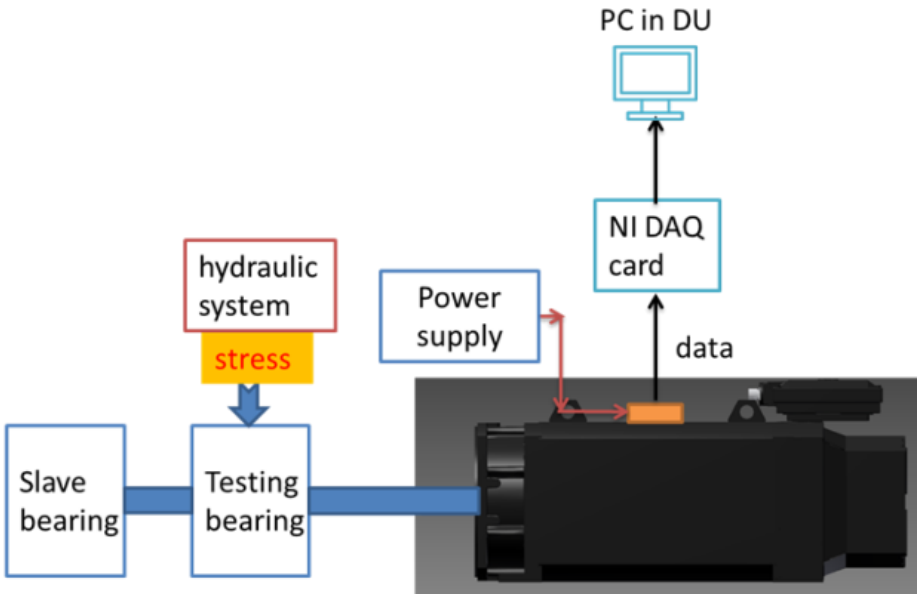

(b) 59 kW induction machine bearing test bench

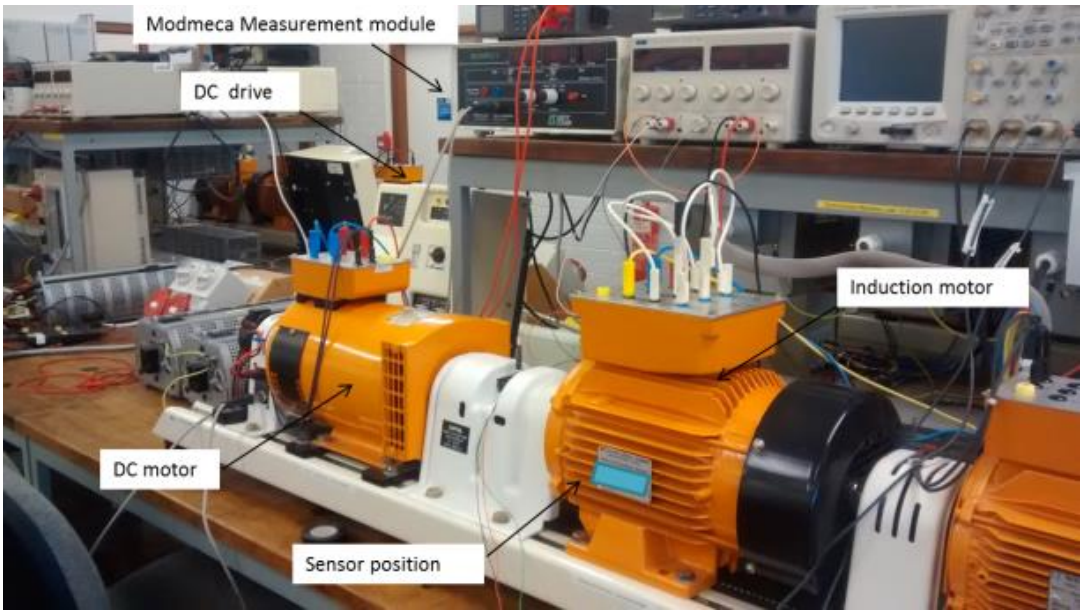

(c) Photograph of 1.5 kW induction machine test bench

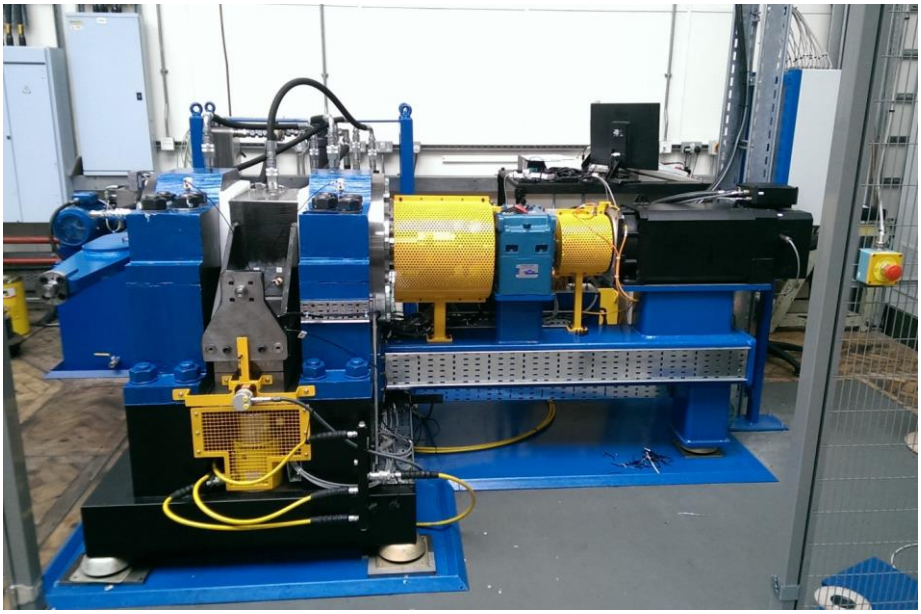

(d) Photograph of 59 kW induction machine bearing test bench

Figure 5.2 Induction machine load monitoring test benches

The experimental study includes tests of static and dynamic load. In the first test bench, the induction machine operates normally with or without loads. During the no-load test, the machine is operated at synchronous speed. After that, one DC motor generates a constant load to test the induction machine, while the GMR sensor has been implemented on the machine's yoke and detects any change in the stray flux. In the dynamic load test, the DC motor applies a constant load and the stray magnetic flux is measured from the machine start-up process up to steady-state operation.

The magnetic flux data are analysed using two different approaches. For the data collected from the static load test, they are analysed by comparing amplitudes. The magnetic sensor data during machine start-up are analysed in the time-frequency domain. By monitoring changes in the stray flux field, the change in dynamic load can be observed. To compare the stability of the transient response, two induction motor systems with different ranges of load have been tested.

Static and transient feature extraction methods are applied to the magnetic stray flux data. Values of amplitude and peak magnetic stray flux are found from in the static test results. The spectrograms illustrate the transient information of magnetic stray flux. The spectrogram provides patterns to estimate the harmonic contents of a time-varying signal, which helps in developing a visual correlation of load variations and detected signals.

5.3 Static test results and analysis

in the motor load test, the DC motor generates loads ranging from 0 to 5 N·m. The stray flux is measured in the *z*-direction of the magnetic field on the machine frame. The GMR sensor detects the radial magnetic flux of the external magnetic field of the test machine. The output voltage waveform of the GMR sensor is almost sinusoidal as shown in Fig. 5.3 *a*.

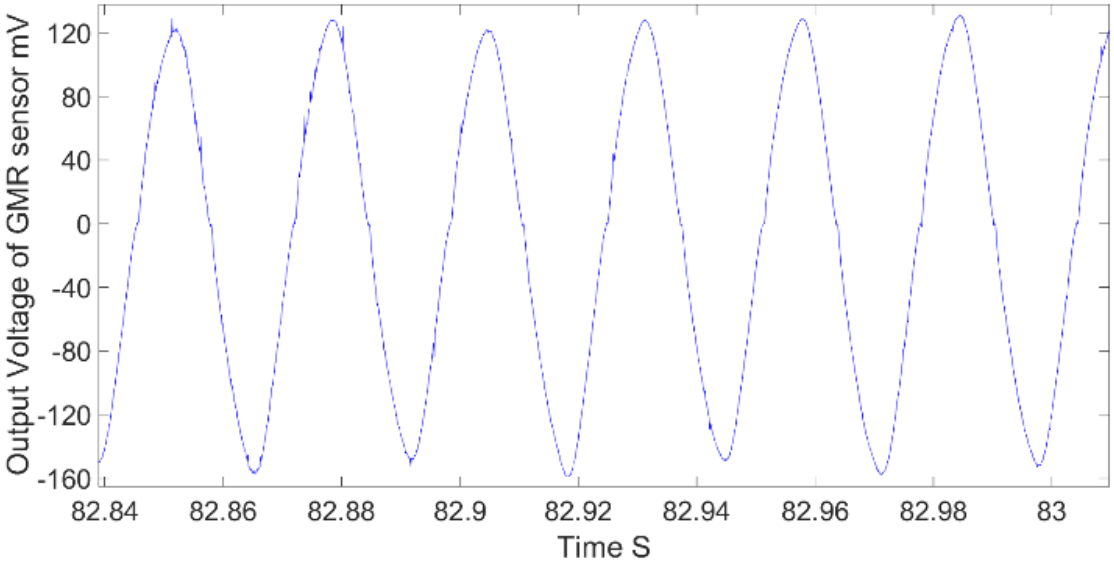

(a) GMR sensor voltage output waveform

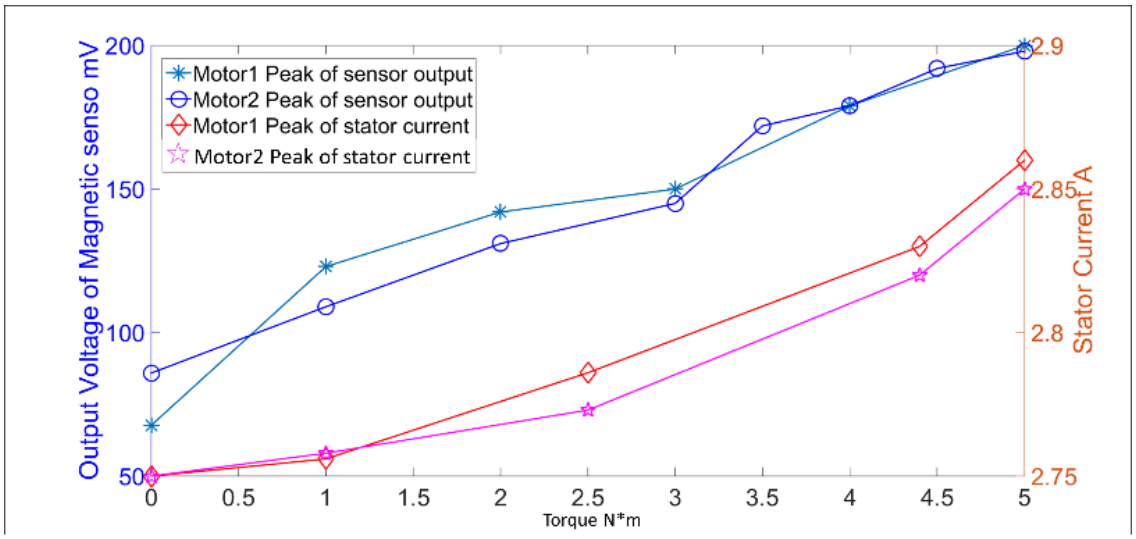

(b) Comparisons of stator current and peak values of the GMR sensor output under different loads

Figure 5.3 Stator current and peak values of the GMR output under different loads

Different steady-state features are captured, as presented in Fig. 5.3*b*. It can be seen that the stray flux increases with loading in steady-state operation, and its peak values increase from 68.1 to 198 mV and 87.1 to 200mV respectively. In Fig. 5.3*b*, the stator current is also shown.

From the previous analysis in 5.1, the stator current can increase the stray magnetic flux which is measured in the z-direction around the machine in this study. As a result, the load state of the induction machine can be monitored by the GMR sensor in the steady state.

5.4 Transient data and feature extraction for characterization

The transient state of machine loading can also be monitored through two different indicators. These are the first peak value of the GMR voltage output waveform, and the transient response time in the spectrogram results. Fig. 5.4 shows the measured output voltage waveforms from the GMR sensor during the two operating conditions of the machine. By controlling the DC motor as a variable load, the test machine starts with a fixed load while the load changes from 5, 4.5, 4, 3.5, 3, 2 to 1 N·m for the starting tests. The test results are presented in Fig. 5.4. It is observed that there is a peak value at around 80 mS in every waveform of the stray magnet flux and the peak value of this waveform increases with load. The air-gap magnetic flux reaches a maximum value at the beginning of the start-up period. It is evident that the stray flux can indicate load variations in the machine starting transients.

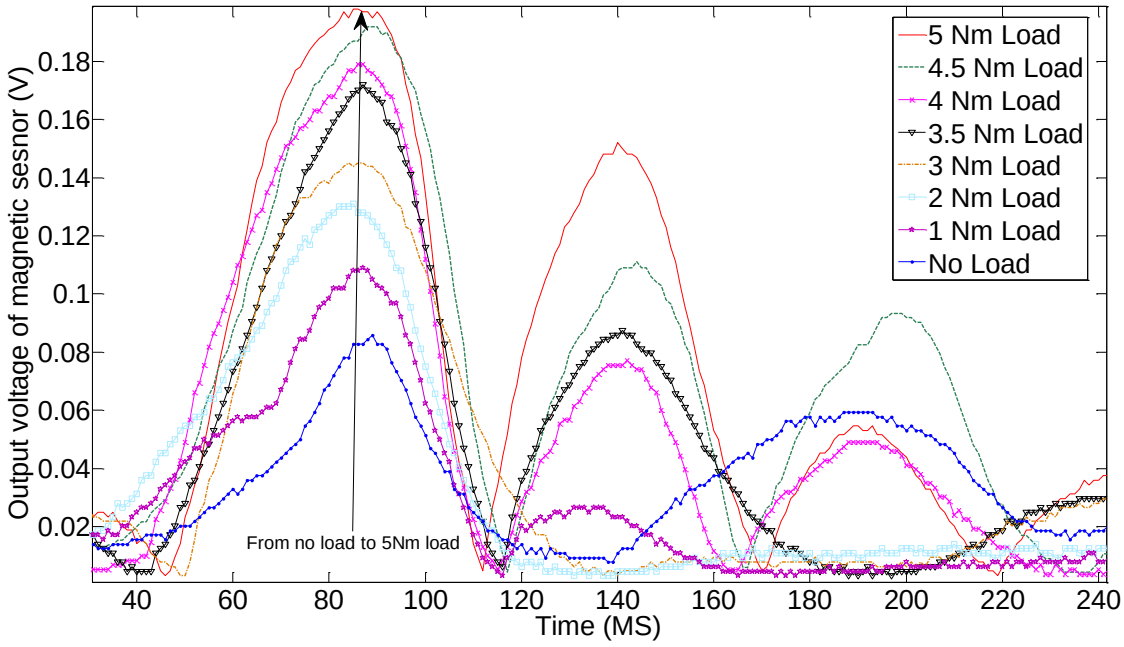

(a) Induced voltage of the GMR sensor during starting-up of motor 1

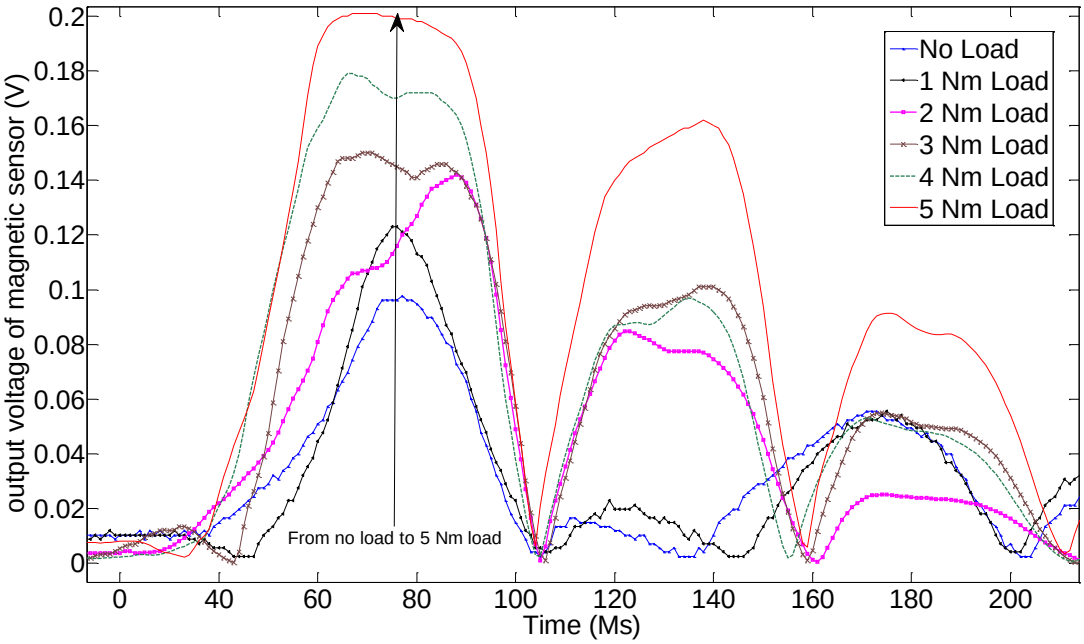

(b) Induced voltage of the GMR sensor during starting-up of motor 2

Figure 5.4 Results for motors 1 and 2

In order to investigate the repeatability of the proposed load monitoring method, two identical induction motors were tested in an experiment as illustrated in Figs. 5.4 a and b. It can be seen in Fig. 5.4a that their first peaks and transient response times have the same trends as the load varies.

The output results for start-up are illustrated in the time-frequency domain in Fig. 5.5. The transient response time is the time from the machine starting point to the steady-state. Whenever the test machine starts, there is a trigger signal sent from machine control board to the NI DAQ card. Additionally, from the spectrogram, the time of entry into the steady-state can be found. Thus, by calculating the difference between the two, the transient response time is obtained. The transient response time is the response time of a system from change to a steady state. In this particular case, the transient response time is the time of the tested machine from the start-up to the steady state. As discussed in Section 5.1, variations in load will lead changes in transient time during the start-up of the induction machines. In this case, as the load torque increases, the transient response time in induction motors rises to reach the same speed as in the previous load situation. Figs. 5.5 a and 5.5b show spectrograms of the magnetic sensor signals during motor start-up. In particular, at the beginning of the start-up transient time, the spectrum results demonstrate significant variations, as illustrated in Fig 5.5. Fig. 5.5 a and Fig. 5.5b show a slight difference in the spectrograms of the two motors during starting-up.

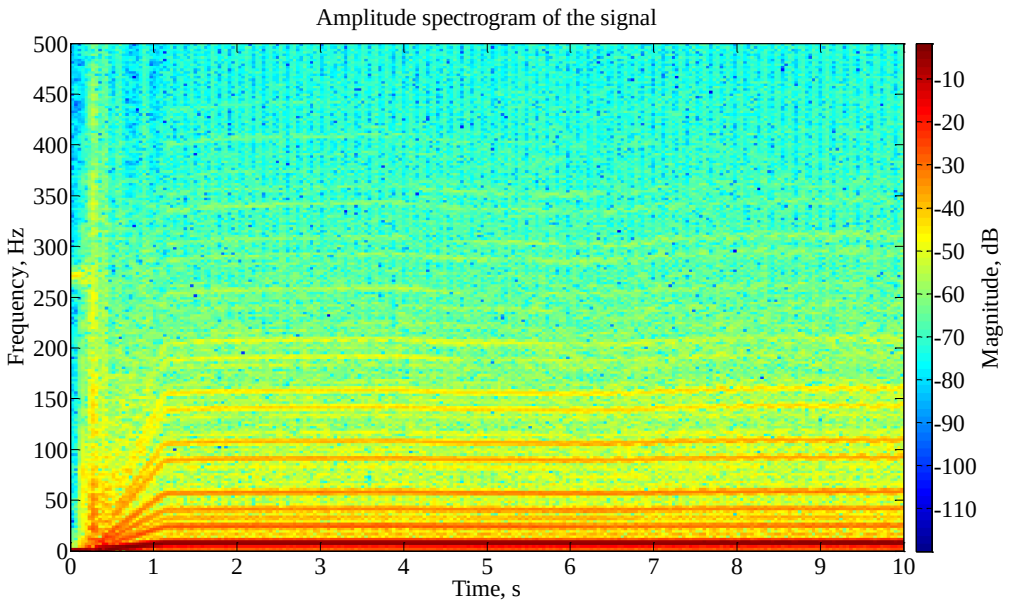

(a) Motor 1 spectrogram for start-up

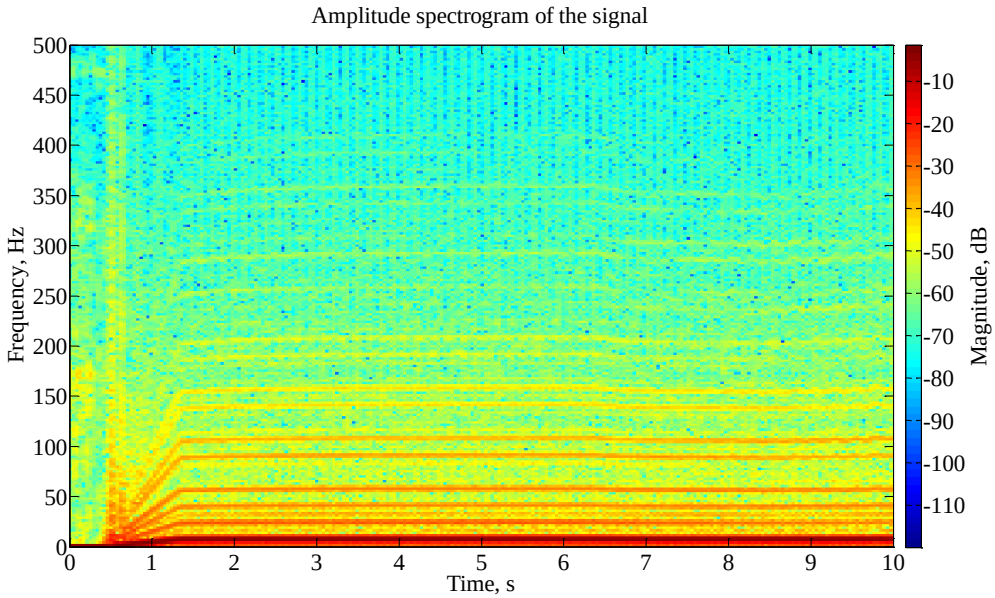

(b) Motor 2 spectrogram for start-up

Figure 5.5 Spectrograms of the magnetic sensor output in the time-frequency domain by STFT

Their individual machine characteristics can be compared in terms of transient responses; for example, in the time-spectrograph analysis as shown in Fig. 5.6. The comparison between the GMR sensor output in steady state and the transient response time in a transient state are illustrated in Fig. 5.6. The transient response time is more sensitive than the peak value in detecting the variation in load. From Fig.5.6, the slope of the transient response time is greater than the peak value during load variations, which leads to better performance of the monitoring

system. The peak value data are captured during the steady state, and the response time is collected in the transient state. The transient state can be considered as a collection of numerous steady states, and thus contains richer information than the steady-state data. Thus, the transient response time can provide better sensitivity performance than the peak values in monitoring load variation.

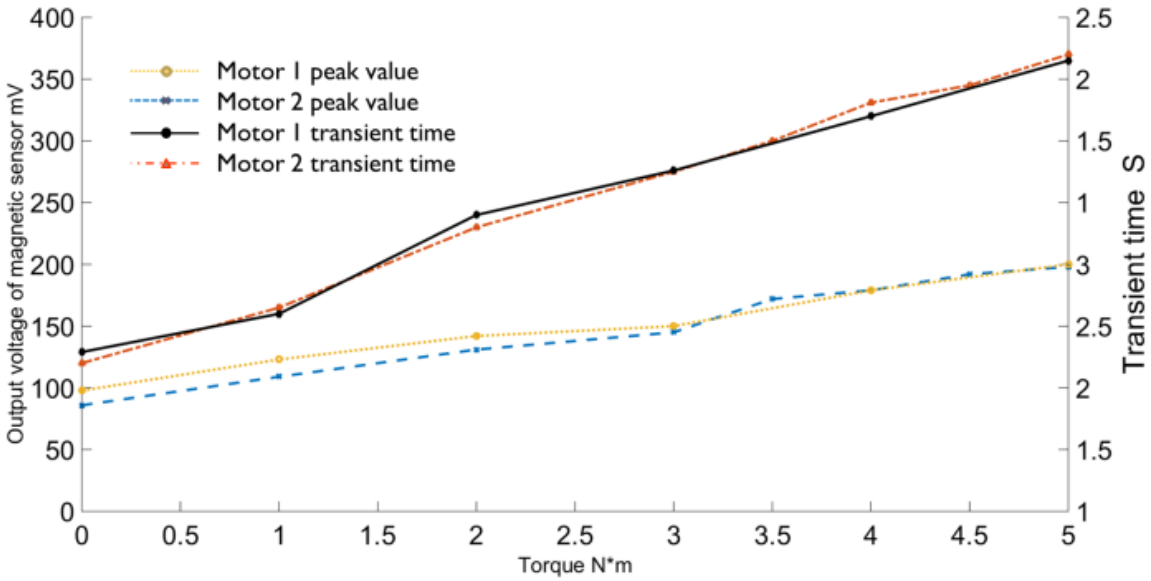

Figure 5.6 Comparison of the peak value and transient response time during starting up

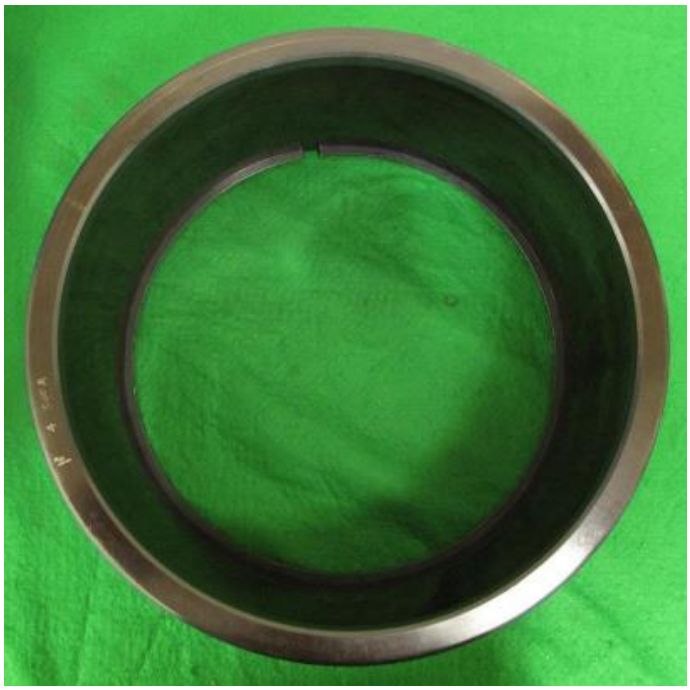

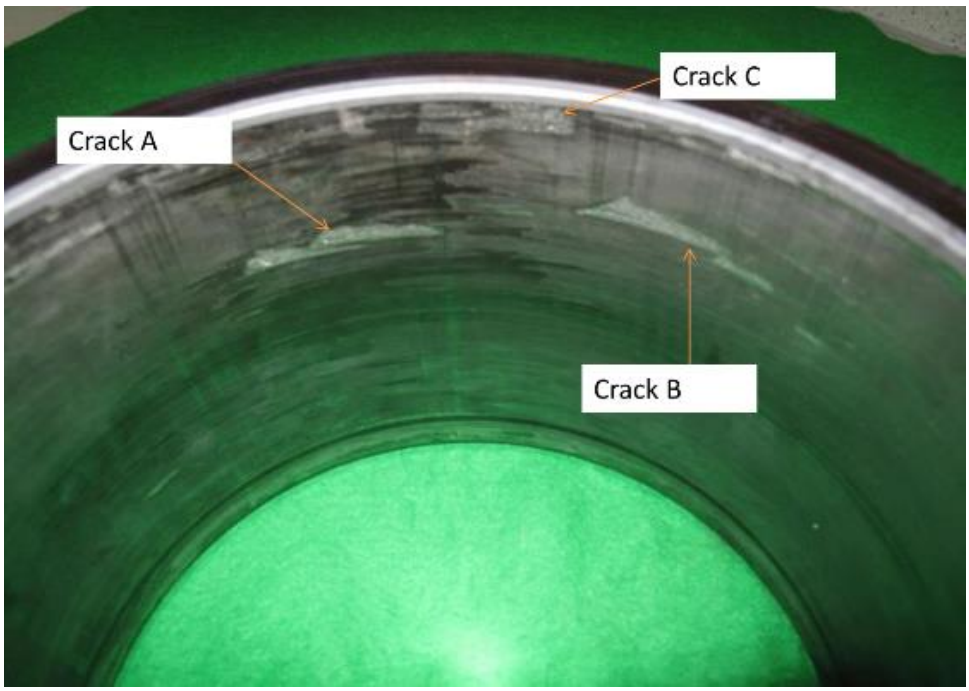

Figure 5.5 Test bearing status

To validate the proposed system and feature extraction method in monitoring induction machines, a second load monitoring test was applied to a 59 kW motor. The first case study was carried out with steady-state features applied. As shown in the bearing test bench (Fig. 5.2), the motor shaft is directly linked to a test bearing. As the hydraulic system exerts an additional constant load on the bearing, bearing cracks or failures may be generated as a result of excessive fatigue cycling. Any cracks and faults on the test bearing will lead to a load increase. The proposed method and transient feature (spectrogram) were applied for load monitoring, especially at motor start-up, to estimate the bearing condition. Figs. 5.7 shows the bearing state (outer race and inner race) before and after a ten-day accelerated fatigue test. The test data from the second test bench was processed and the spectrogram results are shown in Fig. 5.8. The start-up process is divided into several steps due to the heavy load and large power rating of the experimental system. After several days of continuous testing, the start transient response time was obtained and plotted in Fig. 5.9. As the transient response time increases, some bearing faults start to appear, as illustrated in Fig. 5.7. It is thus proven that the spectrogram (and the transient response time in particular) is a valid feature for the monitoring of bearing fatigue.

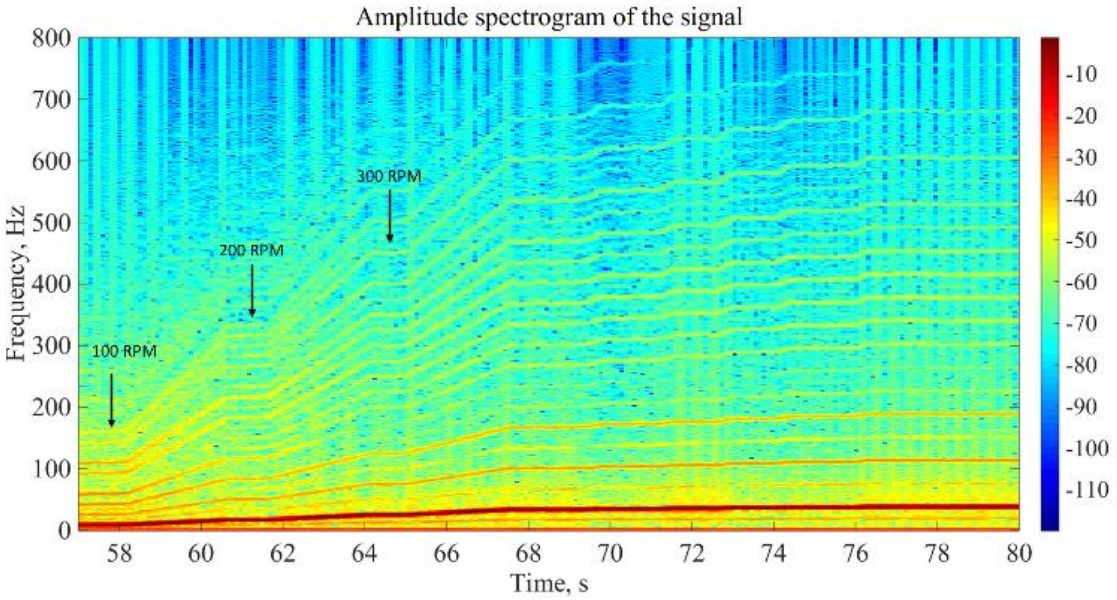

Figure 5.6 Data analysis using STFT in spectrogram with bearing test rig

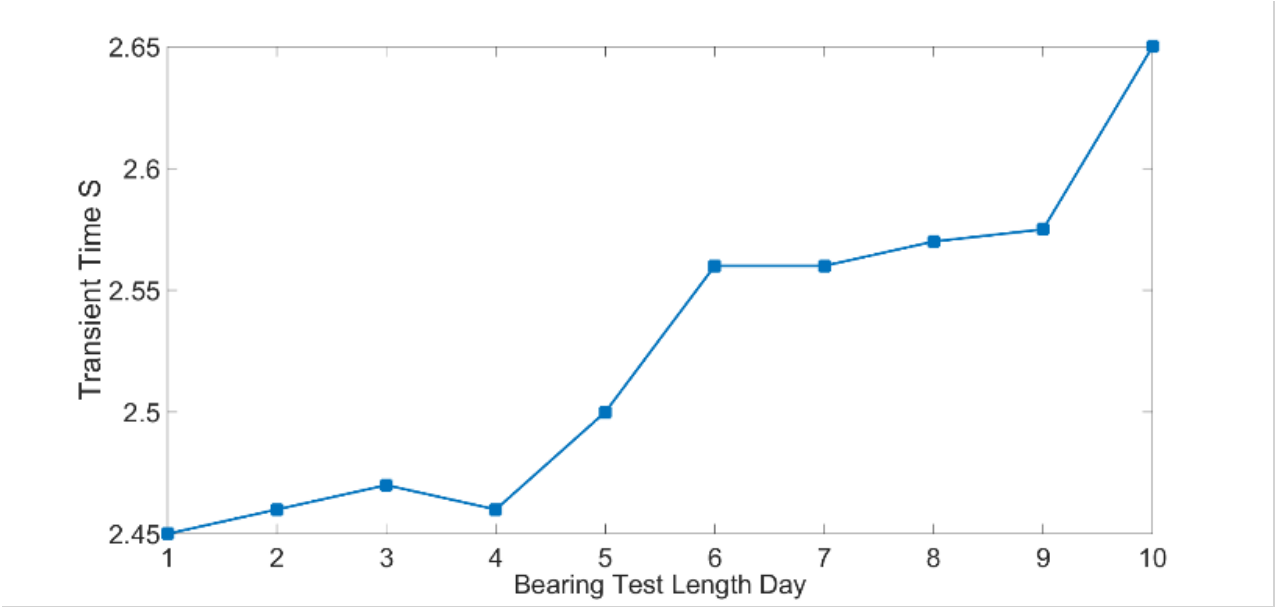

Figure 5.7 Transient time during the experiment

5.5 Chapter summary

Experimental studies have been carried out through steady-state and transient magnetic field measurements. In steady-state operation, the features are applied for load monitoring and feature extraction. When induction motors start up with load, the first peak of the output voltage of the magnetic sensor is a good indicator. Secondly, the spectrogram is used to provide patterns between time and frequency. By referencing the transient time information of the stray flux spectrogram patterns, load variations can be identified during the experiments. Compared with

steady-state analysis, the transient response time can provide more effective and better results for the dynamic load states. Overall, the experimental tests on three induction motors have confirmed the effectiveness of the proposed method of load monitoring. The proposed stray flux system shows the capability to monitor the abnormalities and variations in load in three induction machines even at a very low speed (200 RPM).

Chapter 6 Electrical Winding Failures

The non-intrusive monitoring of health state of induction machines used in industrial processes and harsh environments poses a technical challenge. In the previous review, winding failures were found to be a major fault accounting for over 45% of total machine failures. This chapter focuses on the influence of winding faults on stray magnetic flux in induction machines. Finite element analysis and experimental tests on a 1.5-kW machine are presented to validate the proposed health monitoring method. With time-frequency spectrogram analysis, it is proven to be effective in detecting winding faults by referencing stray flux information. The novelty of this work lies in the implementation of GMR sensing and the analysis of machine winding faults.

6.1 Finite element model

A three-phase induction machine is firstly modelled and built in finite element software, and the same induction machine is later tested in an experimental test rig. The specifications of the induction machine are shown in Table 6-I. Furthermore, the electromagnetic field distribution in a healthy state and with winding failure is analyzed as well.

Table 6-1 Specifications of the tested induction machine

Item	Value
Rated power	1.5 kW
Pole number	4
Phase number	3
Rated stator current	7 A
Rated stator voltage	220 V
Rated speed	1460 rpm
Stator slot	36
Rotor slot	28
Outer diameter of stator	140 mm

Inner diameter of stator	88 mm
Air-gap length	0.8 mm

6.1.1 Numerical results with winding faults

6.1.1.1 Healthy state of magnetic flux field

In order to investigate the change in the stray flux field, a steel housing and yoke is also built in the FE model. The magnetic flux distribution and stray flux in a healthy state are calculated and illustrated in Figs. 6.1 and 6.2, respectively. In this context, the baseline information for stray flux can be observed in the healthy state and also helps in determining the specifications of the magnetic sensors.

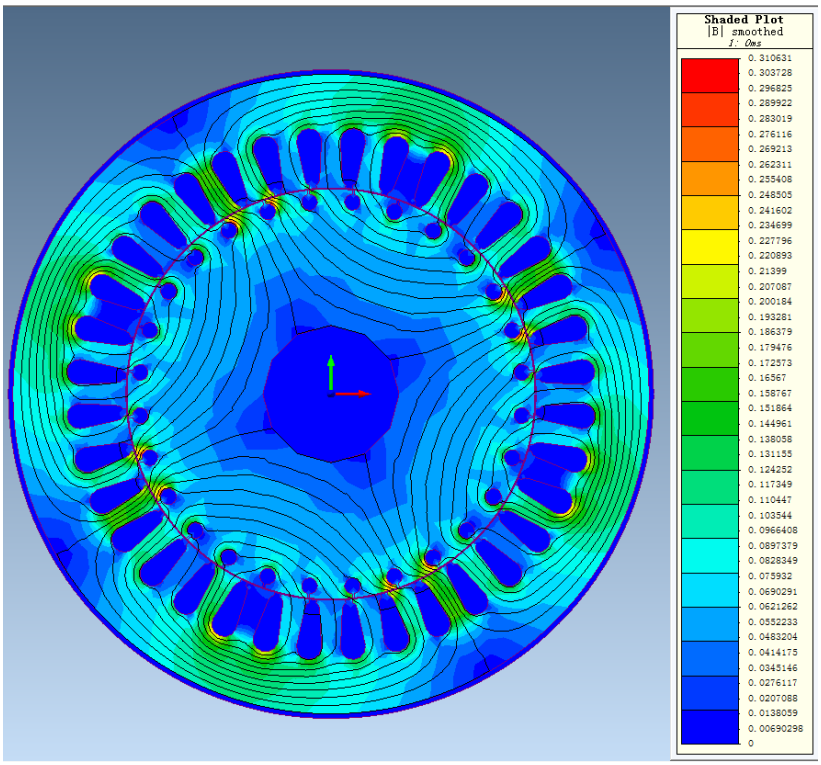

Figure 6.1 Magnetic flux distributions of FE model.

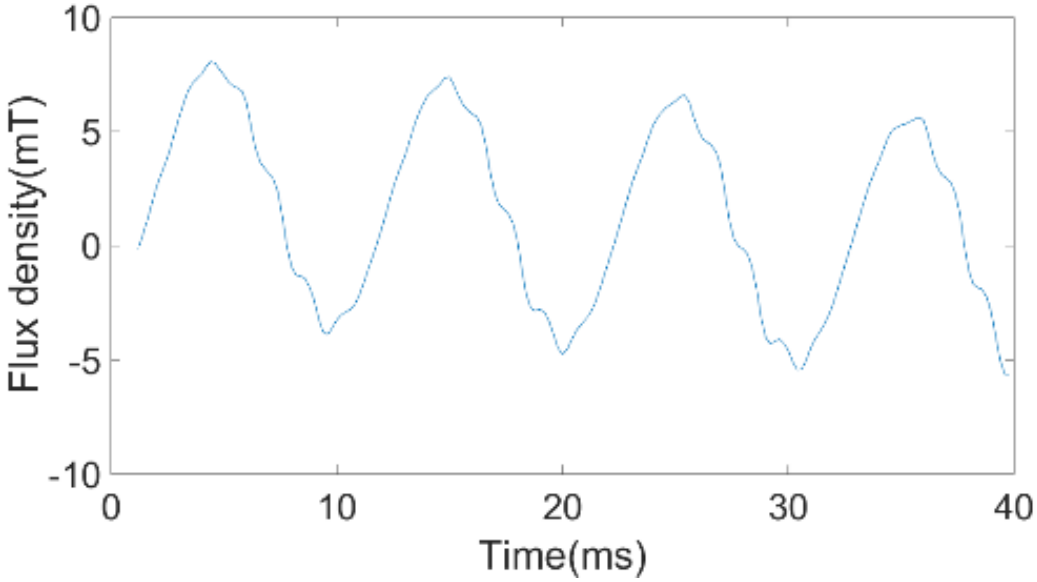

Figure 6.2 Stray flux density in the induction machine housing.

6.1.1.2 Phase -to-phase short-circuit simulation.

By changing the connections and winding parameters, a phase-to-phase short-circuit is formed and simulated in the FE model. As the circuit current creates an imbalance inside the induction machine, the magnetic field and stray flux distribution are different from those in the healthy state, as shown in Fig. 6.3.

Once a winding fault occurs inside an induction machine, the three-phase currents become unbalanced and distort the magnetic and stray flux. Stray flux results at the same detection point are shown in Fig. 6.4.

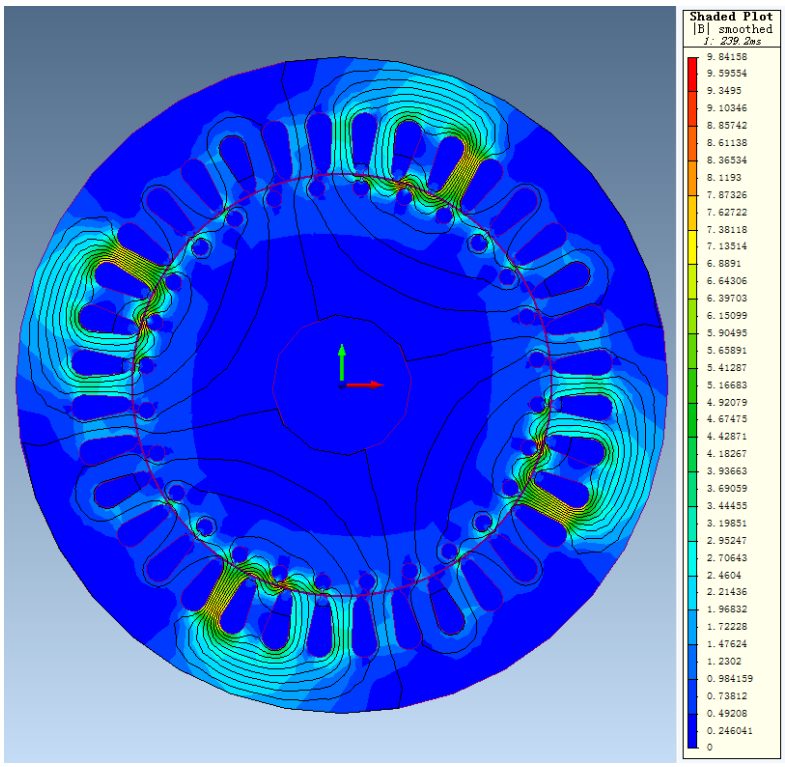

Figure 6.3 Magnetic flux distribution with a phase-to-phase fault.

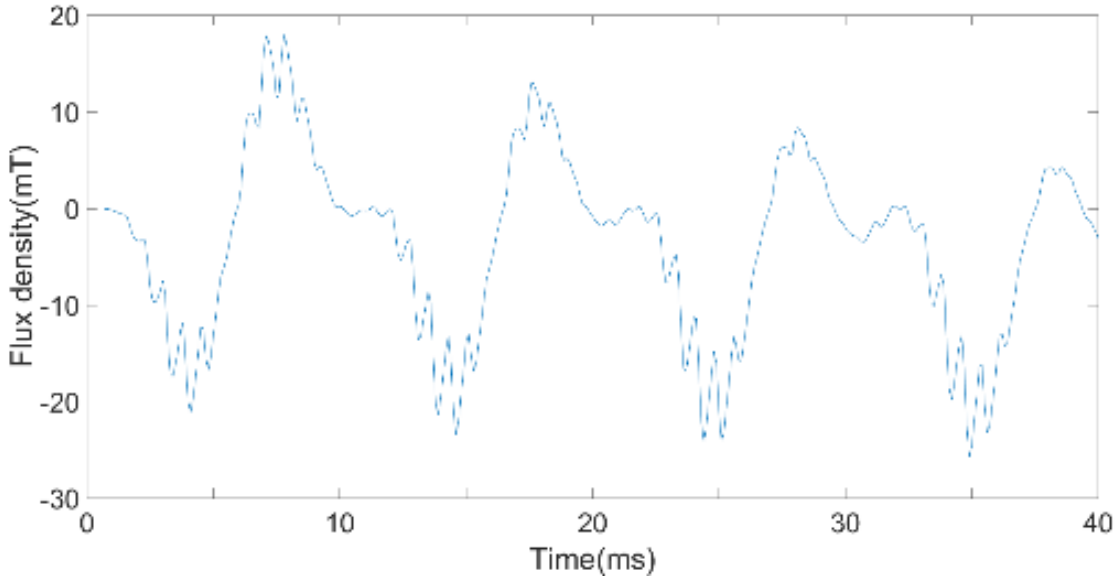

Figure 6.4 Stray magnetic flux with a stator winding fault.

6.1.2 Thermal simulation

As mention in the chapter 2, thermal degradation directly influences the winding insulation and leads to winding circuit failures. Additionally, any winding faults in induction machines will impact on the thermal performance of the machine and the undesirable heating patterns may cause catastrophic damage to the machine if left untreated. Furthermore,

temperature changing inside of the machine affect the magnetic permeability, which leads to change in the magnetic field of the machines. Therefore, it is necessary to investigate the thermal model of the electrical machine.

6.1.2.1 3D Temperature field of the induction machines

In magnetic analysis, induction machines can be analyzed using a 2D magnetic model with reasonable accuracy. But for thermal problems, it is necessary to use 3D models and also to consider ventilation and heat transfer with in the machine. The induction machine model used in this section has been augmented with some ducts in the rotor for cooling, including totally enclosed air-cooling convection.

The following assumptions are made for temperature field modelling:

- All the slice faces of the induction machine model are perfectly insulated.
- The insulators in the slot are identical.
- The heat convection coefficient is identical at all positions in the air gap.

The reason for a temperature increase in the machine is heat losses. The total loss is given by:

$$P_{all} = P_{1cu} + P_{2cu} + P_{iron} + P_M + P_S \tag{6.1}$$

where P_{all} is the total loss, P_{1cu} is the copper loss in the stator, P_{2cu} is the copper loss in the rotor, P_{iron} is the iron loss, P_M is the mechanical loss, and P_S is the stray load loss. By determining the individual losses in the generator, it is then possible to sum them to find the total loss. Then all the sources of heat for different generator components can be set by referring to the corresponding losses.

In an air-cooled machine, the heat radiation is very small and is thus neglected in this study for purposes of simplification. The main routes for heat transfer are through convection and conduction. The 3D steady state heat conduction is:

$$\frac{\partial}{\partial x}\left(k_x \frac{\partial T}{\partial x}\right) + \frac{\partial}{\partial y}\left(k_y \frac{\partial T}{\partial y}\right) + \frac{\partial}{\partial z}\left(k_z \frac{\partial T}{\partial z}\right) = 0 \tag{6.2}$$

where k_x, k_y, k_z are the heat conduction coefficients in the x-, y- and z- directions respectively.

Additionally, the heat convection coefficient h also needs to be calculated to set the boundary conditions for the outer surface of the stator core. This is calculated as follow [8]:

$$h = \rho\ cp\ D\frac{v}{4L*[1-EXP(-M)]} \tag{6.3}$$

$$M = 0.1448L^{0.96}/D^{1.16}\{k/(\rho\ cp\ v)\}^{0.214} \tag{6.4}$$

where D is the outside diameter, L is the characteristic length of the surface, v is the fluid velocity, ρ is the fluid density, c_p is the fluid specific heat capacity, and k is the thermal conductivity.

6.1.2.2 Thermal modelling of healthy induction machines

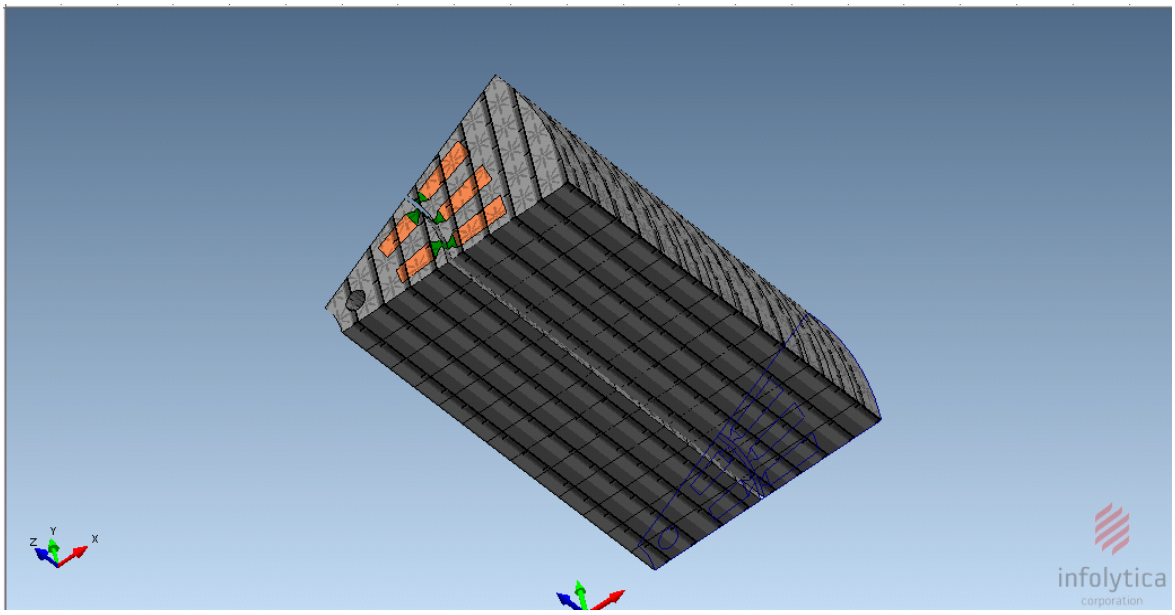

Figure 6.5 3D model of an induction machine

As heat is transferred in the x, y, and z directions, the thermal simulation cannot be fully explained by a 2D model, so a time-consuming 3D model is needed. Fig. 6.5 shows a 3D model of the induction machine designed using ThermNet (coupled with MagNet). To reduce the solution time for thermal simulations, the 3D induction machine model is built with a portion of the motor body for one phase with one pole. The types of convection heat transfer used in the induction machines are natural convection and forced convection.

By adding all the losses calculated from MagNet, the temperature field distribution in the induction machine with natural convection is illustrated in Fig. 6.6. It can be observed that the hottest part is in the center of the rotor, with a recorded temperature of 125.48°C.

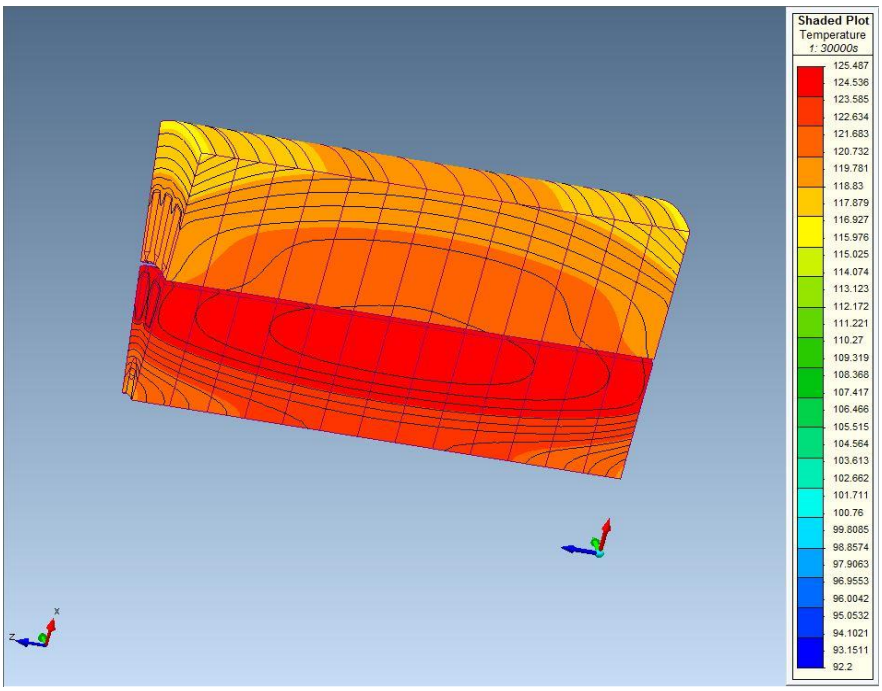

Figure 6.6 3D temperature field with natural convection

On the basis of the natural convection model, forced convection can be added to the FEA. Generally, the forced convection in induction machines can be achieved by installing a fan on the shaft and rotating it with the rotor. In this case, the air is blown into the airgap and ventilation duct. In the FEA, it is assumed that the direction of forced convection is from the left of the model to the right in all diagrams. When air flows through the induction machine, the convection heat transfer coefficient h is different in the axial direction. Consequently, the simulation model has been sliced into 13 sections along the axial direction. According to equations 6.3 and 6.4, each part has been set with a different convection heat transfer coefficient. Figs. 6.7 and 6.8 show the 3D temperature distribution of the healthy induction machine model.

After hours computation, the temperature field of the induction machine mode has reached a steady state. Figs. 6.9 and 6.10 demonstrate that the hottest part of this whole model is the outlet of the air path, which leads to the probability of damage to the winding insulation. But the highest temperature in the generator is only 107.5°C, which is already much cooler than that with natural convection. Moreover, the temperature distributions in the three different coils in the stator are the same; so those are for the two coils in the rotor.

By setting the losses calculated from the faults induction machine model in MagNet (with winding short-circuits), the temperature field of the faulty induction machine model is obtained, as shown in Figs. 6.11 and 6.12. The short-circuit occurs only in one coil of the rotor winding. From Fig. 6.9, the temperature field distribution of the short-circuited coil is different

from that of the healthy one. More specifically, the area of the highest temperature (117.7°C) in the rotor shorted coil is larger than in the healthy case, which makes it more likely to cause a winding failure.

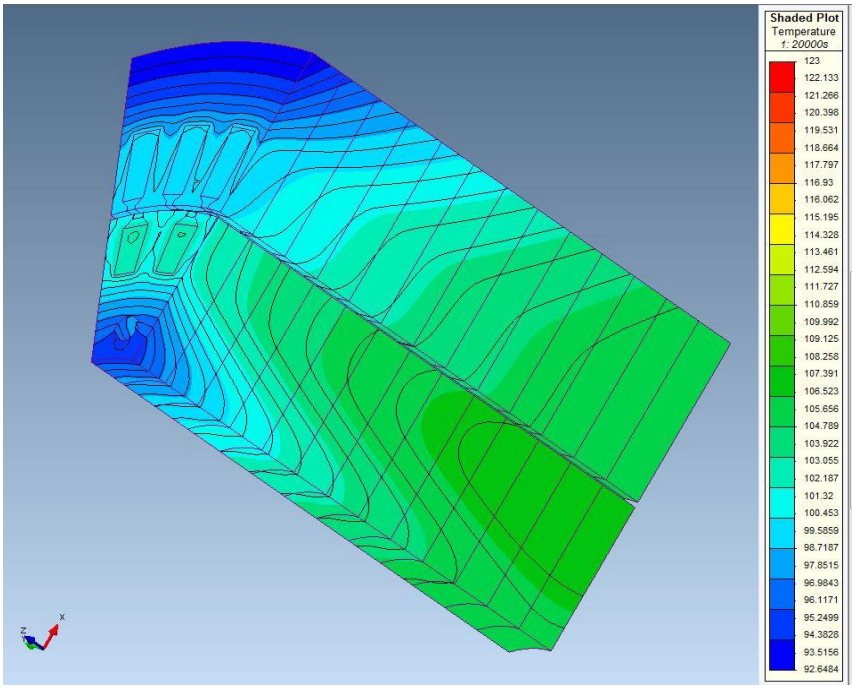

Figure 6.7 3D temperature field with forced convection

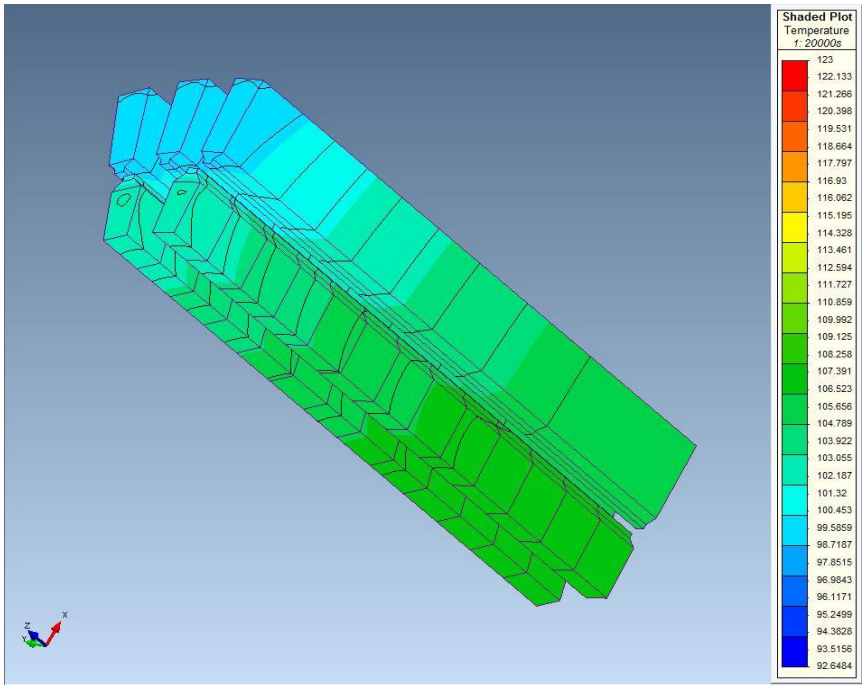

Figure 6.8 3D temperature field under healthy conditions

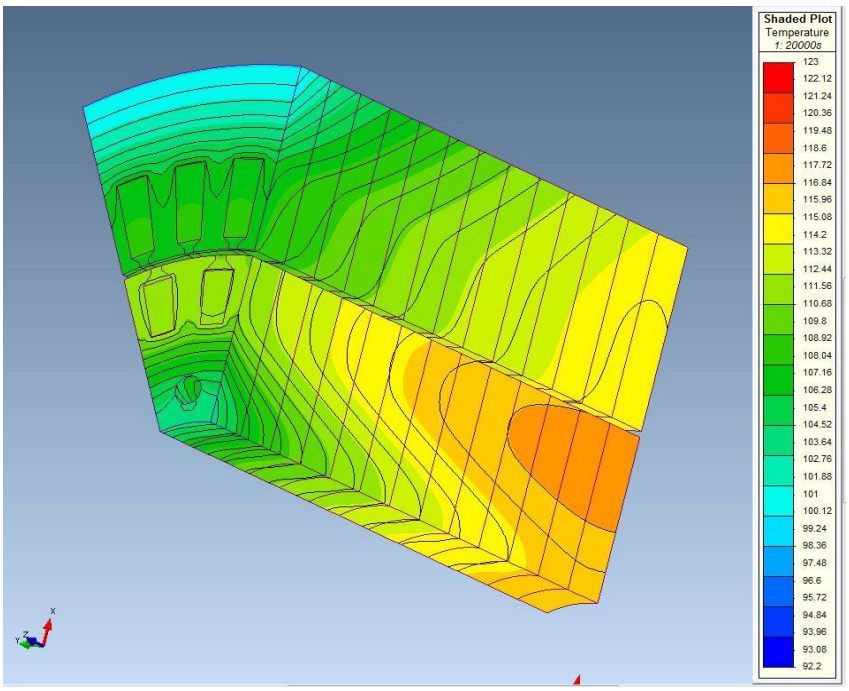

Figure 6.9 3D temperature field with rotor short-circuits

Comparing the healthy and faulty induction machine models, the major difference is the heat source which is induced by the current flowing through the copper winding. During a winding short-circuit event, the current generates heat and creates initially hotspots. When stabilized, the winding temperature in the fault model is much higher than that in the healthy model, giving rise to the likelihood of insulation failure and fault propagation.

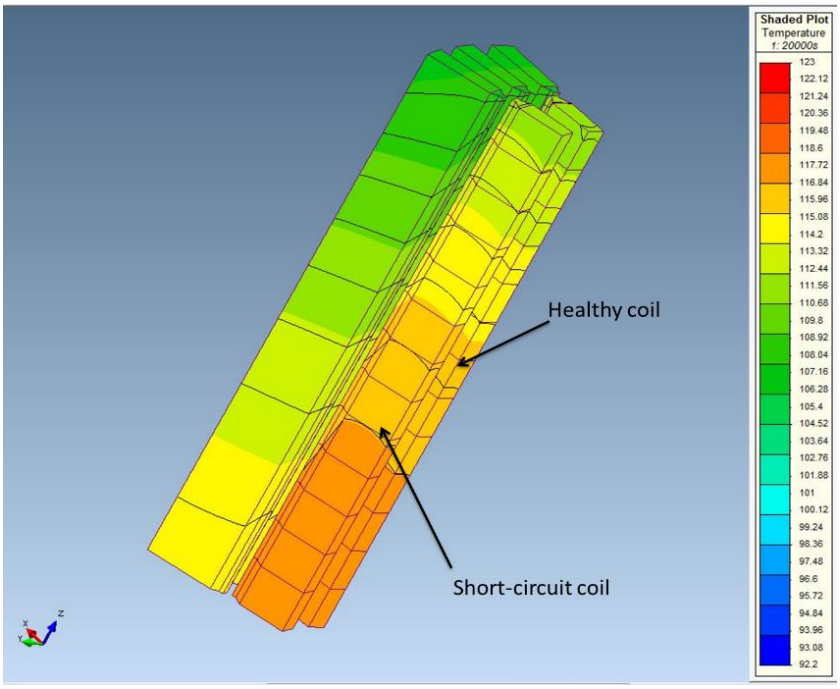

Figure 6.10 3D temperature field with rotor short-circuits

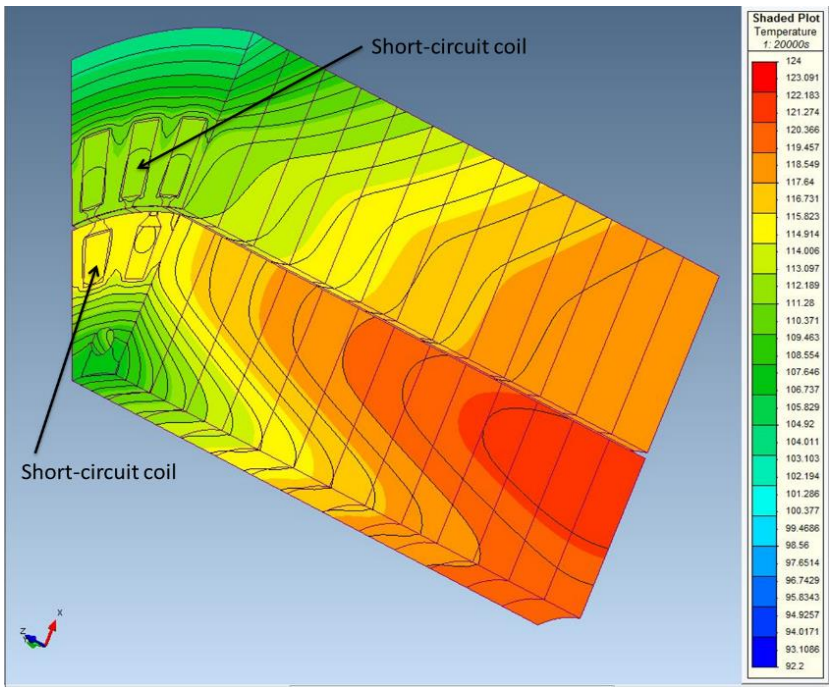

Figure 6.11 3D temperature field with short-circuits in both the rotor and stator windings

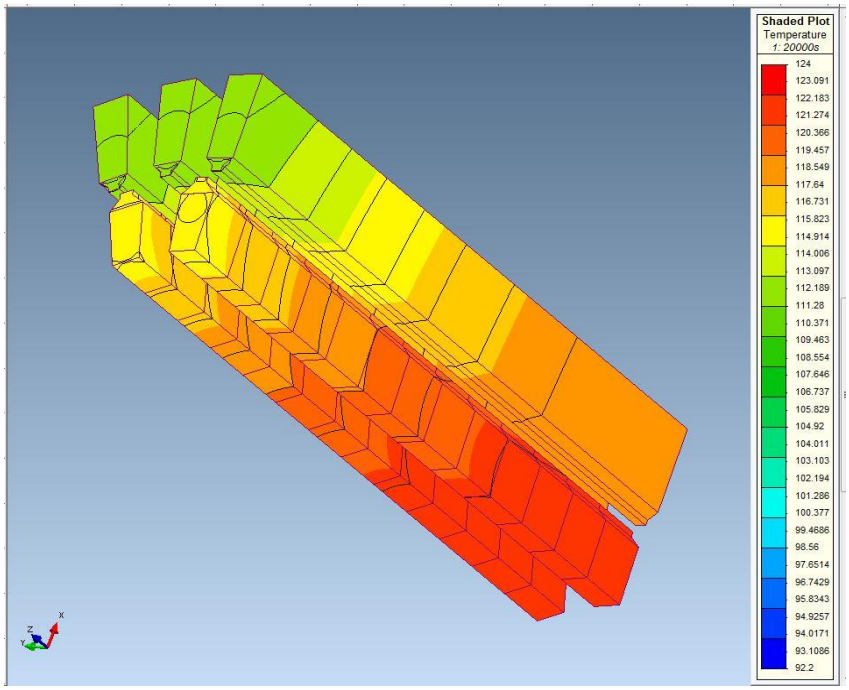

Figure 6.12 3D temperature field with short-circuits in both the rotor and stator windings

When turn-to-turn winding faults occurr in the stator or the rotor, the excessive heat generated from short-circuits will diffuse through the air gap so that the average temperature of the generator increases, leading to hotspots, insulation degradation or new short-circuits in neighboring windings of the induction machine. When winding faults are present in both the stator and the rotor, the damage can be more severe or even catastrophic for the generator. Figs. 6.11 and 6.12 show the temperature field distribution of the induction machine with short-

circuits occurring at one rotor coil and one stator coil. From the simulation results with rotor and stator short-circuits, the highest temperature (123.09°C) is similar to the case of a natural convection machine but much higher than the previous fault simulation in air-cooled cases. Furthermore, the isotherm of the stator windings at the air inlet is quite different from in the healthy model and faulty rotor winding models. Compared with the two healthy stator windings, the trend of the bulging isotherm in the faulty windings is more significant than in the healthy ones.

6.2 Experimental vilaidation

6.2.1 Experimented test bench set-up

An experimental test rig has been set up to validate the proposed technology at Massachusetts Institute of Technology, Boston, USA, as shown in Fig. 6.13. The test machine is a four-pole three-phase induction machine with a steel housing and frame. The stator windings are star-connected and the rotor is short-circuited. The machine is controlled by a converter via a Labview interface in the control PC. A DC motor is coupled to the test machine as the load. The GMR sensor is installed at the middle of the housing to capture the leaking stray flux. The output signal of the magnetic sensors is collected by a NI data acquisition card with sampling frequency of 5-kHz. By changing the wire connection at the fault point, different stator winding faults can be emulated and tested in the experimental test rig, including phase-to-phase and phase-to-ground short-circuits. The aim of this sensor is to detect the stray flux, which is perpendicular to the machine yoke. The sensor has to be placed with glue and tape in the middle of the machine cage in order to minimize the influence of the ending windings as shown in Fig 6.13 b. The sensor can be implemented on any place in the middle of the machines cage to collect the stray magnetic field information.

Stray flux is a magnetic flux that radiates from the inside of the machine frame and is inherently and strictly connected to the magnetic state of the machine. Stray flux is induced by stator and rotor currents, each of which produces magnetic flux with different spectral components. In this case, if a short-circuit occurs inside the machine, the stray flux will change depending on the variation in the machine stator and rotor currents. Therefore, several types of electrical failure have been created during the experiment, such as a phase-to-phase short-circuit. By collecting stray flux information, stray flux information of electrical failure of the machine can be obtained.

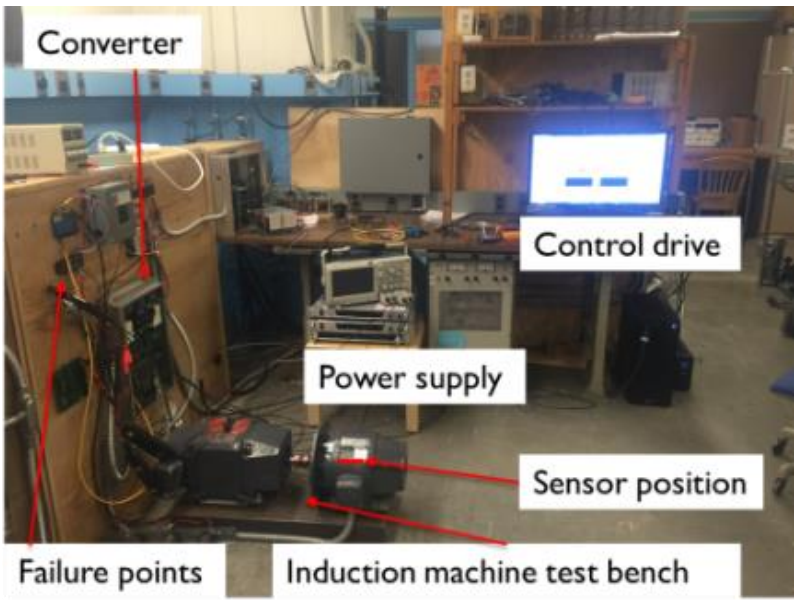

(a) Induction machine failure test bench

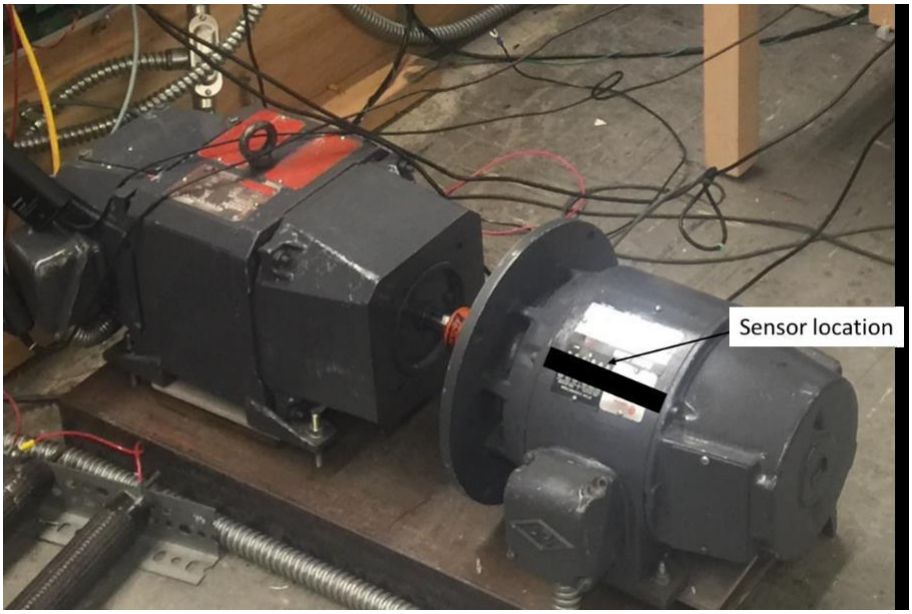

(b) Stray flux sensor location

Figure 6.13 Experimental test rig

From the simulation results, the stray magnetic flux density is within the range which can detected. In this case, the specifications of sensors and sensor arrays are designed to capture the magnetic flux escaping from the machine housing. GMR sensor arrays can meet the design requirements and give good performance in low magnetic fields. After collecting stray flux data, the results can be compared between different health states in both the time and frequency domains.

6.2.2 Experimental Results

The stator winding fault test is used to detect stray flux field variations during different situations. The stray flux is measured in the radial direction of the machine housing when the test machine is running at steady state. To build the healthy baseline information for stray flux, the GMR sensors firstly capture the stray flux of a healthy machine with different output voltages from the converter. The line-to-neutral voltages are set at 10 V, 90 V, 70 V, 40 V and 20 V. The output signals of the GMR sensors are presented in Fig. 6.14.

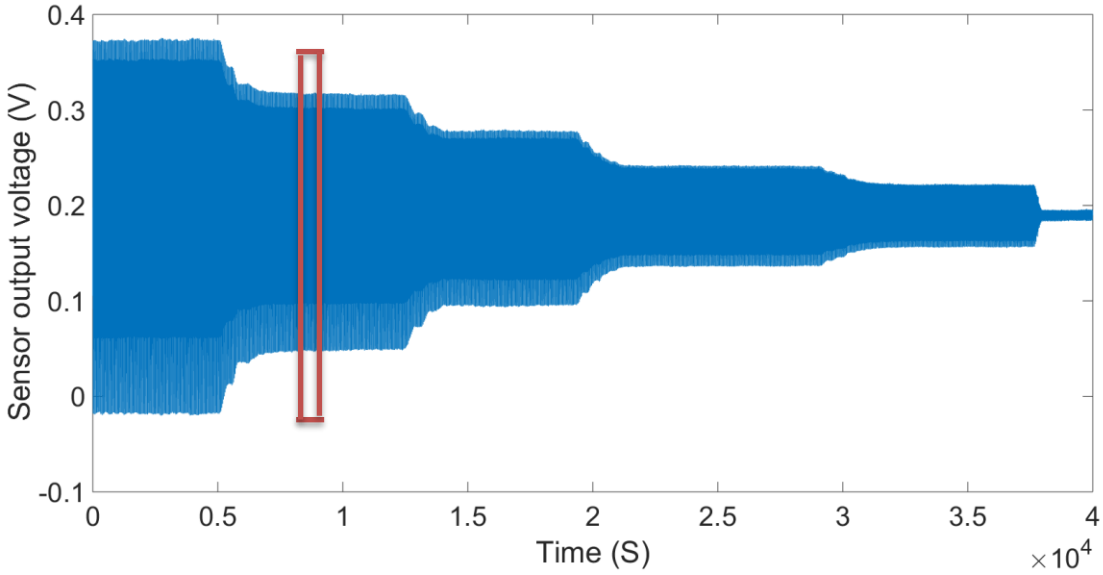

a) Stray flux data at different voltage outputs

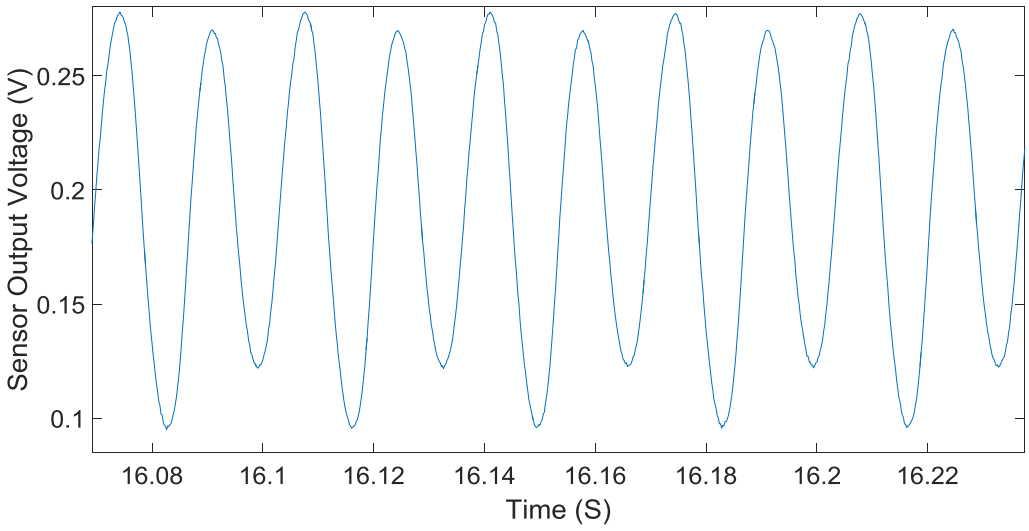

b) Stray flux data at 70 V

Figure 6.14 Stray flux baselines for the healthy induction machine.

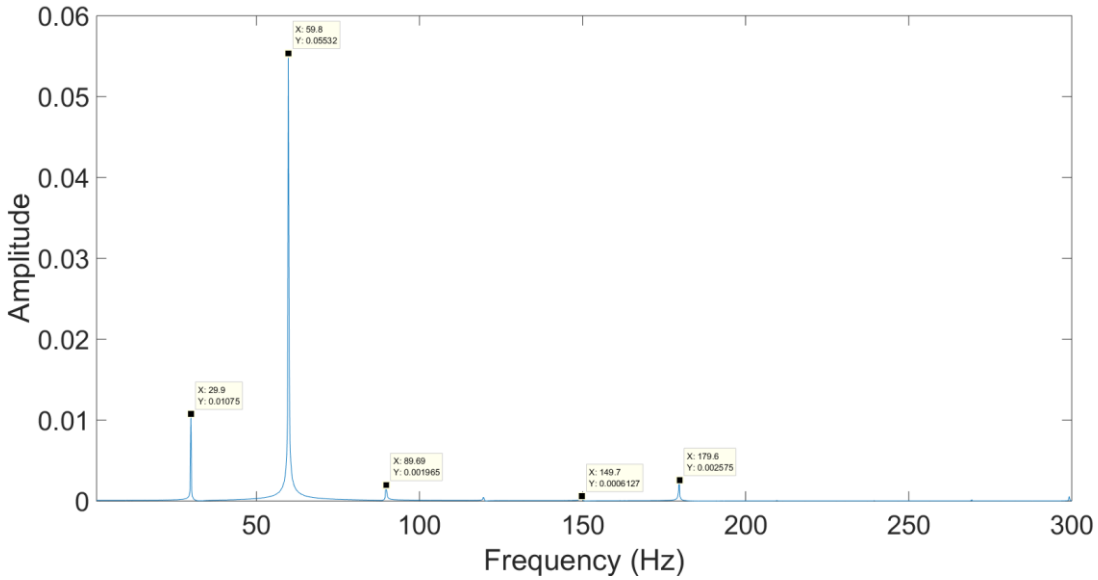

Figure 6.15 Stray flux spectrum of the healthy induction machine

In theory, the stray flux in the radial direction is created by both stator and rotor currents. More specifically, current flow in the stator windings generates the main air-gap flux. Due to attenuation phenomena in the stator lamination and machine housing, the stray flux can be seen as a reduced air-gap flux. The attenuation can be decoupled and represented as a global transmission coefficient which links the two together.

Fig. 6.15 provides the stray flux spectrum of the healthy induction machine. The different frequency components reflect the characteristics of the test machine. The fundamental frequency is 60 Hz, and there are several harmonic components, which are influenced by slotting effects and the geometry of the machine. With the influence of eddy currents in the housing, there is also a slight difference between simulation and experimental results.

By created a phase-to-phase winding fault, the stray flux of the test machine changes, as shown in Fig. 6.16. As a short-circuit occurs in the stator windings, the current flowing in the faulted phase is increased. Therefore, the induction machine becomes unbalanced, which is shown in the stray flux results.

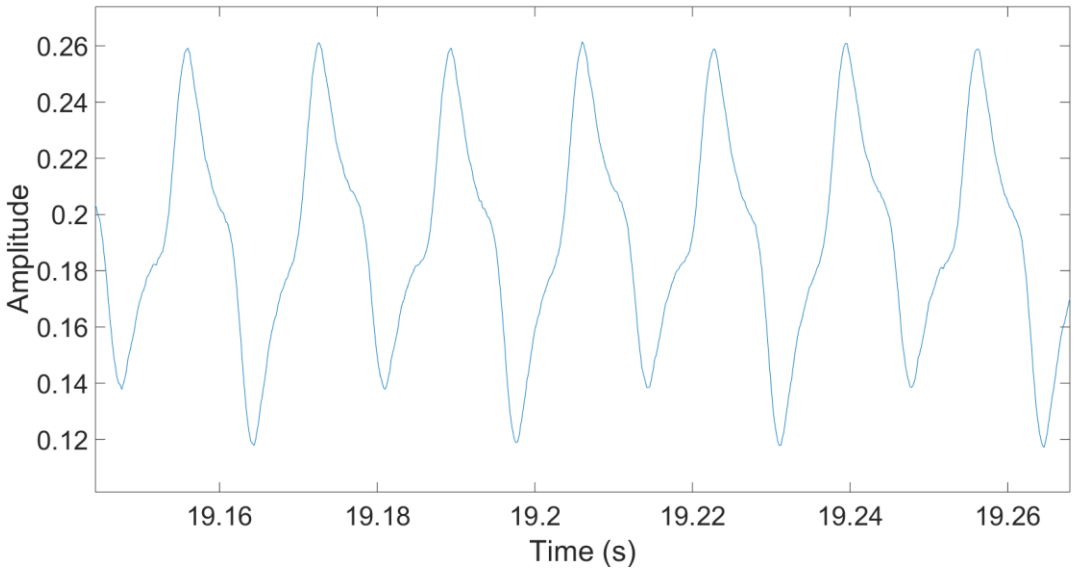

Figure 6.16 Stray flux of induction machine with a phase to phase fault.

By apply Fast Fourier Transform (FFT) analysis, the stray flux signal can be observed in the frequency domain. Fig. 6.17 shows the stray flux spectrum of an induction machine with a phase-to-phase short-circuit. Compared with the healthy state (Fig 6.16), the amplitude of several harmonic components has already changed. The third harmonic (180 Hz) is increased about 6-fold from 0.002575 to 0.01502. Additionally, the 150-Hz harmonic is also doubled. However, the fundamental component and its side band remain at the same level as in the normal state. From the stator current signature analysis, the thrid harmonic component is also proven to be useful in identify an imbalance and winding faults. As a result, the third harmonic component is used as an indicator for phase-to-phase winding short-circuits in induction machines.

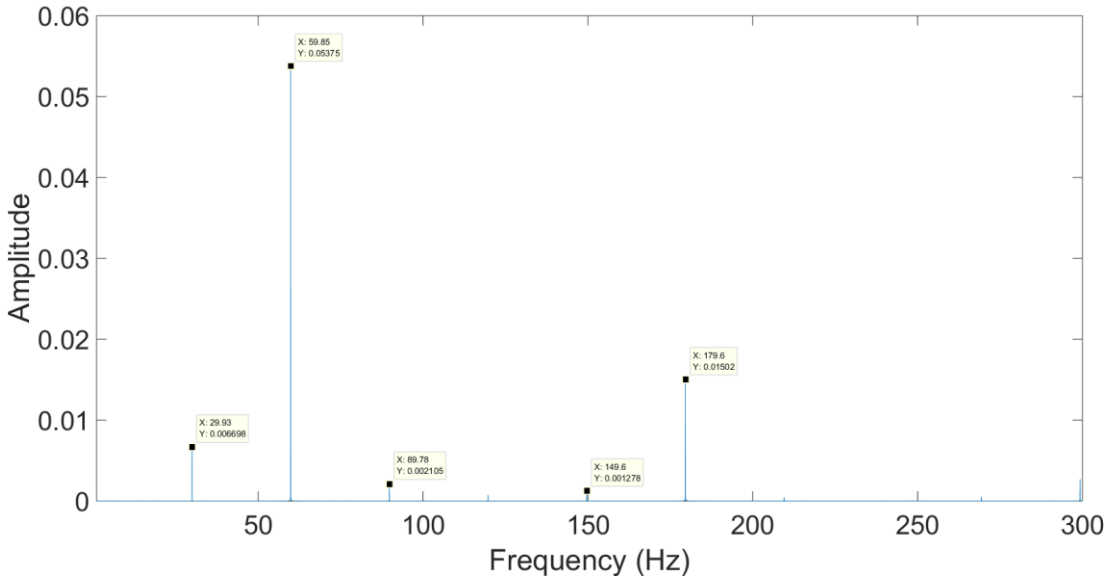

Figure 6.17 Stray flux spectrum of induction machine with phase to phase failure.

Subsequently, another winding failure is also created in the experiment, which is a phase-to-ground short-circuit. This short-circuit usually occurs between the stator winding and stator lamination. With degradation in the insulation of the stator winding, it is possible for it to come into direct contact with laminations, which generates the phase-to-ground winding short-circuit failure. To investigate this failure, one phase winding is connected to the ground for a simulation in the induction machine test bench. The stray flux sensor is placed at the same location as in the previous two experiments. Fig 6.18 shows the stray flux sensor output in the phase-to-ground winding short-circuit.

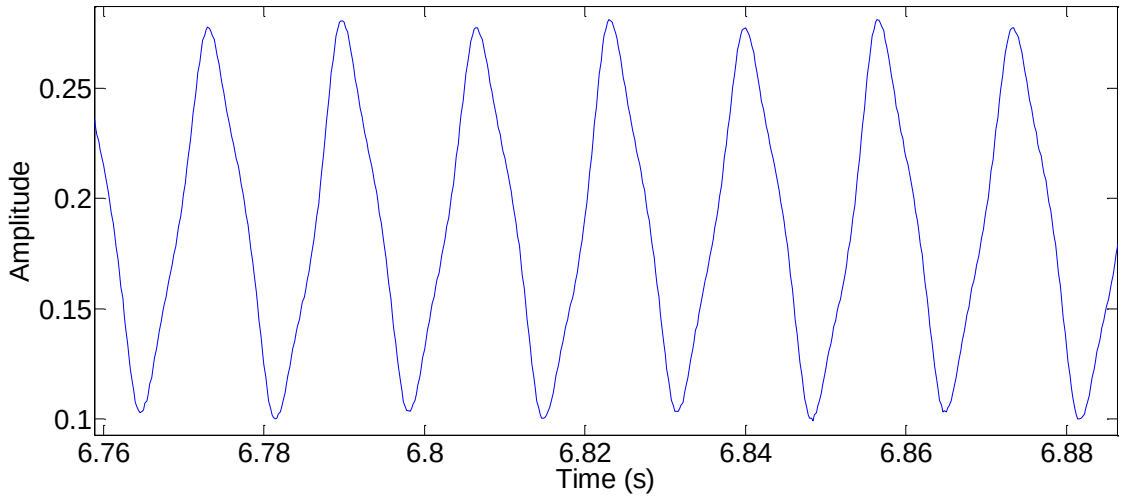

Figure 6.18 Stray flux with phase-to-ground winding failure in the induction machine

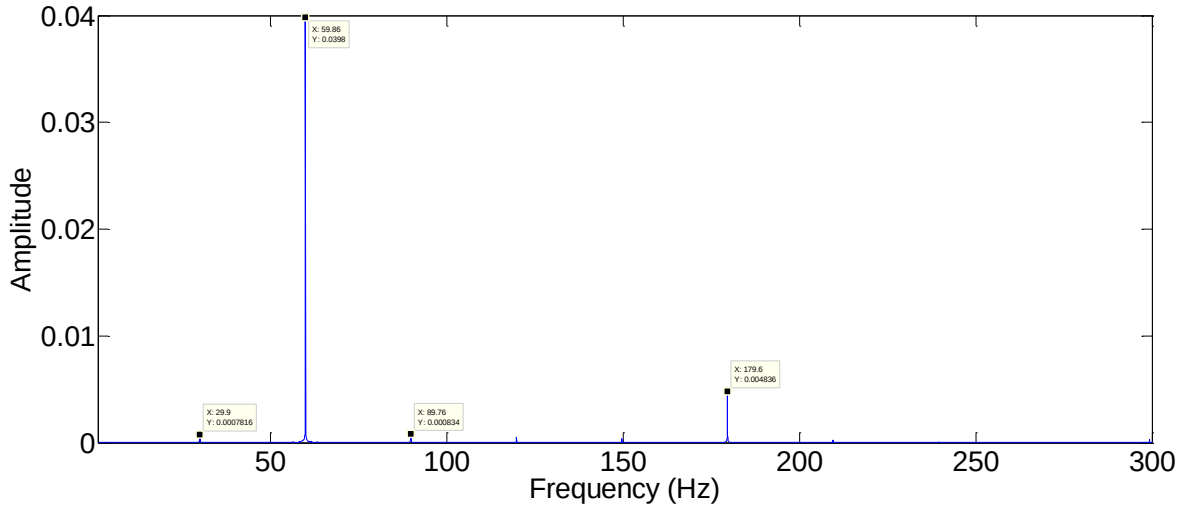

Figure 6.19 Stray flux spectrum of induction machine with phase-to-ground failure

Fig 6.19 shows the stray flux signal with a phase-to-ground failure in the frequency domain. As the power supply is the same as in the previous experiment, the amplitude of the fundamental frequency harmonic is reduced to 0.0398 compared to that of the phase to phase short-circuit winding failure. Additionally, the amplitude of the third harmonic is also larger than that in the healthy state, as unbalanced three-phase current flows in the stator windings. Subsequently, the harmonic components at 30 Hz and 90 Hz decrease to 0.0007816 and 0.000834 respectively once the phase-to-ground short-circuit occurs in the induction machine, this likely to be an indicator to distinguish between phase-to-phase short-circuit and phase-to-ground short-circuits.

As discussed in Chapter 3, stray flux can represent as the main flux in air gap and reflect the stator current. Previous researches of stator winding short circuit fault in the electrical machines have provided several harmonic components as the indicators, which is shown as follow [88]:

$$f_{st} = f_s \left[m\left(\frac{1-s}{2p}\right) \pm k \right] \tag{6.5}$$

where f_{st} is indicator frequency, f_s is fundamental frequency, s is slip, p is number of pole, $m = 0, 1,2,3$, and $k = 0,1,3,5$. During the experimental study, the texted machine is running at rated speed with no load, so the slip is zero. When m =1 and $k = 1$, the indicator frequencies are 30Hz and 90Hz.When m =1 and $k = 2$, the indicator frequency is 150Hz. As the stray flux reflect the stator current, the frequency indicators of the stator current can be used as that of the stray flux as well, which has shown in the experimental result analysis above.

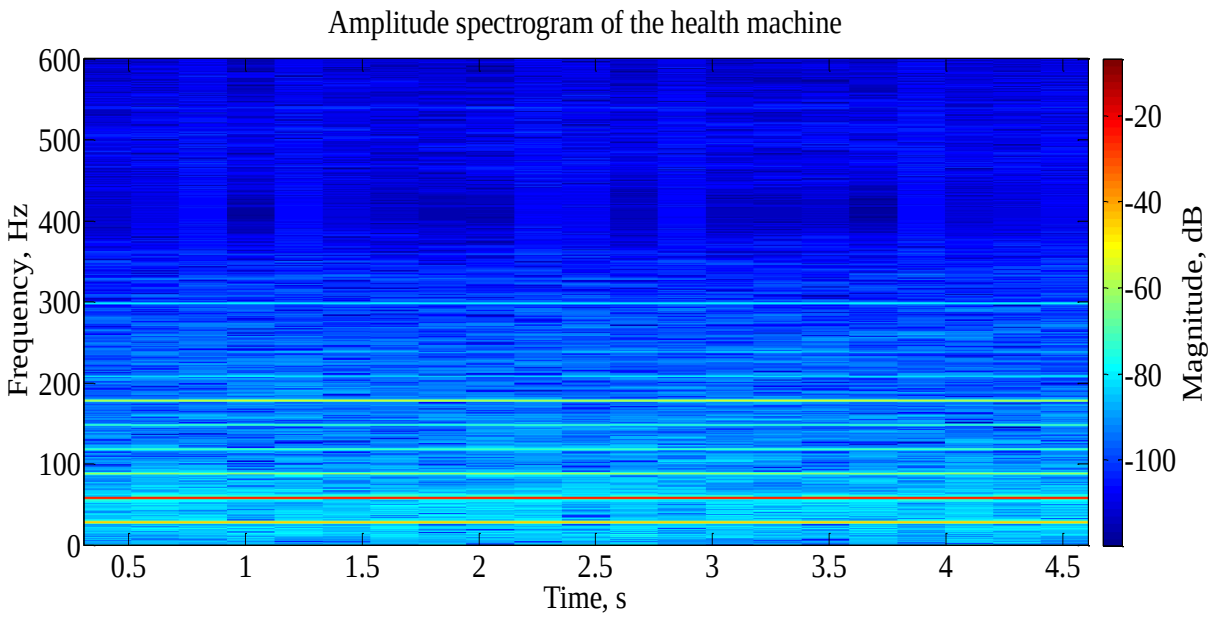

(a) Spectrogram of stray flux in healthy induction machine

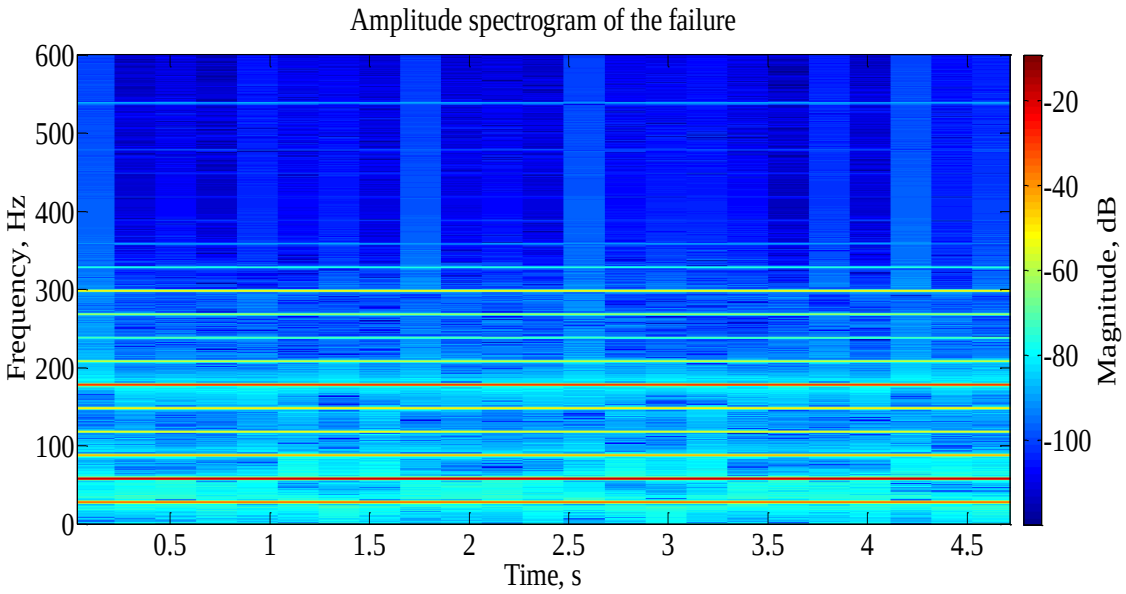

(b) Spectrogram of stray flux in induction machines with phase-to-phase short-circuit

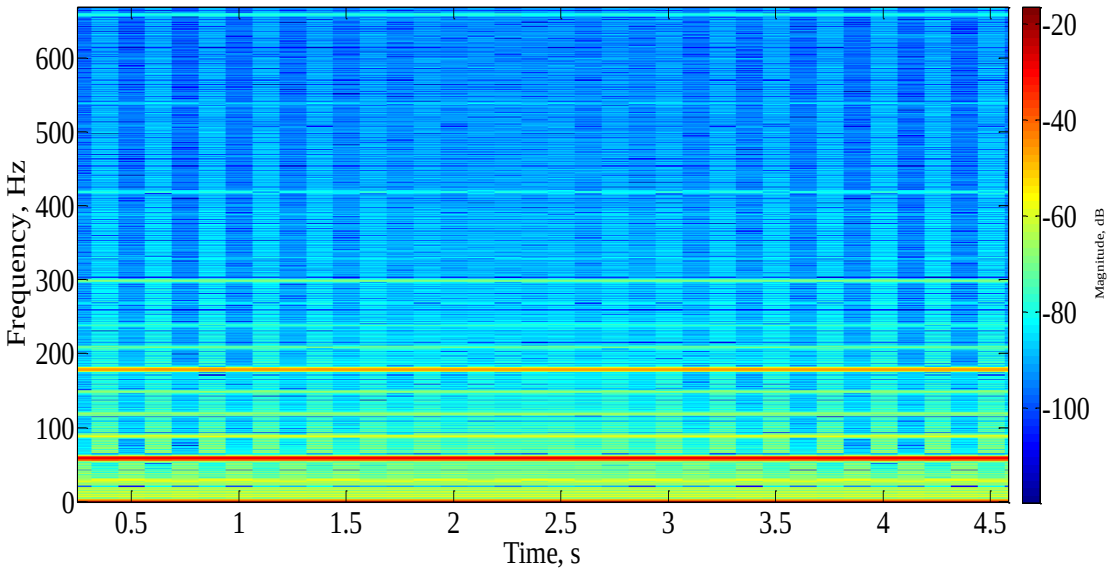

(c) Spectrogram of stray flux in induction machines with phase-to-ground short-circuit

Figure 6.20 Spectrograms of stray flux data in the winding failure experiments

Figure 6.20 (a) shows the healthy state of the machine, and b) and c) represent phase-to-phase and phase-to-ground short-circuits happening in the machine. Both set of data are taken in the steady state. The purpose of using a representation of time evolution is to provide time-varying information from the signal. Additionally, it is easier to show the pattern of the spectrogram compared with FFT. The spectrogram analysis is used to estimate the frequency content of the stray flux signal, and the magnitude squared of the STFT yields the spectrogram of the function, which is represented in colour plots.

Information about harmonic pattern can be observed based on these three spectrograms. In comparison with the FFT results, third harmonic is also increases from -53.83dB to -27.98dB. Additionally, between 200 Hz to 300 Hz, there are several increased harmonics raised which are shown in Fig 6.20 b, at 210 Hz, 239.3 Hz and 269.8 Hz, which are difficult to find in the FFT results. Spectrograms can not only identify tiny abnormalities in frequency component, but can also combine time information. Additionally, once the phase-to-ground short-circuit occurs in the induction machine, the spectrogram in Fig 6.20 c shows the magnitude of decreases in the 210 Hz, 239.3 Hz, 269.8 Hz and 30 Hz components. In this case, these harmonic components could be indicators to distinguish between different types of stator winding failures, and spectrograms can provide easily visible patterns and harmonic distributions.

6.3 Chapter summary

In this chapter, a new non-invasive condition monitoring method for induction machines has been proposed. It measures the stray magnetic flux field outside of the machine frame using GMR magnetic sensors. The proposed method offers wide range spectrum information, and the high resolution detection of low-level magnetic field detection.

Simulation results from different stator winding short-circuits can provide information about changes in stray flux. The thermal simulation of winding failures shows that there will be a temperature increase when a short-circuit occurs in the windings, which then accelerates the degradation of the winding. Based on simulations, GMR sensors and arrays can be chosen and developed to meet test requirements. Experimental results have confirmed that the proposed condition monitoring system is capable of capturing stray magnetic flux even though the leaking flux signal is quite weak. By studying the measured stray flux in the time domain, and especially in the frequency domain, several significant harmonic components can be used as indicators of stator winding faults.

Phase-to-phase and phase-to-ground short-circuit failures are tested in the induction machine experimental bench. From the comparison of these two winding failures, the harmonic component with an amplitude of 30 Hz (half of the fundamental frequency) is reduced once a phase-to-ground failure happens. However, other harmonic components increased compared to the healthy state of the tested induction machines. Thus, depending on the change in the component at half of the fundamental frequency in the stray flux, these two winding failures can be separated.

Chapter 7 Mechanical Failures

As mentioned in chapter 2, apart from electrical winding failures, mechanical failures are the most frequent failures in electrical machines and leads to considerable amounts of downtime. Due to the destructive and rapidly propagating nature of mechanical failures, it is critical to monitor induction machines to prevent further damage. Traditional monitoring techniques are based on variations in fundamental parameters, but those methods cannot distinguish different kinds of mechanical failure. This chapter investigates the influence of several types of mechanical faults on the stray magnetic flux field in the machines, with a view to validating the stray flux-based non-invasive motor monitoring system using an indirect approach. The designed stray magnetic flux monitoring system is proposed to estimate and detect unbalanced loads and bearing misalignments in electrical machines, using both simulation and experimental studies. By using independent component analysis, different mechanical faults and defect characteristics can be distinguished using stray magnetic flux information. Simulation and experimental results are presented to substantiate the idea that a combination of spectrograph, ICA and stray magnetic flux measurement could be a viable method for diagnosing between distinguishing the different mechanical failures.

7.1 Bearing misalignment and unbalanced load

Mechanical failures make the rotor eccentric, and an unexpected radial force is created. This force moves the rotor off-centre, which leads to an unbalanced load on the bearings. This force is called unbalanced magnetic pull (UMP) [2]. By reducing UMP, the bearing load can be reduced as well, which is likely to extend the lifetime of the components. As the bearing and mechanical failures are the major fault issues in the electrical machines, these failures need to be monitored and detected before the rest of the machine is influenced.

In commercial electrical machines, the air gap is designed to be quite small in order to reduce losses and increase efficiency. However, if any mechanical failure happens in the machine, the air gap will become non-uniform, which can lead to poor performance and inefficiency. Furthermore, on off-centre rotor can create UMP during the operation of the

electrical machine working, and rotor eccentricity can also not only increase the existing air-gap harmonics, but also generate additional and unexpected harmonics.

There are many possible causes of rotor eccentricity. Bearing misalignment and an unbalanced load are two of the critical issues, which can lead to varying degree of eccentricity [4]. If let the rotor eccentricity remains untreated, both the rotor and stator will be damaged as shown in Fig 7.1. In this case, developing a non-invasive approach which is easy to implement and give reliable detection has become important.

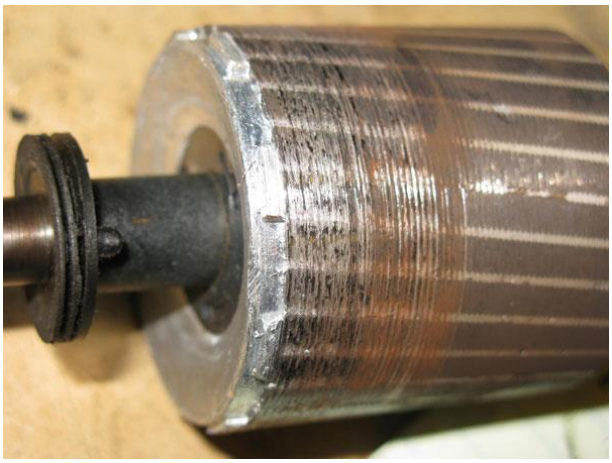

Figure 7.1 Rotor damage due to eccentricity

Bearing misalignment in electrical machines is usually caused by installation problems, where there is a lift-off on one side of the bearing or the shaft. This type of failure can damage the bearing wear and the rotor itself. Once bearing misalignment happens in a machine, the resulting a symmetric air-gap flux density can affect the stator current. As the rotor is supported by the bearing and shaft, any abnormality of the bearing state leads to UMP in the machine [39]. Overall, bearing misalignment will create an air-gap eccentricity failure.

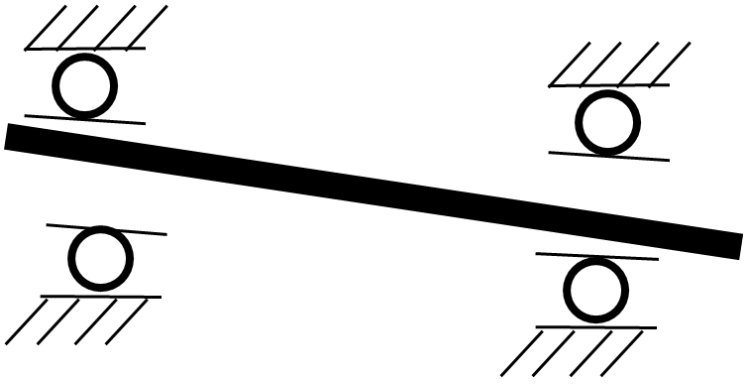

Figure 7.2 Bearing misalignment

As with the air-gap eccentricity, these variations generate stator currents at frequencies given as follow[35]:

$$f_{bearing} = \left| f_s \pm m\frac{n}{2} f_r \left[1 \pm \frac{bd}{pd}\cos\alpha\right]\right| \tag{7.1}$$

where m=1,2,3,……, and f_s is the fundamental frequency; n is the number of bearing balls; f_r is the mechanical rotor speed in hertz; bd is ball diameter, and pd is bearing pitch diameter; and α is the contact angle of the balls on the races.

Bearing misalignment leads to air-gap eccentricity which can be reflected in the fundamental frequency sideband of the stator current:

$$f_{ecc} = f_s \pm m f_r = f_s \left[1 \pm m(\frac{1-s}{p})\right] \tag{7.2}$$

By using this component in the spectrum, bearing misalignment can be detected, where f_{ecc} is the considered as a side-band of the fundamental waveform.

If there is an unbalanced mechanical load influencing the electrical machine, the stator current will also have additional harmonic component. In an electrical machine, any imbalance in the load at a multiple of the rotational speed will produce stator currents at the following frequencies [36] :

$$f_{load} = f_s \pm \frac{2mf_s}{p} \tag{7.3}$$

In this case, once an unbalanced load is applied to the machine system, the low frequency harmonic indicator is likely to overwhelm that for bearing misalignment. This is because both bearing misalignment and unbalanced load can create air-gap eccentricity, which then exert the same influence on the stator current. However, stray flux data can reflect air-gap flux density, as discussed in chapter 3.

7.2 Finite element simulation

As mentioned in section 7.1, static and dynamic eccentricities represent different mechanical failures, which in this case as unbalanced load and bearing misalignments. In order to understand distribution of stray magnetic flux, a finite element (FE) model has been built to investigate the potential influence of mechanical failures in machines. Static and dynamic eccentricities are simulated in this section. There the distribution of stray flux in the presence of the static and dynamic eccentricities can be observed in numerical results, and the simulation results are subsequently validated by the experimental studies in the following parts.

The FEA model is built based on a brushless DC machine which is the test machine in the mechanical failure experiment bench. As the eccentricities representing failure affect the whole air gap of the machine, it is necessary to use the 3D simulation model shown in Fig 7.3, which can provide more accurate results for the stray flux.

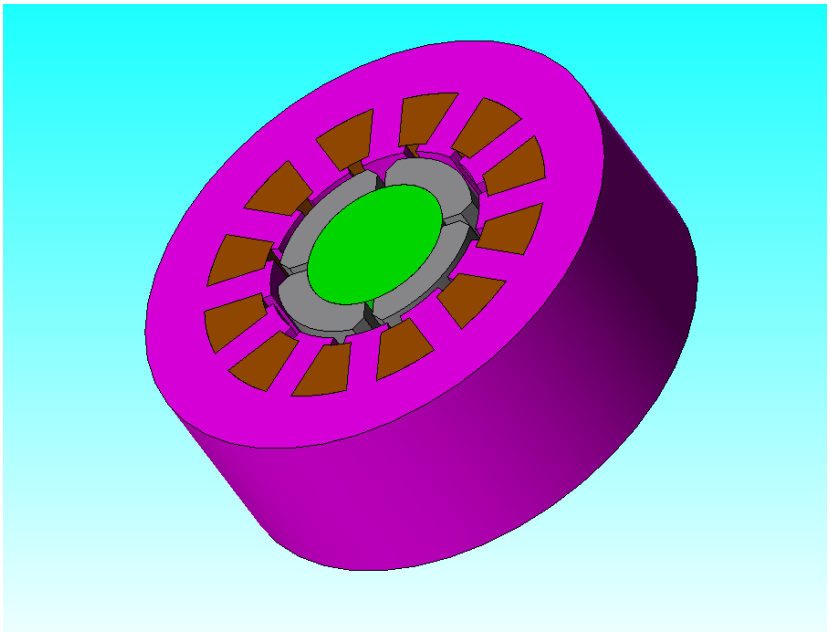

Figure 7.3 3D model of the tested machine

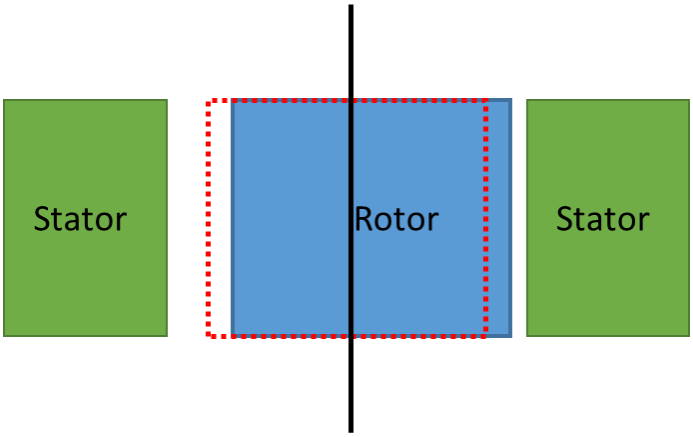

(a) Static eccentricity simulation

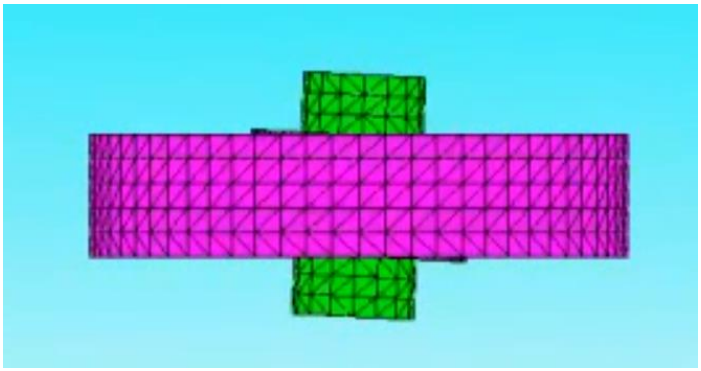

(b) Dynamic eccentricity simulation

Figure 7.4 FEA simulation diagrams of static and dynamic eccentricities

Two types of eccentricity are investigated in the simulation study. Static eccentricity occurs when the rotor rotates along the same central axis, but there is a small displacement of this centre axis, as shown in Fig 7.4 a. To simulate static eccentricity, the rotor has been moved from the rotation centre by 0.1 mm. Meanwhile dynamic eccentricity makes the rotor turn at the same central axis as in the health state, and there is an angular difference between its rotation axis and stator central axis as shown in Fig 7.4 b. By achieving the simulation of dynamic eccentricity, it is clear that there is an angle of 10 degree between the rotor and the central rotation axis.

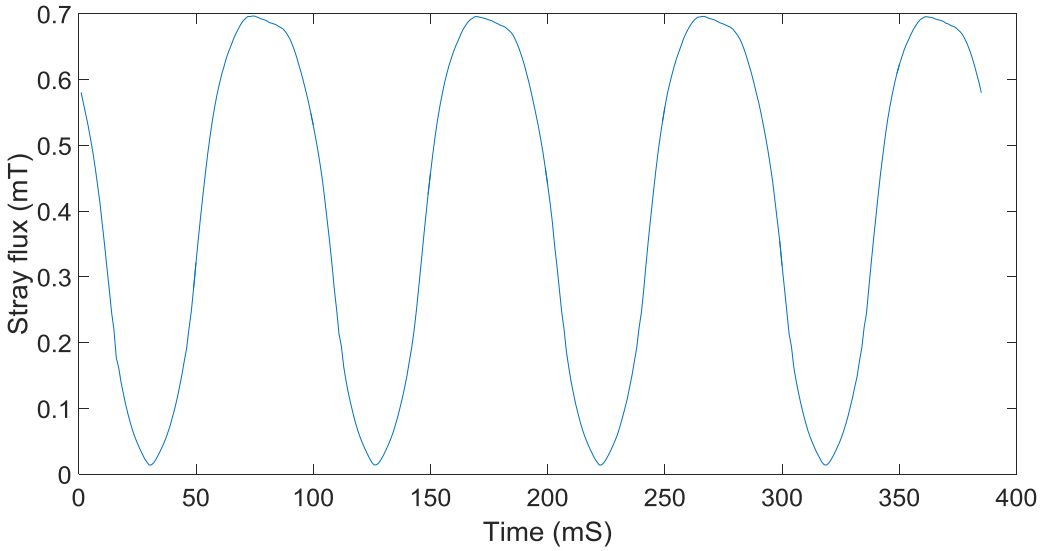

(a) Stray flux of the machine in a health state

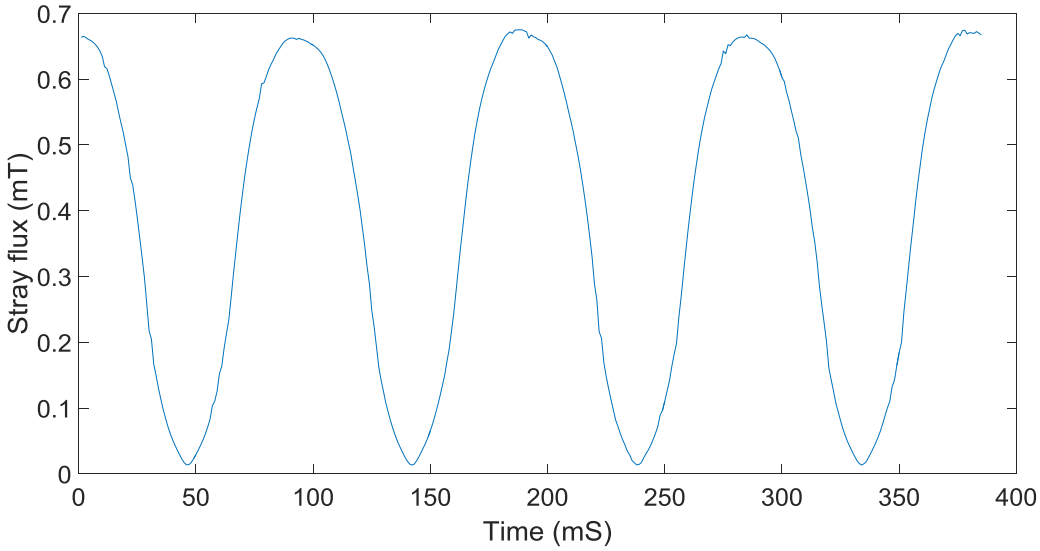

(b) Stray flux in the machine with static eccentricity

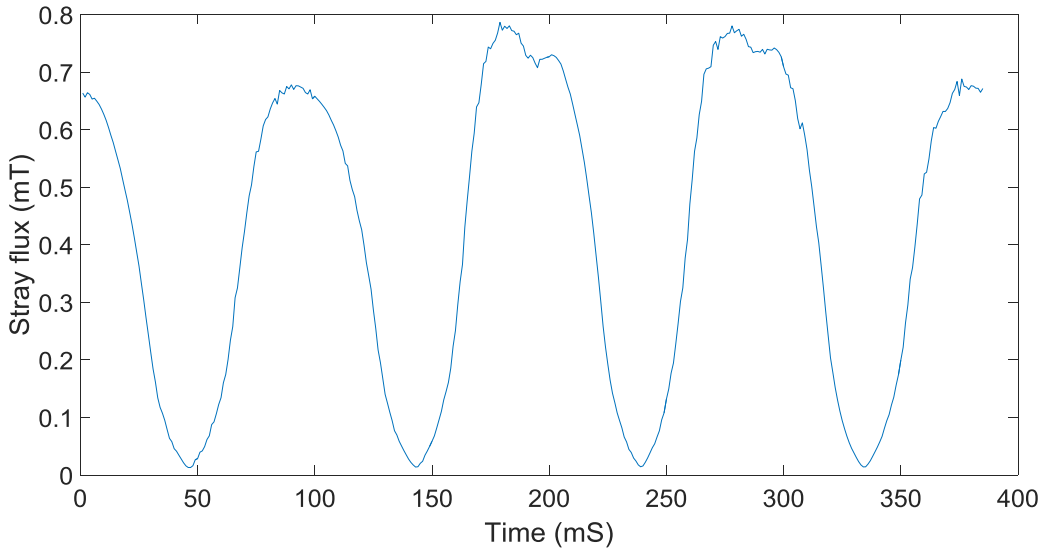

(c) Stray flux in the machine with dynamic eccentricity

Figure 7.5 Simulation results for stray flux information in three different states

The FEA simulation results are presented in Fig 7.5, showing the stray flux waveforms at the same detection point in the healthy state, and with static and dynamic eccentricity. From Fig 7.5 a, the stray flux waveform is almost a sin wave, as the FEA model is for an ideal brushless DC motor. However, there is region of a saturation at the peak of each waveform which is due to the influence of eddy current from the external yoke and stator laminations.

Fig 7.5 b represents the stray flux waveform of a machine with static eccentricity. Compared with the healthy case, the waveform contains several additional harmonic components, as there is some oscillation in the simulation stray flux data. The reason for the change in this stray flux waveform is that the machine's air-gap is no longer symmetrical. However, as the rotation centre has moved by 0.1mm, the air-gap flux density has also changed. The stray flux waveform for dynamic eccentricity is shown in Fig 7.5 c. As the air-gap changes during the machine's operation, the stray flux waveform includes many of unexpected harmonic components. From using the simulation software, different types of eccentricity have different effects on the stray flux waveform, and it's possible to analyse mechanical failures, such as unbalanced loads and bearing misalignments with referenced to stray flux information.

7.3 Experiment set up and validation

A mechanical failures test bench is built to validate the proposed method and monitoring system at Georgia Institute of Technology, Atlanta, USA. The test machine is a brushless DC

machine, which is widely used in industrial applications. The rated power is 2.5Kw and the system is supplied by a voltage source inverter with 220V/280v. The pole number of the machine is 6 and the no-load speed is 540 rpm with star connection. The frame and yoke are made of steel. Fig 7.6 a shows the overall test bench set up, and sensor's placement is shown in Fig 7.6 b. The unbalanced load has been emulated by installing ponderable clips on the fans of the motor, which is directly linked to the main shaft of the machine as shown in Fig 7.6 c. In this circumstance, by applying clips of different weight, two different unbalanced load situation can be performed in the experimented test rig. The GMR sensor is placed as shown in Fig 7.6 b to detect the stray magnetic flux. The output signal from the sensor is measured and captured by an NI data acquisition card and a PC with a sampling frequency of 5000 Hz. Furthermore, the bearing misalignment is created by changing the healthy main shaft bearing with a faulty one. The stray magnetic flux data is recorded while the motor is running at the steady state with different unbalance load and bearing misalignments.

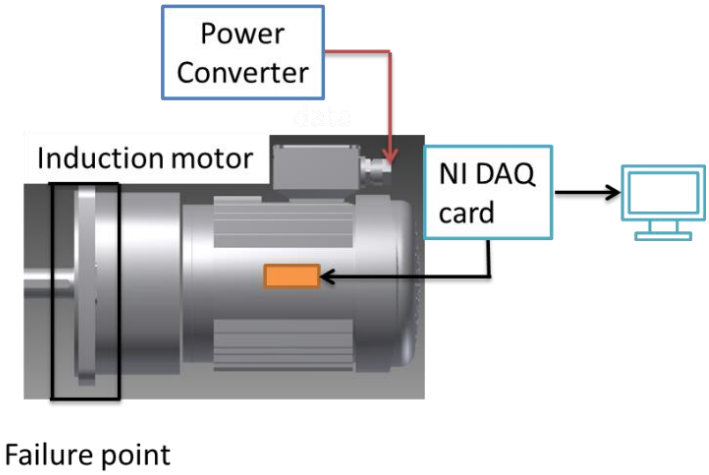

(a) Mechanical failure test bench system diagram

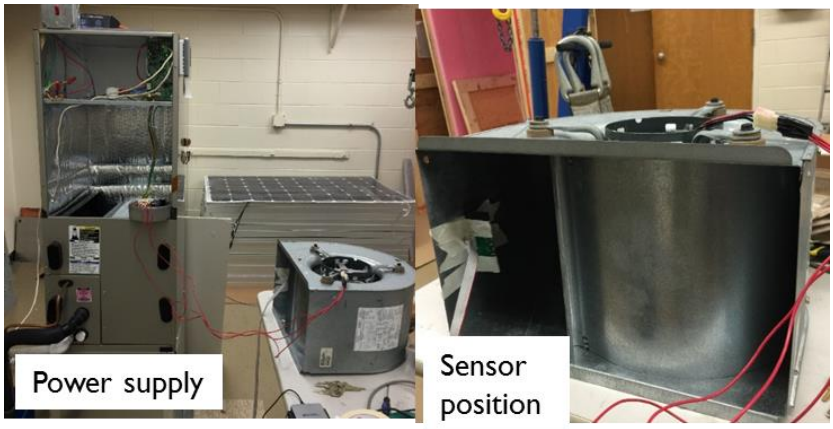

(b) Photographs of experimental test bench and GMR sensor positioning

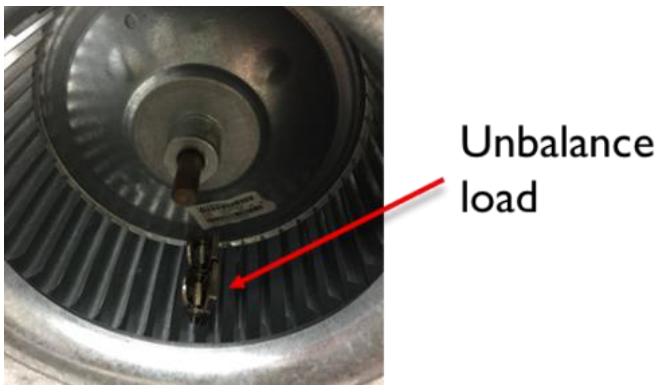

(c) Photograph of the application of unbalanced load with weighted clips

Figure 7.6 Mechanical failure test bench and system diagram

7.4 Data analysis and feature extraction

The proposed GMR sensor has been implemented outside of the tested machine as shown in the previous section. Stray flux information was captured, from a healthy state first as a baseline. Unbalanced load and bearing misalignments were also applied in the test bench. Fig 7.7 shows the signal output of the GMR sensors, which includes much noise. There are two main reasons for this noise. Firstly, due to the choice of its postioning, the GMR sensor is placed at the very outside of the external frame which inclues a large external air gap. Sencodly, the tested brushless DC motor is driven by a PWM conveter, from which the modulation waveform contains lots of harmonics and noise.

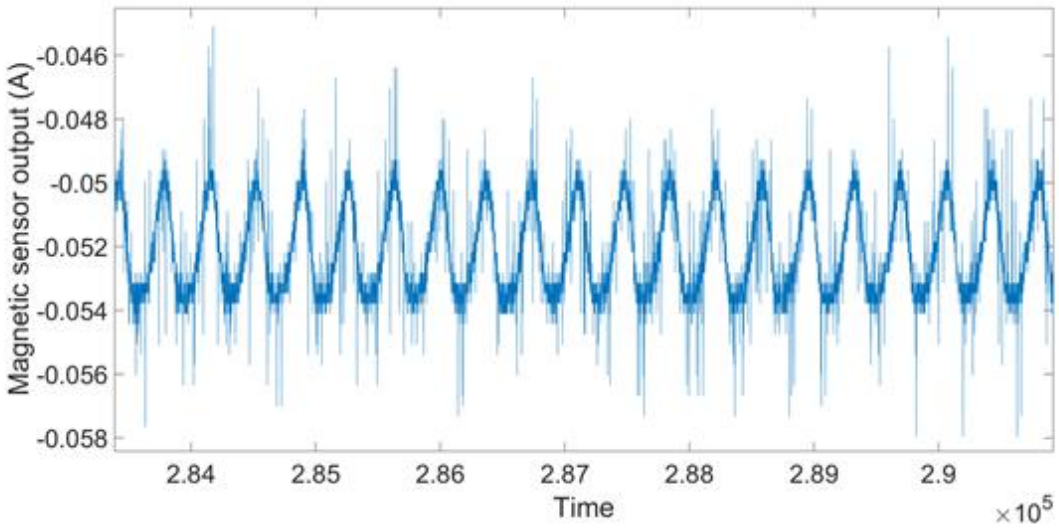

Figure 7.7 Output signals of magnetic sensors

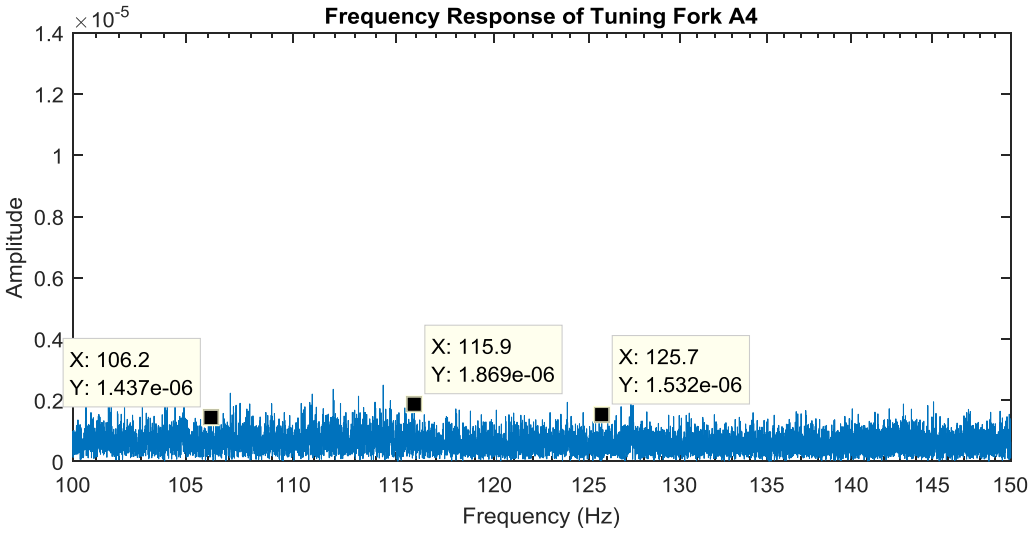

(a) Stray flux spectrum of the healthy test machine

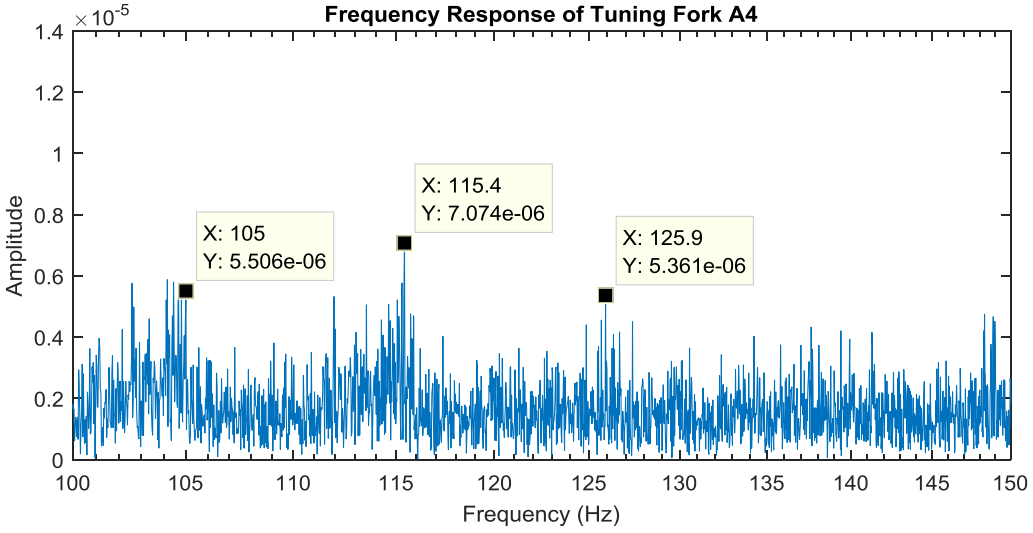

(b) Stray flux spectrum of the test machine under unbalanced load with one clip

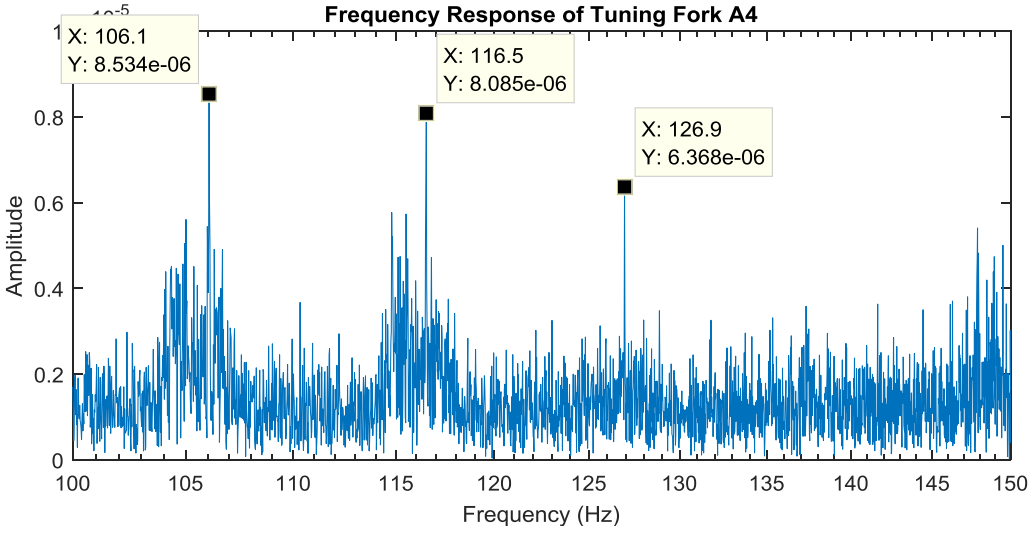

(c) Stray flux spectrum of the test machine under unbalanced load with two clips

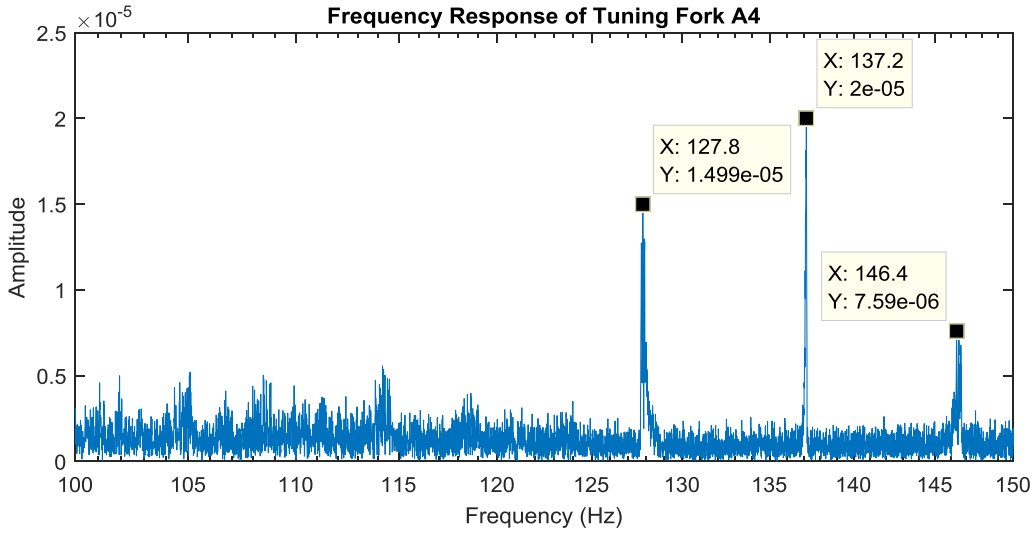

(d) Stray flux spectrum of the test machine with bearing misalignment

Figure 7.8 Stray flux spectrums of the test machine with different mechanical failures

The fast Fourier transformation is applied to address variations in the different harmonic components of stray flux data analysis. Fig 7.8 a shows the stray flux spectrum of the healthy test machine. As the machine is running at 180 RPM, the fundamental frequency f_s is 9 Hz, which is 0.000291 T. Additionally, reference to equation 7.3, the various indication harmonics can be calculated by choosing different integer m. The experimental results analysis in this section provides the changes of harmonic components at 105Hz(m=35), 117Hz(m=39), and 126Hz(m=42) for unbalanced load. This spectrum information can be set as the baseline data for comparison with different mechanical failures. Furthermore, there is also some noise in the high frequency region which might be caused by the PWM converter.

In Fig 7.8 b and c, the stray flux data is also analysed in the frequency domain with different unbalanced load (one and two weighted clips, 30g for each). Due to the increase in load, the amplitude of the fundamental frequency f_s 9 Hz is increased from 0.0004171 and 0.0008427 T respectively. Meanwhile, the frequency components at 105 Hz are also increased to 0.000005506 T with one clip load and to 0.000008534 T with two clips. The frequency components at 117Hz are also increased to 0.000007074 T with one clip load and to 0.000008085 T with two clips. The frequency components at 126Hz are also increased to 0.000005361 with one clip and 0.000006368 with two clips. As mentioned in Section 7.1 and

equation 7.2, once the unbalanced load occurs in the machine, the amplitude of the frequency component will be also increased as same as the stator current.

Fig 7.8 d presents the stray flux spectrum with a bearing misalignment in the tested brushless DC machine. Compared with the healthy state, the fundamental frequency f_s stays almost the same at 0.0002946 T. However, there are several high frequency components increases such as 137.2 Hz and 146.4 Hz, when bearing misalignment in present. Additionally, these frequency components are not influenced by the unbalanced load situation which may be a very good candidate to distinguish the bearing misalignment from unbalanced load. This is because the faulty bearing also has its own additional rotation frequency except the supply frequency. These higher order harmonic components can be indicators of bearing misalignment.

From the output of the GMR sensor, the signal includes lots of noise, which means that the target information is buried. Independent component analysis (ICA) is a technique that transforms a multivariate random signal into a signal having components that are mutually independent in the strict statistical sense. Recently, this technique has been demonstrated to be able to extract independent components from mixed signals. Here independence means that the information carried by one component cannot be inferred from that of other components. Statistically, this means that the joint probability of independent quantities is obtained as the product of the probability of each.

The ICA algorithm normally finds the independent components of a data set by minimizing or maximizing some measure of independence. A review of the solution to ICA problems shows that various theoretic information criteria have been used [101], such as mutual information, negentropy, and maximum entropy, as well as the maximum likelihood approach. The fixed-point algorithm is used due to its suitability for handling raw time domain data and its good convergence properties.

The ICA is one of the most important methods for blind source separation, which aims to provide independent signals from the signals with complex structure. ICA is statistically independent and nongaussian, which the any results of the components are not influenced by any other components. Considering the situation of bearing monitoring experiment in this research, different harmonics mixes with the fundamental frequency and noise. To describe this situation, the equation can be shown as following [112]:

$$X = AS \tag{7.4}$$

where elements of X is different harmonics in the collected stray flux data, elements of S is the original signals, A is the mixing matrix. To separate the harmonics from the mixtures of signals, it can be assumed that the mixing matrix A can be inverted with appropriate mixing coefficients:

$$S = WX \tag{7.5}$$

Where W is the coefficient matrix. In this case, the problem of ICA turns to calculate the statistical independent components of different solutions of X. As mentioned before, there are serval methods to solve ICA problem. Referenced the concept of mutual information, the first different entropy is shown as following:

$$H(y) = -\int f(y) \log f(y) dy \tag{7.6}$$

where H is the first different entropy, $y = (y_{1,} y_{2,} \dots, y_n)$ is random vector, $f(y)$ is density. As the largest entropy is the one with a Gaussian variable, the definition of negentropy can be found by normalizing the differential entropy.

$$J(y) = H\left(y_{gauss}\right) - H(y) \tag{7.7}$$

where y_{gauss} is a Gaussian random vector with the same matrix as y . The negentropy is zero with Gaussian variable and always nonnegative. In this case, mutual information can be shown as following:

$$I\left(y_{1,} y_{2,} \dots, y_n\right) = J(y) - \sum_i J(y_i) \tag{7.8}$$

where I is mutual information. As the mutual information includes the independence of random variable, it can be used to get the ICA transform. Due to the matrix W is found, the mutual information of the different situations of mixed matrix X can be minimized [112]. In this case, the independent components can be found.

Basically, feature extraction maps the processing of data from higher dimensional space to lower dimensional space. This step is intended to avoid the phenomenon of the curse of dimensionality. ICA was used here to reduce the feature dimensionality that contains 95% of the variation in eigenvalues. In this work, feature extraction produced several independent components (ICs) based on the eigenvalues. Also, from feature extraction using ICA, we can understand that there is a change from data features becomes components which are independent and uncorrelated, respectively. The first three independent and principal components are plotted in Fig 7.9. It can be observed that the clusters for the four conditions

are well separated. It can be seen that feature extraction using ICA can effectively separate well almost all conditions without overlapping.

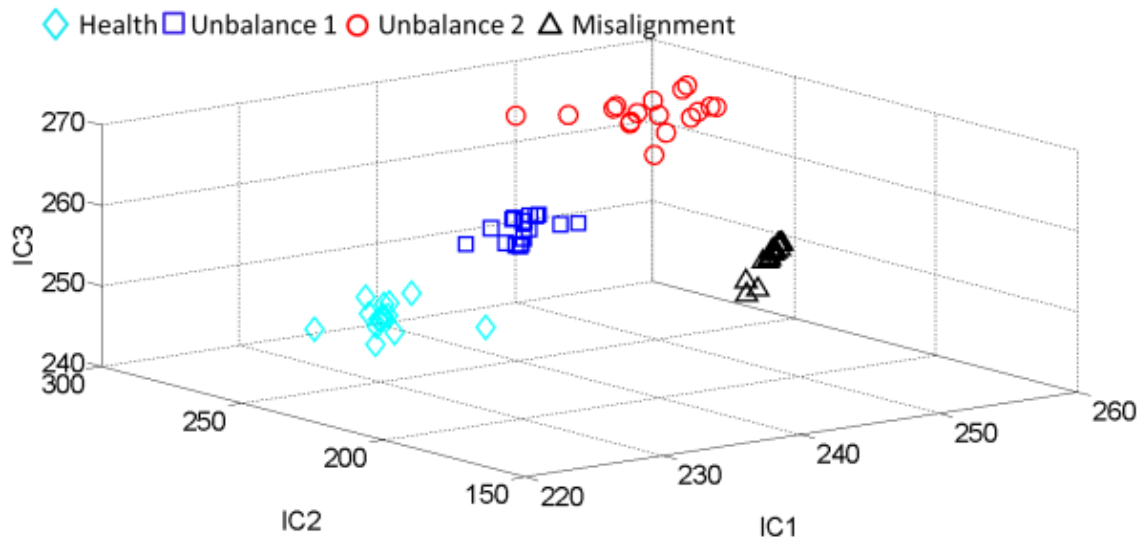

Figure 7.9 ICA analysis results of different mechanical failures

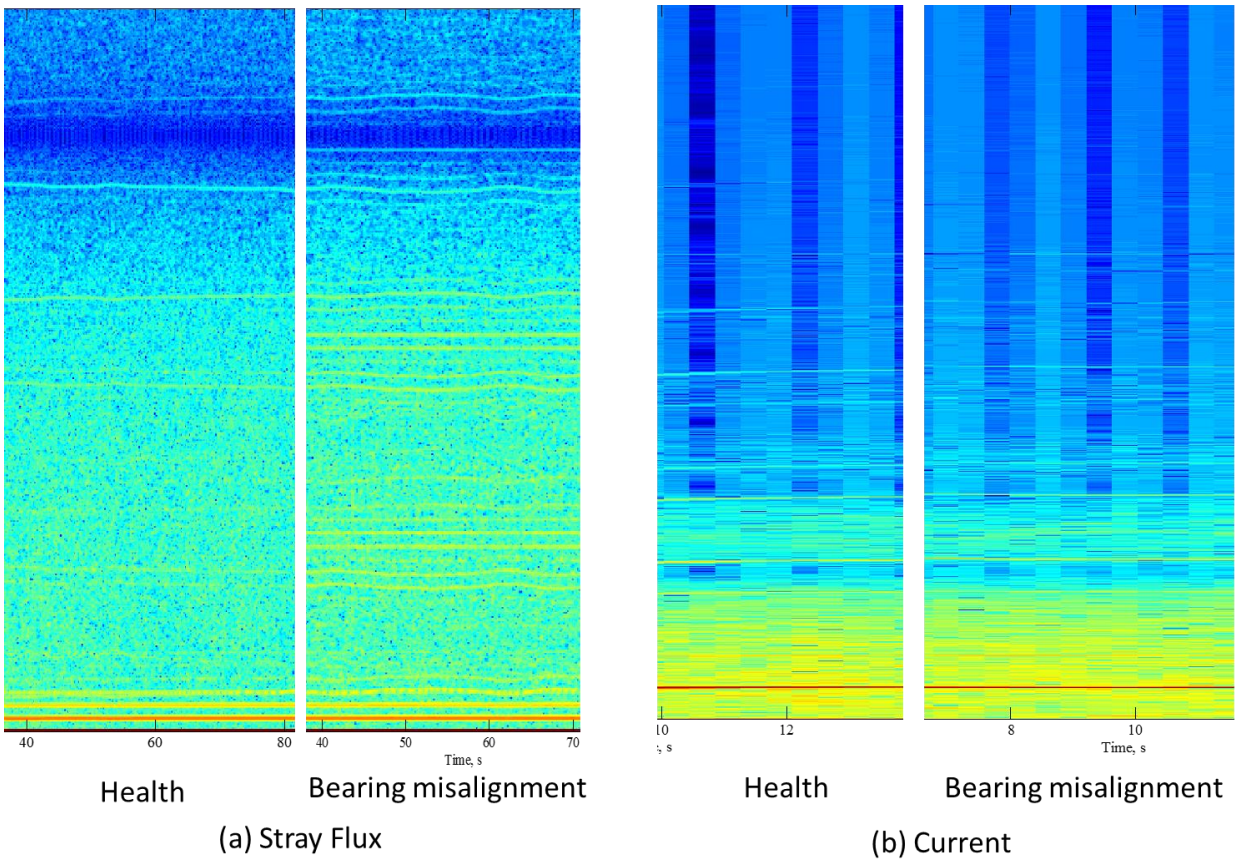

Figure 7.10 Comparison of spectrograms between stray flux and stator current

A comparison of the spectrograms for stray flux and stator current is shown in Fig 7.10. One of the advantages of the spectrogram is that it is easy to identify patterns in the time-

frequency domain. Fig 7.10 a presents a comparison of the stray flux data in the healthy state and with a bearing misalignment. Several high frequency harmonics appear in the stray flux spectrogram for bearing misalignment between 200 Hz to 600 Hz. However, in Fig 7.10 b, by measuring the stator current in the steady state, spectrograms of a healthy machine and one with a bearing misalignment are illustrated. It is unlikely that there is any obvious frequency components changing as the stray flux. The reason for this is that the stray flux information reflects the air-gap flux, which is directly linked to the health state of the machine; however, the stator current feature may be overwhelmed other components such as those for unbalanced load. By using the GMR sensor, stray flux monitoring gives a better performance in mechanical failure detection than the current basic monitoring technology.

7.5 Chapter summary

In this chapter, the proposed GMR sensor monitoring system detects two mechanical failures which are unbalanced load and bearing misalignment. Both of these types of mechanical failure can lead to machine air-gap eccentricity. Furthermore, the air gap eccentricity causes imbalance in magnetic pull and a nonsymmetrical air gap flux density distribution, which may cause unexpected vibrations and reductions in machine performance and efficiency. A comparison of stray flux data and current data for mechanical failures is also provided in this chapter. Where current data shows global information of the whole windings of the machine, the analysis of stray flux can illustrate local information which includes more detail and better resolutions

An FEA simulation model has been built in this chapter to investigate the influences of static and dynamic eccentricity on stray flux. The simulation results illustrate that both static and dynamic eccentricity can cause additional harmonic in the stray flux, which provide support for numerical analysis. A brushless DC test bench is built to simulate unbalanced load and bearing misalignment. By referencing the stray flux spectrum, it was found that the fundamental frequency component f_s and the side band $2f_s$ increased dramatically during the different states of unbalance load applied in the test bench. Additionally, the stray flux spectrum for bearing misalignment shows increases in several higher order harmonic components compared with healthy state base-line information. ICA is applied to these four sets of stray flux data, and it can be observed that the clusters the for four conditions are well separated, which suggests that this can be a good method to distinguish different types of failures. A comparison of stray flux and current detection is applied using the spectrogram, which it shows that stray flux gives a

better performance than current-based monitoring technology, as the richness signal information.

Chapter 8 Conclusions and Future Work

The key points and essential outcomes of the thesis are summarised in this chapter. Recommendations for the future work are also mentioned.

8.1 Research conclusion

Condition monitoring of electrical machines can not only reduce downtime but also increase reliability. To identify the research objectives, a comprehensive literature review has been carried out in this research, concerning failure modes and their causes. It is illustrated that stator winding failures and mechanical failures involving unbalance loads and bearing misalignments are the major types of failure occurring in these machines. Additionally, dynamic load is another major reason for failure. Therefore, it is necessary to develop a suitable condition monitoring system for electrical machines.

Previous research studies have mainly been based on different types of monitoring technologies, especially those based on stator current monitoring technology. However, the challenge of current monitoring methods include that they are invasive approaches and it is hard to distinguish between different types of failure. By comparing different monitoring techniques, it seems that stray flux analysis may be a good potential approach to electrical machine monitoring, as it is non-invasive approach, and delivers rich information. In this study, a novel magnetic sensor-based health monitoring system is designed and validated against different types of failures in electrical machines.

The research in this thesis is focused on developing and investigating stray magnetic field-based condition monitoring for electrical machines through analytical, numerical and experimental studies. The theoretical background of stray flux in electrical machines is described in chapter 3. By making several assumptions, a simple analytical model is built to represent the relationship between air-gap flux density and stray flux, which is influenced by the geometry of the machine and the electromagnetic properties of the stator lamination and

external frame only. Air-gap flux is an important parameter in an electrical machine's monitoring and analytical modelling, and the proposed stray flux monitoring system is also able to identify abnormalities in the electrical machine. In this case, a bridge can be built between the stray flux signal and different failures in electrical machine. Additionally, the feature extraction method used in this research is explained, which is the short time Fourier transform. The STFT can provide a spectrogram of the harmonics in an electrical machine depending on time variation. In the transient state, the spectrogram shows patterns of the distribution of changes in harmonics.

A novel stray flux-based machine health monitoring system is developed in this research, including a magnetic sensing system, and a wired and wireless data acquisition system. Comparison with other magnetic sensors, GMR sensors can provide a large detection range, high sensitivity and high bandwidth, and these devices are used in this research. Numerical models of the stray magnetic field are built to investigate the distribution of stray flux in electrical machines. From the simulation results, the location of the placement of the GMR sensor is determined, which is at the middle of the machine's external frame. Additionally, the z-direction of the stray flux is found to provide the strongest signal among the three directions. Combined with a signal conditioning circuit, a GMR sensor PCB board is designed and tested in chapter 3. Subsequently, the NI USB-6125 card is applied to the wired data acquisition system with a fully functional Labview program. Moreover, a wireless sensor network is also built to achieve wireless communication and high sampling rates of data acquisition.

Real-time load monitoring is carried out through the application of the proposed stray flux system design. Existing load monitoring methods for electrical machines are generally effective, but suffer from sensitivity problems at low speeds and non-linearity problems at high supply frequencies. The proposed GMR condition monitoring system is used to illustrate the load state during machine's operation. Three induction motors with different starting loading profiles are tested at two separate test benches and their results are analysed in the time-frequency domain. Their steady features and dynamic load response time through spectrograms under variable loads are extracted and correlated with load variations based on spectrogram information.

The relationship between stray flux information and stator winding failures is also investigated using the proposed stray magnetic field monitoring system. Simulation results from different stator winding short-circuits can provide the information about changes in stray flux. The thermal simulation of winding failures shows that there will be a temperature increasing when a short-circuit happens in the windings, which accelerates the degradation of

the winding. Based on the simulations, GMR sensors and arrays can be chosen and developed to meet test requirements. Experimental results have confirmed that the proposed condition monitoring system is capable of capturing stray magnetic flux even though the leaking flux signal is quite weak. By studying the measured stray flux in the time domain and especially in the frequency domain, several significant harmonic components can be used as indicators of stator winding faults. Phase-to-phase and phase-to-ground short-circuit failures are tested in the induction machine experimental bench. In comparing these two types of winding failures, the harmonic component with an amplitude of 30 Hz (half of fundamental frequency) is reduced once a phase-to-ground failure happens. However, other harmonic components are increased with reference to the healthy state of the tested induction machines. Thus, depending on the change in this frequency component of stray flux, these two winding failures can be separated.

Mechanical failures are major issues in machine diagnosis. The developed GMR sensor monitoring system can detect two types of mechanical failure which are unbalanced load and bearing misalignment. Both of these mechanical failures can lead to eccentricity in the machine's air-gap. Furthermore, air gap eccentricity causes unbalanced magnetic pull and a non-symmetrical air gap flux density distribution, which may casuse unexpected vibration and reductions in machine performance and efficiency. An FEA simulation model has been built in chapter 7 to investigate the influence of static and dynamic eccentricity on the stray flux. The simulation results illustrate that both static and dynamic eccentricity can cause additional harmonics in the stray flux, which provide support for numerical analysis. A brushless DC test bench is built to simulate the unbalance load and bearing misalignment. By referencing the stray flux spectrum, the fundamental frequency component fs and the side band 2fs increased dramatically during the different states of unbalanced load occurring in the test bench. Additionally, the stray flux spectrum for bearing misalignment shows increases in several higher order harmonic components compared with healthy state base-line information. ICA is applied to these four sets of stray flux data, and it can be observed that the clusters for the four conditions are well separated, which means that this may be a good method to distinguish between different types of failures. A comparison between stray flux and current detection is applied using spectrograms, showing stray flux analysis gives better performance than current-based monitoring, due to the richness information in the signal.

8.2 Future work

Future work in stray flux condition monitoring in electrical machines will be geared towards improvements in the performance of failure detection and feature extraction, such as

in providing early warning systems and lifetime predictions. These improvements will also help in moving towards commercial feasibility. As it is a non-invasive, low-cost approach, the proposed stray flux monitoring system can be implemented in industrial drive systems to increase reliability and reduce maintenance costs.

Although the stray flux model in this research is built with numerical and analytical approaches, the analytical model is a simplified model to demonstrate the methodology and theoretical background of stray flux monitoring. In reality, different aspects of machine design will influence the stray flux information collected, such as in terms of phase shift and noise. Additionally, finite element analysis is time-consuming. To develop a detailed analytical stray flux model, it would not only be helpful to build a model-based condition monitoring system so as to reduce calculation time, but also to improve the understanding of the principles of stray flux distribution inside electrical machines.

At this moment, the proposed stray flux condition monitoring system usese GMR sensors to collect the weak magnetic flux information. Although GMR sensors can provide accurate stray flux information, the drawback of this approach is that one GMR sensor can only collect stray flux information at one point. Future work may focus on implementing magnetic cameras in the stray flux condition monitoring system. Magnetic cameras could be applied to capture not only the stray flux at one point, but also stray flux density distributions over larger areas. However, the sampling frequency of magnetic cameras are relatively low at the moment, and this might be improved in future research work. Additionally, to improve sensitivity and dynamic range, the tunnel magnetoresistance (TMR) sensor could be applied in the monitoring system instead of the current GMR sensor, and this might can provide more accurate local health information about the machine.

As an electrical machine is totally enclosed, the investigation of the mechanisms and degradations associated with different failures, especially of the winding, insulation and bearings, are still not fully understood. Moreover, every component of an electrical machine may suffer from thermal, electrical and machine stresses. These factors may influence each other, and so the complexities of the failure procedure are increased. To determine the mechanisms of the different failures, a lifetime model of each component may be able to be built in the future to help in achieving early warning and prognosis.

Stray flux monitoring technology has its own disadvantages, such as the issue of noise. Future studies of stray flux monitoring should consider data fusion and the implementation of advanced signal processing and decision making algorithms. By combining stray flux analysis

with other monitoring techniques such as of temperature, current and vibration, the accuracy and capability of distinguishing between different types of failure can be increased in future research. Furthermore, non-negative matrix factorization (NMF) is an approach to decompose the features from data, which is more effective than ICA and could be used in the future. The experiments and failure samples of electrical machines used in this research are limited due to restrictions of the research resources. Future work also needs to focus on conducting more experimental studies and failure tests for a stray flux condition monitoring system. In this case, the relationship between the stray magnetic field and failures in electrical machines can be more fully understood.

References

[1] Z. Pinjia, L. Bin, and T. G. Habetler, "An active stator temperature estimation technique for thermal protection of inverter-fed induction motors with considerations of impaired cooling detection," in *Electric Machines and Drives Conference, 2009. IEMDC '09. IEEE International*, 2009, pp. 1326-1332.

[2] B. Yazici, G. B. Kliman, W. J. Premerlani, R. A. Koegl, and A. Abdel-Malek, "An adaptive, on-line, statistical method for detection of broken bars in motors using stator current and torque estimation," in *Industry Applications Conference, 1997. Thirty-Second IAS Annual Meeting, IAS '97., Conference Record of the 1997 IEEE*, 1997, pp. 221-226 vol.1.

[3] B. Boulkroune, M. Galvez-Carrillo, and M. Kinnaert, "Additive and multiplicative fault diagnosis for a doubly-fed induction generator," in *Control Applications (CCA), 2011 IEEE International Conference on*, 2011, pp. 1302-1308.

[4] I. Rodriguez, R. Alves, and V. Guzman, "Analysis of air gap flux to detect induction motor faults," in *Universities Power Engineering Conference, 2006. UPEC '06. Proceedings of the 41st International*, 2006, pp. 690-694.

[5] J. Li, D. Choi, and Y. Cho, "Analysis of rotor eccentricity in switched reluctance motor with parallel winding using fem," *Ieee Transactions on Magnetics*, vol. 45, pp. 2851-2854, Jun 2009.

[6] A. H. Bonnett, "Analysis of winding failures in three-phase squirrel cage induction motors," *Industry Applications, IEEE Transactions on*, vol. IA-14, pp. 223-226, 1978.

[7] T. De Rybel, A. Singh, J. A. Vandermaar, M. Wang, J. R. Marti, and K. D. Srivastava, "Apparatus for online power transformer winding monitoring using bushing tap injection," *Ieee Transactions on Power Delivery*, vol. 24, pp. 996-1003, Jul 2009.

[8] M. A. Awadallah and M. A. Morcos, "Application of AI tools in fault diagnosis of electrical machines and drives - An overview," *Ieee Transactions on Energy Conversion*, vol. 18, pp. 245-251, Jun 2003.

[9] P. S. Barendse, B. Herndler, M. A. Khan, and P. Pillay, "The application of wavelets for the detection of inter-turn faults in induction machines," in *Electric Machines and Drives Conference, 2009. IEMDC '09. IEEE International*, 2009, pp. 1401-1407.

[10] Q. D. Sun, Z. X. Zhou, and W. Q. Guo, "An approach of insulation state on-line monitoring and fault diagnosis for generator and its application," in *Power and Energy Engineering Conference (APPEEC), 2010 Asia-Pacific*, 2010, pp. 1-6.

[11] Y. Amirat, V. Choqueuse, M. E. H. Benbouzid, and J. F. Charpentier, "Bearing fault detection in DFIG-based wind turbines using the first Intrinsic Mode Function," in *Electrical Machines (ICEM), 2010 XIX International Conference on*, 2010, pp. 1-6.

[12] C. Harlisca, L. Szabo, L. Frosini, and A. Albini, "Bearing faults detection in induction machines based on statistical processing of the stray fluxes measurements," in *Diagnostics for Electric Machines, Power Electronics and Drives (SDEMPED), 2013 9th IEEE International Symposium on*, 2013, pp. 371-376.

[13] A. Cassat, C. Espanet, and N. Wavre, "BLDC motor stator and rotor iron losses and thermal behavior based on lumped schemes and 3-D FEM analysis," *Ieee Transactions on Industry Applications*, vol. 39, pp. 1314-1322, Sep-Oct 2003.

[14] A. Yazidi, H. Henao, and G. A. Capolino, "Broken rotor bars fault detection in squirrel cage induction machines," in *Electric Machines and Drives, 2005 IEEE International Conference on*, 2005, pp. 741-747.

[15] Z. Yujiao, R. Jiangjun, H. Tao, Y. Xiaoping, Z. Houquan, and Y. Gao, "Calculation of temperature rise in air-cooled induction motors through 3-d coupled electromagnetic fluid-dynamical and thermal finite-element analysis," *Magnetics, IEEE Transactions on*, vol. 48, pp. 1047-1050, 2012.

[16] K. Bacha, M. Gossa, H. Henao, and G. A. Capolino, "Comparative investigation of diagnosis media of stator voltage asymmetry and rotor broken bars in induction machines," in *IEEE Industrial Electronics, IECON 2006 - 32nd Annual Conference on*, 2006, pp. 5040-5045.

[17] C. Kral, A. Haumer, M. Haigis, H. Lang, and H. Kapeller, "Comparison of a cfd analysis and a thermal equivalent circuit model of a tefc induction machine with measurements," *Ieee Transactions on Energy Conversion*, vol. 24, pp. 809-818, Dec 2009.

[18] Y. Wenxian, P. J. Tavner, and M. Wilkinson, "Condition monitoring and fault diagnosis of a wind turbine with a synchronous generator using wavelet transforms," in *Power Electronics, Machines and Drives, 2008. PEMD 2008. 4th IET Conference on*, 2008, pp. 6-10.

[19] C. J. Crabtree, S. Djurovic, P. J. Tavner, and A. C. Smith, "Condition monitoring of a wind turbine DFIG by current or power analysis," in *Power Electronics, Machines and Drives (PEMD 2010), 5th IET International Conference on*, 2010, pp. 1-6.

[20] M. R. Wilkinson, F. Spinato, and P. J. Tavner, "Condition monitoring of generators other subassemblies in wind turbine drive trains," in *Diagnostics for Electric Machines, Power Electronics and Drives, 2007. SDEMPED 2007. IEEE International Symposium on*, 2007, pp. 388-392.

[21] S. J. Watson, B. J. Xiang, Y. Wenxian, P. J. Tavner, and C. J. Crabtree, "Condition monitoring of the power output of wind turbine generators using wavelets," *Energy Conversion, IEEE Transactions on*, vol. 25, pp. 715-721, 2010.

[22] L. M. Popa, B. B. Jensen, E. Ritchie, and I. Boldea, "Condition monitoring of wind generators," in *Industry Applications Conference, 2003. 38th IAS Annual Meeting. Conference Record of the*, 2003, pp. 1839-1846 vol.3.

[23] Y. Wenxian, P. J. Tavner, C. J. Crabtree, and M. Wilkinson, "Cost-effective condition monitoring for wind turbines," *Industrial Electronics, IEEE Transactions on*, vol. 57, pp. 263-271, 2010.

[24] G. Gao and W. Chen, "Design challenges of wind turbine generators," in *Electrical Insulation Conference, 2009. EIC 2009. IEEE*, 2009, pp. 146-152.

[25] J. Vieira, M. Nunes, and U. H. Bezerra, "Design of optimal PI controllers for doubly fed induction generators in wind turbines using genetic algorithm," in *Power and Energy Society General Meeting - Conversion and Delivery of Electrical Energy in the 21st Century, 2008 IEEE*, 2008, pp. 1-7.

[26] L. Zarri, M. Mengoni, Y. Gritli, A. Tani, F. Filippetti, G. Serra, and D. Casadei, "Detection and localization of stator resistance dissymmetry based on multiple reference frame controllers in multiphase induction motor drives," *Industrial Electronics, IEEE Transactions on*, vol. 60, pp. 3506-3518, 2013.

[27] T. Utsumi and I. Yamaguchi, "Detection and location of inter-turn short-circuit in linear induction motor," in *Diagnostics for Electric Machines, Power Electronics and Drives, 2003. SDEMPED 2003. 4th IEEE International Symposium on*, 2003, pp. 63-68.

[28] J. Penman, H. G. Sedding, B. A. Lloyd, and W. T. Fink, "Detection and location of interturn short-circuits in the stator windings of operating motors," *Energy Conversion, IEEE Transactions on*, vol. 9, pp. 652-658, 1994.

[29] C. Demian, A. Mpanda-Mabwe, H. Henao, and G. A. Capolino, "Detection of induction machines rotor faults at standstill using signals injection," *Ieee Transactions on Industry Applications*, vol. 40, pp. 1550-1559, Nov-Dec 2004.

[30] G. Joksimovic and J. Penman, "The detection of interturn short-circuits in the stator windings of operating motors," in *Industrial Electronics Society, 1998. IECON '98. Proceedings of the 24th Annual Conference of the IEEE*, 1998, pp. 1974-1979 vol.4.

[31] H. Douglas, P. Pillay, and P. Barendse, "The detection of interturn stator faults in doubly-fed induction generators," in *Industry Applications Conference, 2005. Fourtieth IAS Annual Meeting. Conference Record of the 2005*, 2005, pp. 1097-1102 Vol. 2.

[32] C. Kral, F. Pirker, and G. Pascoli, "Detection of rotor faults in squirrel-cage induction machines at standstill for batch tests by means of the Vienna Monitoring Method," *Ieee Transactions on Industry Applications*, vol. 38, pp. 618-624, May-Jun 2002.

[33] V. Dinkhauser and F. W. Fuchs, "Detection of rotor turn-to-turn faults in doubly-fed induction generators in wind energy plants by means of observers," in *Power Electronics and Applications, 2009. EPE '09. 13th European Conference on*, 2009, pp. 1-10.

[34] A. Fazli, M. Fazli, S. Hesami, A. Seif, and A. Shafighi Malekshah, "The detection of VFC and STATCOM faults in Doubly Fed Induction Generator," in *Environment and Electrical Engineering (EEEIC), 2012 11th International Conference on*, 2012, pp. 161-165.

[35] K. D. Sousa, A. A. Hafner, H. J. Kalinowski, and J. C. C. da Silva, "Determination of temperature dynamics and mechanical and stator losses relationships in a three-phase induction motor using fiber bragg grating sensors," *Ieee Sensors Journal*, vol. 12, pp. 3054-3061, Oct 2012.

[36] L. Frosini, A. Borin, L. Girometta, and G. Venchi, "Development of a leakage flux measurement system for condition monitoring of electrical drives," in *Diagnostics for Electric Machines, Power Electronics & Drives (SDEMPED), 2011 IEEE International Symposium on*, 2011, pp. 356-363.

[37] E. Al-Ahmar, M. E. H. Benbouzid, Y. Amirat, and S. E. Ben Elghali, "DFIG-based wind turbine fault diagnosis using a specific discrete wavelet transform," in *Electrical Machines, 2008. ICEM 2008. 18th International Conference on*, 2008, pp. 1-6.

[38] C. Harlisca, L. Szabo, L. Frosini, and A. Albini, "Diagnosis of rolling bearings faults in electric machines through stray magnetic flux monitoring," in *Advanced Topics in Electrical Engineering (ATEE), 2013 8th International Symposium on*, 2013, pp. 1-6.

[39] S. Djurovic, S. Williamson, and A. Renfrew, "Dynamic model for doubly-fed induction generators with unbalanced excitation, both with and without winding faults," *Electric Power Applications, IET*, vol. 3, pp. 171-177, 2009.

[40] M. J. Islam, H. V. Khang, A. Repo, and A. Arkkio, "Eddy-current loss and temperature rise in the form-wound stator winding of an inverter-fed cage induction motor," *Magnetics, IEEE Transactions on*, vol. 46, pp. 3413-3416, 2010.

[41] R. Romary, R. Pusca, J. P. Lecointe, and J. F. Brudny, "Electrical machines fault diagnosis by stray flux analysis," *2013 Ieee Workshop on Electrical Machines Design, Control and Diagnosis (Wemdcd)*, 2013.

[42] Y. S. Chen, Y. D. Cheng, J. J. Liao, and C. C. Chiu, "Electromagnetic-rotordynamic integrated vibration analysis for electrical machines," *Proceedings of the Institution of Mechanical Engineers Part C-Journal of Mechanical Engineering Science*, vol. 223, pp. 2549-2559, Nov 2009.

[43] M. R. Bissonnette, "End-winding vibration monitoring and interpretation," in *Electrical Insulation (ISEI), Conference Record of the 2012 IEEE International Symposium on*, 2012, pp. 285-290.

[44] S. Ul Haq and T. Bashir, "Evaluation of induction motor groundwall insulation using infrared thermography," *Second International Conference on Emerging Technologies 2006, Proceedings*, pp. 416-420, 2006.

[45] D. Casadei, F. Filippetti, A. Stefani, C. Rossi, A. Yazidi, and G. A. Capolino, "Experimental fault characterization of doubly fed induction machines for wind power generation," *2006 International Symposium on Power Electronics, Electrical Drives, Automation and Motion, Vols 1-3*, pp. 1281-1286, 2006.

[46] D. Casadei, F. Filippetti, A. Stefani, C. Rossi, A. Yazidi, and G. A. Capolino, "Experimental fault characterization of doubly fed induction machines for wind power generation," in *Power Electronics, Electrical Drives, Automation and Motion, 2006. SPEEDAM 2006. International Symposium on*, 2006, pp. 1281-1286.

[47] S. P. Verma and R. S. Girgis, "Experimental verification of resonant frequencies and vibration behaviour of stators of electrical machines. Part 1: Models, experimental procedure and apparatus," *Electric Power Applications, IEE Proceedings B*, vol. 128, pp. 12-21, 1981.

[48] V. Kontargyri, C. Tsirekis, S. Kabanaros, A. Sakarellos, A. Moronis, N. Kolliopoulos, and S. Kaminaris, "An expert system for fault diagnosis, repairing and maintenance of electrical machines," *Aee '07: Proceedings of the 6th Wseas International Conference on Applications of Electrical Engineering*, pp. 166-171, 2007.

[49] M. R. Wilkinson and P. J. Tavner, "Extracting condition monitoring information from a wind turbine drive train," in *Universities Power Engineering Conference, 2004. UPEC 2004. 39th International*, 2004, pp. 591-594 vol. 1.

[50] L. R. Cusido, A. Garcia, J. A. Rosero, and J. A. Ortega, "Fault detection in induction machines by using continuous and discrete wavelet decomposition," in *Power Electronics and Applications, 2007 European Conference on*, 2007, pp. 1-8.

[51] D. Basak, A. Tiwari, and S. P. Das, "Fault diagnosis and condition monitoring of electrical machines - A review," *2006 IEEE International Conference on Industrial Technology, Vols 1-6*, pp. 2987-2992, 2006.

[52] S. Nandi and H. A. Toliyat, "Fault diagnosis of electrical machines - A review," *Iemdc'99 - Ieee International Electric Machines and Drives Conference, Proceedings*, pp. 219-221, 1999.

[53] A. Yazidi, H. Henao, G. A. Capolino, M. Artioli, F. Filippetti, and D. Casadei, "Flux signature analysis: An alternative method for the fault diagnosis of induction machines," in *Power Tech, 2005 IEEE Russia*, 2005, pp. 1-6.

[54] H. Henao, C. Demian, and G. A. Capolino, "A frequency-domain detection of stator winding faults in induction machines using an external flux sensor," *Ieee Transactions on Industry Applications*, vol. 39, pp. 1272-1279, Sep-Oct 2003.

[55] H. Henao, C. Demian, and G. A. Capolino, "A frequency-domain detection of stator winding faults in induction machines using an external flux sensor," *Industry Applications, IEEE Transactions on*, vol. 39, pp. 1272-1279, 2003.

[56] S. M. J. R. Fatemi, H. Henao, and G. A. Capolino, "Gearbox monitoring by using the stray flux in an induction machine based electromechanical system," *2008 Ieee Mediterranean Electrotechnical Conference, Vols 1 and 2*, pp. 463-468, 2008.

[57] M. S. N. Sdid and M. E. H. Benbouzid, "H-G diagram based rotor parameters identification for induction motors thermal monitoring," *Energy Conversion, IEEE Transactions on*, vol. 15, pp. 14-18, 2000.

[58] S. H. Kia, H. Henao, and G. A. Capolino, "A high-resolution frequency estimation method for three-phase induction machine fault detection," *Ieee Transactions on Industrial Electronics*, vol. 54, pp. 2305-2314, Aug 2007.

[59] K. A. Folly and S. Sheetekela, "Impact of fixed and variable speed wind generators on the transient stability of a power system network," in *Power Systems Conference and Exposition, 2009. PSCE '09. IEEE/PES*, 2009, pp. 1-7.

[60] E. Levi, A. Lamine, and A. Cavagnino, "Impact of stray load losses on vector control accuracy in current-fed induction motor drives," *Energy Conversion, IEEE Transactions on*, vol. 21, pp. 442-450, 2006.

[61] A. Yazidi, H. Hena, G. A. Capolino, M. Artioli, and F. Filippetti, "Improvement of frequency resolution for three-phase induction machine fault diagnosis," in *Industry Applications Conference, 2005. Fourtieth IAS Annual Meeting. Conference Record of the 2005*, 2005, pp. 20-25 Vol. 1.

[62] A. H. Bonnett and C. Yung, "Increased efficiency versus increased reliability," *Industry Applications Magazine, IEEE,* vol. 14, pp. 29-36, 2008.

[63] A. M. da Silva, R. J. Povinelli, and N. A. O. Demerdash, "Induction machine broken bar and stator short-circuit fault diagnostics based on three-phase stator current envelopes," *Industrial Electronics, IEEE Transactions on,* vol. 55, pp. 1310-1318, 2008.

[64] S. H. Kia, H. Henao, G. A. Capolino, and C. Martis, "Induction machine broken bars fault detection using stray flux after supply disconnection," in *IEEE Industrial Electronics, IECON 2006 - 32nd Annual Conference on*, 2006, pp. 1498-1503.

[65] K. Bacha, H. Henao, M. Gossa, and G. A. Capolino, "Induction machine fault detection using stray flux EMF measurement and neural network-based decision," *Electric Power Systems Research,* vol. 78, pp. 1247-1255, Jul 2008.

[66] J. Cusido, J. A. Rosero, J. A. Ortega, A. Garcia, and L. Romeral, "Induction motor fault detection by using wavelet decomposition on dq0 components," in *Industrial Electronics, 2006 IEEE International Symposium on*, 2006, pp. 2406-2411.

[67] J.-q. Li, L. Ma, and D.-y. Wang, "Influence of stator turn-to-turn short-circuit on magnetic field of DFIG," in *Electrical Machines and Systems (ICEMS), 2011 International Conference on*, 2011, pp. 1-5.

[68] S. N. Huang and H. Y. Yu, "Intelligent fault monitoring and diagnosis in electrical machines," *Measurement,* vol. 46, pp. 3640-3646, Nov 2013.

[69] A. J. M. Cardoso, S. M. A. Cruz, and D. S. B. Fonseca, "Inter-turn stator winding fault diagnosis in three-phase induction motors, by Park's vector approach," *Energy Conversion, IEEE Transactions on,* vol. 14, pp. 595-598, 1999.

[70] B.-q. Xu, H.-m. Li, and L.-l. Sun, "Joint detection of stator winding inter-turn short-circuit and rotor bar breaking fault in squirrel cage induction motors," in *Power System Technology, 2002. Proceedings. PowerCon 2002. International Conference on*, 2002, pp. 761-764 vol.2.

[71] T. Utsumi and I. Yamaguchi, "Location of inter-turn short-circuit in linear induction motor by dc measurement," in *Diagnostics for Electric Machines, Power Electronics and Drives, 2005. SDEMPED 2005. 5th IEEE International Symposium on*, 2005, pp. 1-5.

[72] Q. F. Lu, Z. T. Cao, and E. Ritchie, "Model of stator inter-turn short-circuit fault in doubly-fed induction generators for wind turbine," in *Power Electronics Specialists Conference, 2004. PESC 04. 2004 IEEE 35th Annual*, 2004, pp. 932-937 Vol.2.

[73] L. Qian, T. Breikin, and W. Hong, "Modelling and fault diagnosis for DFIGs with multi-phase inter-turn short-circuit," in *Advanced Mechatronic Systems (ICAMechS), 2011 International Conference on*, 2011, pp. 155-160.

[74] R. F. M. Brandao, J. A. B. Carvalho, and F. P. M. Barbosa, "Monitoring systems for wind generators maintenance," in *Universities Power Engineering Conference (UPEC), 2010 45th International*, 2010, pp. 1-4.

[75] P. A. Zotos, "Motor failures due to steep fronted switching surges: the need for surge protection - user's experience," *Industry Applications, IEEE Transactions on,* vol. 30, p. 1514, 1994.

[76] T. A. Lipo and K. C. Chang, "A new approach to flux and torque-sensing in induction machines," *Industry Applications, IEEE Transactions on,* vol. IA-22, pp. 731-737, 1986.

[77] C. Siwei and T. G. Habetler, "A new method to detect stator turn-to-turn faults in a closed-loop multiple-motor drive system," in *Diagnostics for Electric Machines, Power Electronics and Drives, 2009. SDEMPED 2009. IEEE International Symposium on*, 2009, pp. 1-6.

[78] A. Yazidi, G. A. Capolino, F. Filippetti, and D. Casadei, "A new monitoring system for wind turbines with doubly-fed induction generators," in *Electrotechnical Conference, 2006. MELECON 2006. IEEE Mediterranean*, 2006, pp. 1142-1145.

[79] L. Frosini, A. Borin, A. Albini, and F. Benzi, "New techniques to simulate and diagnose stator winding faults in low voltage induction motors," in *Electrical Machines (ICEM), 2012 XXth International Conference on*, 2012, pp. 1783-1789.

[80] J. Castellon, J. Bouquart, J. P. Reboul, and A. Toureille, "A new tool to study the ageing of the winding insulation of electrical machines," in *Electrical Insulation and Dielectric Phenomena, 1997. IEEE 1997 Annual Report., Conference on*, 1997, pp. 447-450 vol.2.

[81] T. M. Wolbank, P. Nussbaumer, H. Chen, and P. E. Macheiner, "Non-invasive detection of rotor cage faults in inverter fed induction machines at no load and low speed," *2009 Ieee International Symposium on Diagnostics for Electric Machines, Power Electronics and Drives*, pp. 143-149, 2009.

[82] L. Frosini, A. Borin, L. Girometta, and G. Venchi, "A novel approach to detect short-circuits in low voltage induction motor by stray flux measurement," in *Electrical Machines (ICEM), 2012 XXth International Conference on*, 2012, pp. 1538-1544.

[83] L. Qian and T. Breikin, "Observer based fault detection for stator inter-turn short-circuit in wind turbine DFIGs," in *Modelling, Identification and Control (ICMIC), The 2010 International Conference on*, 2010, pp. 483-488.

[84] S. Williamson and S. Djurovic, "Origins of stator current spectra in DFIGs with winding faults and excitation asymmetries," in *Electric Machines and Drives Conference, 2009. IEMDC '09. IEEE International*, 2009, pp. 563-570.

[85] F. Blaabjerg, R. Teodorescu, M. Liserre, and A. V. Timbus, "Overview of control and grid synchronization for distributed power generation systems," *Ieee Transactions on Industrial Electronics,* vol. 53, pp. 1398-1409, Oct 2006.

[86] C. Kral, A. Haumer, and S. Lee, "A practical thermal model for the estimation of permanent magnet and stator winding temperatures," *Power Electronics, IEEE Transactions on,* vol. PP, pp. 1-1, 2013.

[87] D. F. Leite, M. B. Hell, P. H. Diez, B. S. L. Gariglio, L. O. Nascimento, and P. Costa, "Real-time model-based fault detection and diagnosis for alternators and induction motors," in *Electric Machines & Drives Conference, 2007. IEMDC '07. IEEE International*, 2007, pp. 202-207.

[88] A. Gandhi, T. Corrigan, and L. Parsa, "Recent advances in modeling and online detection of stator interturn faults in electrical motors," *Industrial Electronics, IEEE Transactions on,* vol. 58, pp. 1564-1575, 2011.

[89] F. Spinato, P. J. Tavner, G. J. W. van Bussel, and E. Koutoulakos, "Reliability of wind turbine subassemblies," *Renewable Power Generation, IET,* vol. 3, pp. 387-401, 2009.

[90] K. Alewine and W. Chen, "A review of electrical winding failures in wind turbine generators," *Electrical Insulation Magazine, IEEE,* vol. 28, pp. 8-13, 2012.

[91] Z. Daneshi-Far, G. A. Capolino, and H. Henao, "Review of failures and condition monitoring in wind turbine generators," in *Electrical Machines (ICEM), 2010 XIX International Conference on*, 2010, pp. 1-6.

[92] M. El Hachemi Benbouzid, "A review of induction motors signature analysis as a medium for faults detection," *Industrial Electronics, IEEE Transactions on,* vol. 47, pp. 984-993, 2000.

[93] A. Siddique, G. S. Yadava, and B. Singh, "A review of stator fault monitoring techniques of induction motors," *Energy Conversion, IEEE Transactions on,* vol. 20, pp. 106-114, 2005.

[94] M. Moghadasian, R. Kiani, F. Betin, A. Sivert, V. Lanfranchi, A. Yazidi, and G. A. Capolino, "Sensorless position control of six-phase induction machine using fuzzy-PI system," in *Industrial Electronics (ISIE), 2011 IEEE International Symposium on*, 2011, pp. 739-744.

[95] J. Martinez, P. C. Kjar, P. Rodriguez, and R. Teodorescu, "Short-circuit signatures from different wind turbine generator types," in *Power Systems Conference and Exposition (PSCE), 2011 IEEE/PES*, 2011, pp. 1-7.

[96] A. Boglietti, A. Cavagnino, M. Lazzari, and M. Pastorelli, "A simplified thermal model for variable speed self cooled industrial induction motor," in *Industry Applications Conference, 2002. 37th IAS Annual Meeting. Conference Record of the*, 2002, pp. 723-730 vol.2.

[97] Y. Gritli, A. Stefani, F. Filippetti, and A. Chatti, "Stator fault analysis based on wavelet technique for wind turbines equipped with DFIG," in *Clean Electrical Power, 2009 International Conference on*, 2009, pp. 485-491.

[98] J. Aguayo, A. Claudio, L. G. Vela, S. Lesecq, and A. Barraud, "Stator winding fault detection for an induction motor drive using actuator as sensor principle," in *Power Electronics Specialist Conference, 2003. PESC '03. 2003 IEEE 34th Annual*, 2003, pp. 1347-1351 vol.3.

[99] S. M. A. Cruz and A. J. M. Cardoso, "Stator winding fault diagnosis in three-phase synchronous and asynchronous motors, by the extended Park's vector approach," in *Industry Applications Conference, 2000. Conference Record of the 2000 IEEE*, 2000, pp. 395-401 vol.1.

[100] D. Shah, S. Nandi, and P. Neti, "Stator-interturn-fault detection of doubly fed induction generators using rotor-current and search-coil-voltage signature analysis," *Industry Applications, IEEE Transactions on*, vol. 45, pp. 1831-1842, 2009.

[101] A. Ceban, R. Pusca, and R. Romary, "Study of rotor faults in induction motors using external magnetic field analysis," *Industrial Electronics, IEEE Transactions on*, vol. 59, pp. 2082-2093, 2012.

[102] Z. Pinjia, D. Yi, T. G. Habetler, and L. Bin, "A survey of condition monitoring and protection methods for medium-voltage induction motors," *Industry Applications, IEEE Transactions on*, vol. 47, pp. 34-46, 2011.

[103] R. Johan and B. Lina Margareta, "Survey of failures in wind power systems with focus on swedish wind power plants during 1997-2005," *Energy Conversion, IEEE Transactions on*, vol. 22, pp. 167-173, 2007.

[104] X. Ying, G. Chenglin, and W. Lingchao, "There-dimensional temperature estimation of squirrel-cage induction motor using finite element method," in *Electrical Machines and Systems (ICEMS), 2011 International Conference on*, 2011, pp. 1-5.

[105] A. Boglietti, A. Cavagnino, M. Popescu, and D. Staton, "Thermal model and analysis of wound rotor induction machine," in *Energy Conversion Congress and Exposition (ECCE), 2012 IEEE*, 2012, pp. 2688-2695.

[106] K. de Morais Sousa, A. A. Hafner, E. G. Carati, H. J. Kalinowski, and J. C. C. da Silva, "Validation of thermal and electrical model for induction motors using fiber Bragg gratings," *Measurement*, vol. 46, pp. 1781-1790, 2013.

[107] S. Djurovic, D. Vilchis-Rodriguez, and A. C. Smith, "Vibration monitoring for wound rotor induction machine winding fault detection," in *Electrical Machines (ICEM), 2012 XXth International Conference on*, 2012, pp. 1906-1912.

[108] T. Sun, Z. Chen, and F. Blaabjerg, "Voltage recovery of grid-connected wind turbines with DFIG after a short-circuit fault," in *Power Electronics Specialists Conference, 2004. PESC 04. 2004 IEEE 35th Annual*, 2004, pp. 1991-1997 Vol.3.

[109] M. N. Zaggout, P. J. Tavner, and L. Ran, "Wind turbine condition monitoring using generator control loop signals," in *Power Electronics, Machines and Drives (PEMD 2012), 6th IET International Conference on*, 2012, pp. 1-6.

[110] G. Peng, D. Infield, and Y. Xiyun, "Wind turbine generator condition-monitoring using temperature trend analysis," *Sustainable Energy, IEEE Transactions on*, vol. 3, pp. 124-133, 2012.

[111] Y. Amirat, V. Choqueuse, and M. E. H. Benbouzid, "Wind turbines condition monitoring and fault diagnosis using generator current amplitude demodulation," in *Energy Conference and Exhibition (EnergyCon), 2010 IEEE International*, 2010, pp. 310-315.

[112] Pöyhönen S, Jover P, Hyötyniemi H. "Independent component analysis of vibrations for fault diagnosis of an induction motor. " InProceedings of IASTED International Conference Circuits, Signals, and Systems, 2003 May, pp. 19-21.

Appendix

GMR sensor board design

As the GMR sensor collects very weak magnetic field signals, the noise in the signal is a major problem in a stray flux monitoring system. If the signal-to-noise ratio is too small, accurate measurement results are unlikely to be obtained. In this case, it is necessary to design the signal conditioning circuit in the GMR sensor board to be suitable for low power and 5V operation.

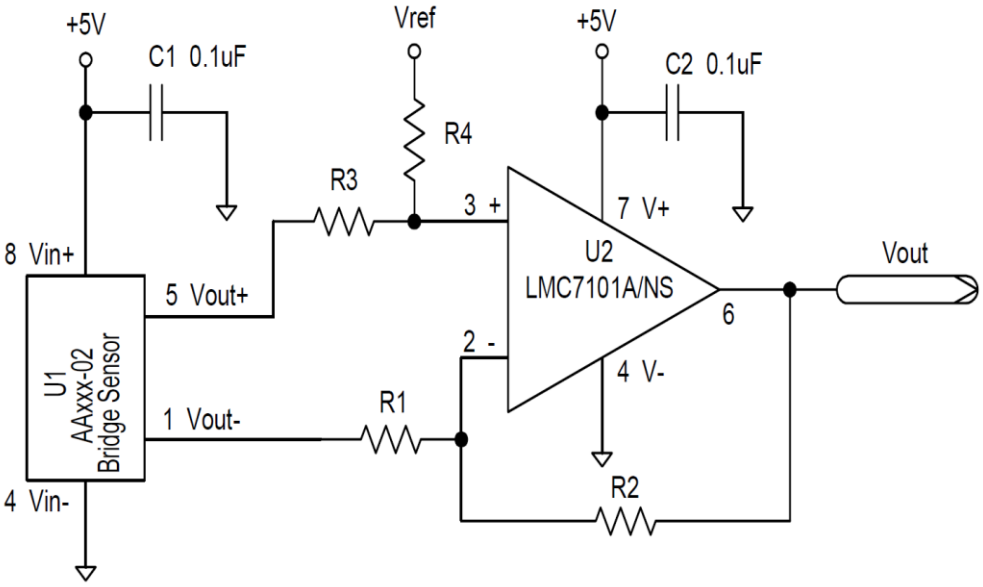

Figure 9.1 Single amplifier circuit

Fig 9.1 shows the single amplifier circuit for one GMR sensor. The advantages of this circuit are that it is simple and cheap and has fewer components. Depending on the amplifier circuit, the GMR sensor board is designed with 5 NVE AA02-02E GMR devices embedded together. Table II shows the PCB elements for a 5-channel GMR sensor board.

Table 9-1 PCB elements list

Element	Quantity	Packaging
Header 10 Pin	1	HDR 2*5 way
resistors 80K	5	0805N
Capacitors 10uF	10	0805N
Capacitors 10nF	5	0805N

INA 126UA	5	8SOIC
GMR sensors AA02-02E	5	8SOIC

The GMR sensor array PCB board has been assembled, which includes two layers for the sensor detection circuit and signal conditioning circuit. Following the application of the NVE GMR sensor, a schematic of the 5-channel GMR sensor array is shown below.

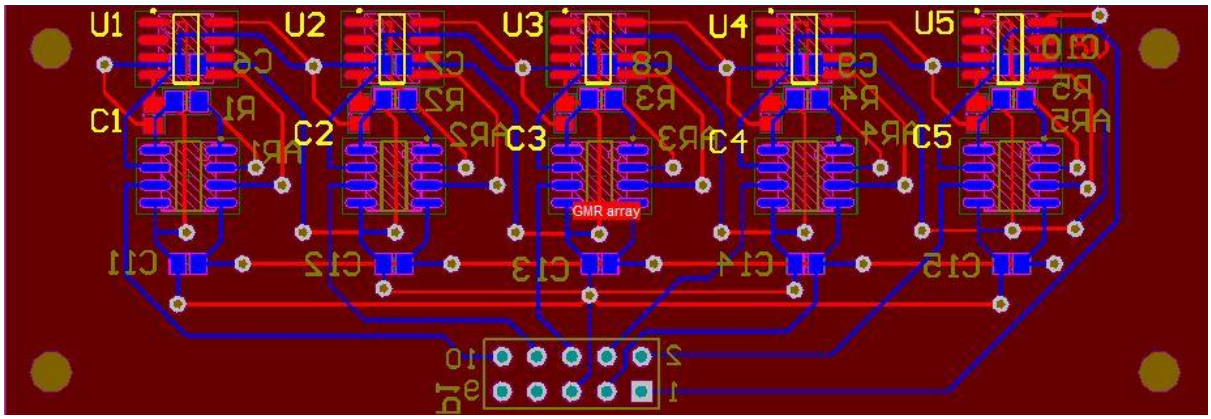

Figure 9.2 PCB layout

The PCB board is 85MM*30MM with 4 via pan (3MM) in each corner to be fastened by screws. In the PCB layout, the blue lines are the wires on the bottom signal conditioning circuit layout, and the red lines are the wires on the top sensors detection circuit layout. The 10 Pin head has integrated the five channels of output, 5V, -5V and ground together.

Test results

The GMR sensor array can detect a magnetic field especially for very weak magnetic field. In this case, the obejct in this test is an electrical magnetic copper coil shown in Fig 9.3, which is able to generate the magnetic field using input signals. In order to test the transient and dynamic satuation of the sensor array, the input of the electrical magnetic coil is a sinusoidal wave. The output of the sine wave is 100Hz, 5Vpp and the offset is 2.5Vpp.

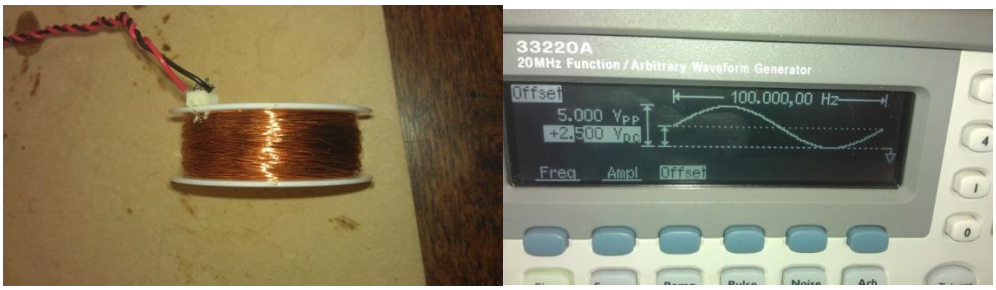

Fig 9.3 Electrical magnetic coil and power suppy for experiment

The PCB board is directly connected to a DC power supply (5V, -5V and ground). Due to limitations of the oscilloscope, for each test there are only two channels showing on the screen.First two GMR sensors are tested at the same time, and the positions of the electrical magnet coil are shown in the following figure.

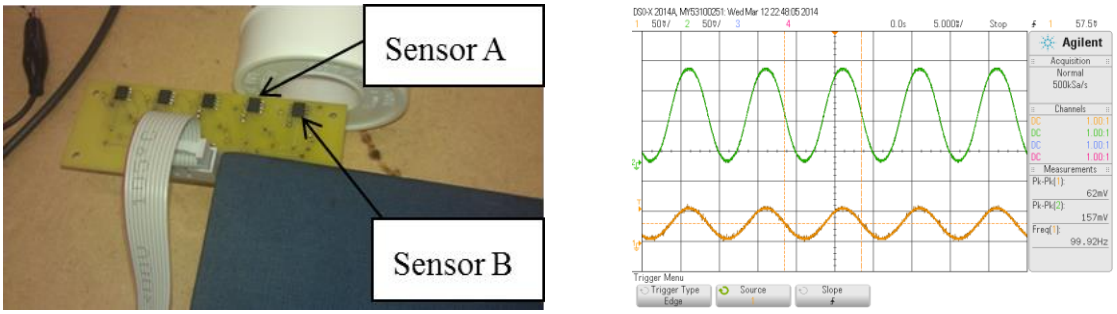

Fig 9.4 Two tested sensors and output signals

The green waveform is the output from sensor A, and the yellow waveform is the output from sensor B. From the results, the amplitude of sensor A is higher than that of sensor B, because sensor A is in the middle of the coil and stays within a much stronger magnetic field. The frequency of the two output waveforms are 100Hz. If the coil moves far from the sensors, by1.5 cm, the results are showing in Fig 9.5.

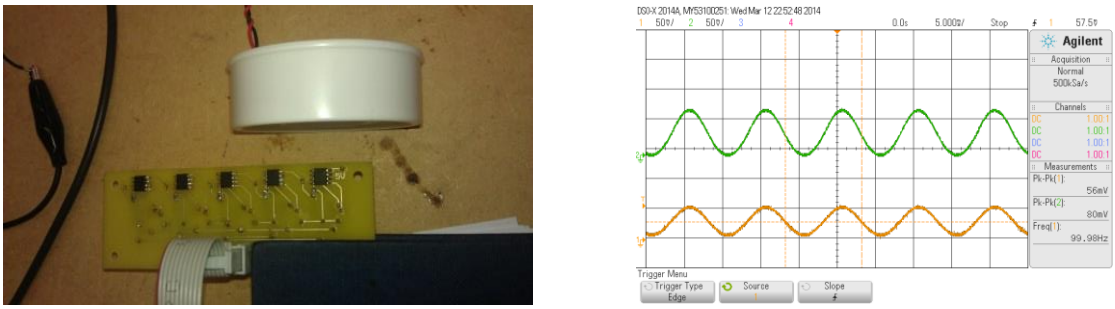

Fig. 9.5 The postions of two tested sensors and output signals

From figure above, the amplitude of the output waveform of sensor A is reduced due to the magnet coil moving further from the PCB board, which leads to the reduction in magnetic field strength. In this case, the testing results are able to show that sensors A and B are working well; furthermore, they are quite sensitive to changes in the magnetic field, and they are able to collect stray flux information from the machines.

Data acquisition design

In the previous section, the GMR sensor board has been designed and tested with the oscilloscope. However, to produce complete and fully functional condition monitoring, a data

acquisition system is needed. Due to the output of the 5 channels, the DAQ system is able to collect the stray flux data with multiple channels and high sampling frequency. The NI USB-6125 is used in this research project for the wire data acquisition system with 16 analog channels (16-bit,250kS/s).

The Labview program is applied to the data acquisition of the GMR sensor array. It is possible to collect data from the NI USB-6125 with adjustable sampling frequency and sampling time. Furthermore, by choosing a different channel, the program is able to apply the fast Fourier transform during the recording of the data. The data is saved to a specified path and given a manual name. Additionally, the program is also able to provide a 3D mesh to show the magnet flux strength in real time.

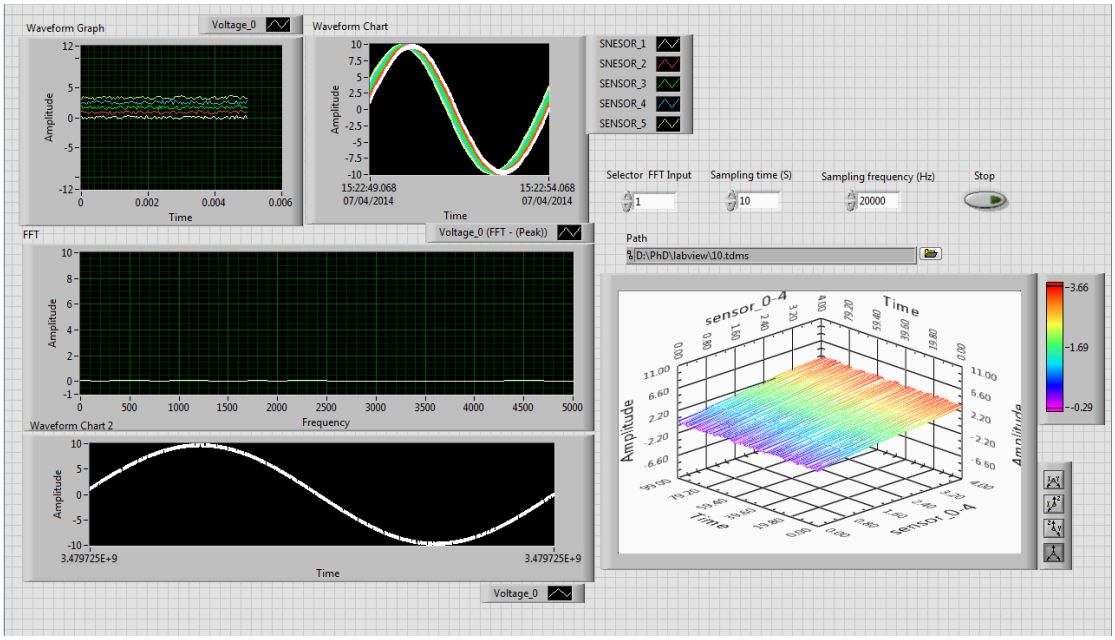

Figure 9.6 Labview design